
**A FIBER BEAM-COLUMN ELEMENT
FOR SEISMIC RESPONSE ANALYSIS
OF REINFORCED CONCRETE STRUCTURES**

by

Fabio F. Taucer

Research Assistant

Enrico Spacone

Doctoral Student

and

Filip C. Filippou

Associate Professor

Department of Civil Engineering

A Report on Research Conducted under
Grant RTA-59M848 from the
California Department of Transportation and
Grant ECE -8657525 from the
National Science Foundation

Report No. UCB/EERC-91/17
Earthquake Engineering Research Center
College of Engineering
University of California, Berkeley

December 1991

ABSTRACT

This study proposes a reliable and computationally efficient beam-column finite element model for the analysis of reinforced concrete members under cyclic loading conditions that induce biaxial bending and axial force. The element is discretized into longitudinal steel and concrete fibers such that the section force-deformation relation is derived by integration of the stress-strain relation of the fibers. At present the nonlinear behavior of the element derives entirely from the nonlinear stress-strain relation of the steel and concrete fibers.

The proposed beam-column element is based on the assumption that deformations are small and that plane sections remain plane during the loading history. The formulation of the element is based on the mixed method: the description of the force distribution within the element by interpolation functions that satisfy equilibrium is the starting point of the formulation. Based on the concepts of the mixed method it is shown that the selection of flexibility dependent shape functions for the deformation field of the element results in considerable simplification of the final equations. With this particular selection of deformation shape functions the general mixed method reduces to the special case of the flexibility method. The mixed method formalism is, nonetheless, very useful in understanding the proposed procedure for the element state determination.

A special flexibility based state determination algorithm is proposed for the computation of the stiffness matrix and resisting forces of the beam-column element. The proposed nonlinear algorithm for the element state determination is general and can be used with any nonlinear section force-deformation relation. The procedure involves an element iteration scheme that converges to a state that satisfies the material constitutive relations within the specified tolerance. During the element iterations the equilibrium and the compatibility of the element are always satisfied in a strict sense by the assumed force and deformation interpolation functions. The proposed method proved to be computationally stable and robust, while being able to describe the complex hysteretic behavior of reinforced concrete members, such as strain hardening, "pinching" and softening under cyclic nodal and element loads.

A new scheme for the application of element loads in flexibility based beam finite elements is also presented in the report. The procedure is a natural extension of the element state determination algorithm and is based on the use of the exact internal force distribution

under the applied element loads. The corresponding fixed end forces at the element ends are determined during iterations of the element state determination.

Correlation studies between the experimental response of several reinforced concrete elements and the analytical results show the ability of the proposed model to describe the hysteretic behavior of reinforced concrete members. The response sensitivity to the number of control sections in the element and the effect of the selected tolerance on the accuracy of the results is discussed in a few parameter studies.

ACKNOWLEDGMENTS

This report is part of a larger study on the seismic behavior of reinforced concrete structures supported by Grant No. RTA-59M848 from the California Department of Transportation (CALTRANS) with respect to reinforced concrete highway structures and by Grant ECE-8657525 from the National Science Foundation with respect to reinforced concrete building structures. This support is gratefully acknowledged. Any opinions expressed in this report are those of the authors and do not reflect the views of the sponsoring agency.

The authors would like to thank Professors G.H. Powell and R.L. Taylor of the University of California, Berkeley and Professor V. Ciampi of the University of Rome, La Sapienza for fruitful discussions during the course of this study.

TABLE OF CONTENTS

ABSTRACT	i
ACKNOWLEDGMENTS.....	iii
TABLE OF CONTENTS	iv
CHAPTER 1 INTRODUCTION.....	1
1.1 General.....	1
1.2 Literature Survey of Discrete Finite Element Models	2
1.2.1 Lumped Models	3
1.2.2 Distributed Nonlinearity Models	7
1.2.3 Fiber Models	15
1.3 Objectives and Scope.....	19
CHAPTER 2 FORMULATION OF BEAM-COLUMN ELEMENT.....	23
2.1 General.....	23
2.2 Definition of Generalized Forces and Deformations	24
2.3 Beam-Column Element Formulation.....	26
2.4 State Determination	30
2.5 Summary of Nonlinear Solution Algorithm.....	38
CHAPTER 3 REINFORCED CONCRETE FIBER BEAM-COLUMN ELEMENT	45
3.1 General.....	45
3.2 Model Assumptions	46
3.3 Generalized Forces and Deformations.....	47
3.4 Fiber Constitutive Models.....	49
3.4.1 Steel Stress-Strain Relation.....	49
3.4.2 Concrete Stress-Strain Relation	52
3.5 Fiber Beam-Column Element Formulation.....	56
3.6 Summary of the Fiber Beam-Column Element State Determination.....	59

CHAPTER 4	NUMERICAL IMPLEMENTATION OF BEAM-COLUMN ELEMENT	. 63
4.1	General.....	63
4.2	Preliminary Considerations.....	65
4.3	Numerical Integration	69
4.4	Definition of Tolerance.....	69
4.5	Application of Element Loads	73
4.6	Material Softening and Unloading in Reinforced Concrete Members.....	83
CHAPTER 5	APPLICATIONS	89
5.1	General.....	89
5.2	Moment-Curvature of a Section.....	90
5.3	Uniaxial Bending of a Cantilever.....	94
5.4	Uniaxial and Biaxial Bending of a Column under Compression.....	98
CHAPTER 6	CONCLUSIONS	107
REFERENCES	111
APPENDIX A	SUMMARY OF SOLUTION ALGORITHM	115
APPENDIX B	APPLICATION OF A UNIFORMLY DISTRIBUTED LOAD ON A LINEAR ELASTIC CANTILEVER	127
APPENDIX C	APPLICATION OF SOLUTION ALGORITHM TO A SIMPLE SOFTENING SYSTEM	133

CHAPTER 1

INTRODUCTION

1.1 General

Structures in regions of high seismic risk will not respond elastically to the maximum earthquake expected at the site during their usable life. Present seismic design recommendations intend that buildings respond elastically only to small magnitude earthquakes, but should be expected to experience different degrees of damage during moderate and strong ground motions. The response of reinforced concrete (RC) buildings to earthquake excitations depends on several factors, such as earthquake characteristics, soil quality and structural properties.

The determination of the structural properties of a reinforced concrete building is an essential step in the evaluation of its earthquake response. Typically, initial stiffness, ultimate capacity, and different global and local ductility demands are some of the parameters included in this assessment. In some cases it may be necessary to evaluate the remaining stiffness and load carrying capacity of a building after a strong ground motion. A complete assessment of the seismic resistant design of reinforced concrete structures often requires a nonlinear dynamic analysis. Due to the complex interactions between the various components of real structures, their dynamic characteristics up to failure cannot be identified solely from dynamic tests of scale models. Moreover, the cost of such tests is often substantial, particularly, for large scale specimens.

Historically these difficulties have been overcome by static tests on components and on reduced-scale subassemblages of structures under cyclic load reversals. Results from these tests are then used in the development and calibration of hysteretic models that permit the extrapolation of the limited test data to other cases and to the dynamic response of complete structures. In these integrated studies several models for the nonlinear response analysis of reinforced concrete structures have been developed. These can be divided into three categories in accordance with the increasing level of refinement and complexity:

Global models. The nonlinear response of a structure is concentrated at selected degrees of freedom. For example, the response of a multistory building may be represented as a system

with one lateral degree of freedom at each floor. Each degree of freedom has the hysteretic characteristics of the interstory shear-lateral drift response. Such models are useful in the preliminary design phase for estimating interstory drifts and displacement ductility demands. The reliability of this class of model in the accurate prediction of global displacements is poor and the recovery of internal member forces from the limited number of degrees of freedom is practically impossible.

Discrete finite element (member) models. The structure is modeled as an assembly of interconnected elements that describe the hysteretic behavior of reinforced concrete members. Constitutive nonlinearity is either introduced at the element level in an average sense or at the section level. Correspondingly, two types of element formulation are possible: (a) lumped nonlinearity, and, (b) distributed nonlinearity member models.

Microscopic finite element models. Members and joints are discretized into a large number of finite elements. Constitutive and geometric nonlinearity is typically described at the stress-strain level or averaged over a finite region. Bond deterioration between steel and concrete, interface friction at the cracks, creep, relaxation, thermal phenomena and geometric crack discontinuities are among the physical nonlinearities that can be studied with this class of model.

The present study concentrates on the second class of model. Discrete finite element models are the best compromise between simplicity and accuracy in nonlinear seismic response studies and represent the simplest class of model that still allows significant insight into the seismic response of members and of the entire structure. Global models are based on too crude approximations and yield too little information on the forces, deformations and damage distribution in the structure. Microscopic finite elements, on the other hand, should be limited to the study of critical regions, since these models are computationally prohibitively expensive for large scale nonlinear dynamic analyses, where the model of even a simple frame involves hundreds of degrees of freedom. Before presenting the beam-column finite element proposed in this study, an overview of existing discrete models is given.

1.2 Literature Survey of Discrete Finite Element Models

A review of existing analytical studies relevant to the nonlinear seismic response of RC frames is presented in the following. A concerted effort to model and analyze these structures in the inelastic range of response has been under way for several years and the current state of the art is summarized in this short survey. Respecting a chronological order, lumped plasticity models are presented first and distributed nonlinearity models follow. Stiffness and

flexibility formulations are also reviewed and their suitability for the analysis of reinforced concrete members is evaluated. Finally, distributed nonlinearity models that subdivide the cross section of the member into fibers are presented in more detail because of their promising performance and their relevance to the beam-column element of this study.

1.2.1 Lumped Models

Under seismic excitation the inelastic behavior of reinforced concrete frames often concentrates at the ends of girders and columns. Thus, an early approach to modeling this behavior was by means of zero length plastic hinges in the form of nonlinear springs located at the member ends. Depending on the formulation these models consist of several springs that are connected in series or in parallel.

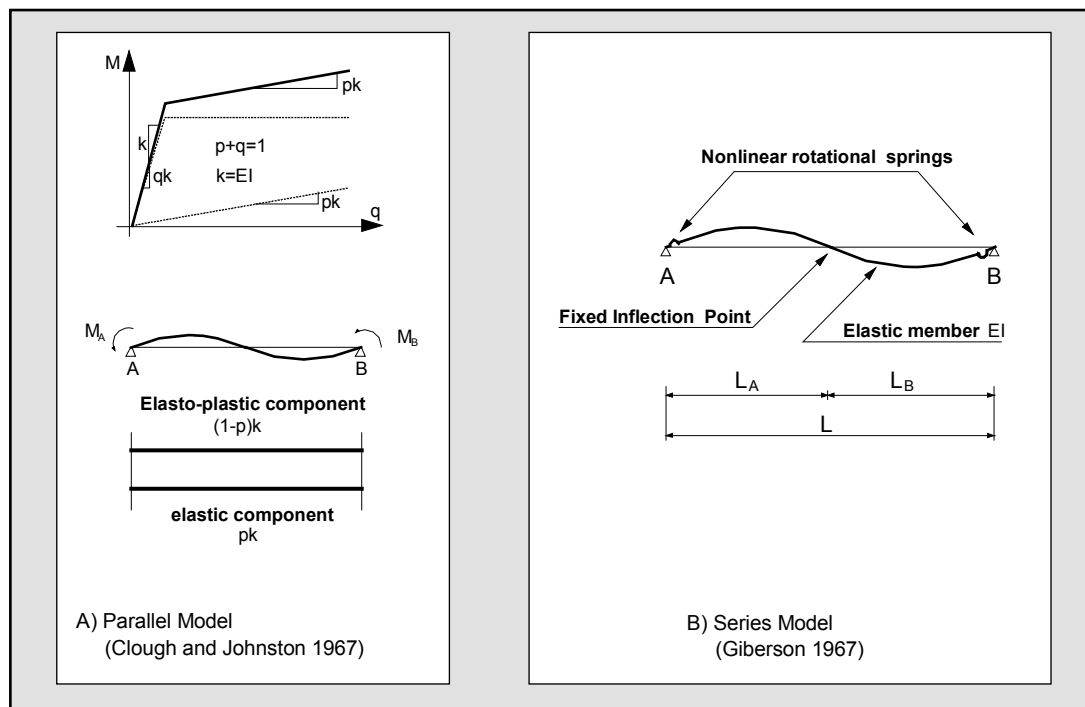


FIGURE 1.1 - SIMPLE LUMPED PLASTICITY ELEMENTS:

A) CLOUGH AND JOHNSTON MODEL

B) GIBERSON MODEL

The earliest parallel component element, shown in Fig. 1.1a, was introduced by Clough and Johnston (1967) and allowed for a bilinear moment-rotation relation: the element consists of two parallel elements, one elastic-perfectly plastic to represent yielding and the other perfectly elastic to represent strain-hardening. The stiffness matrix of the member is the

sum of the stiffnesses of the components. Takizawa (1976) generalized this model to multilinear monotonic behavior allowing for the effect of cracking in RC members. The series model was formally introduced by Giberson (1967), although it had been reportedly used earlier. Its original form, shown in Fig. 1.1b, consists of a linear elastic element with one equivalent nonlinear rotational spring attached to each end. The inelastic deformations of the member are lumped into the end springs. This model is more versatile than the original Clough model, since it can describe more complex hysteretic behavior by the selection of appropriate moment-rotation relations for the end springs. This makes the model attractive for the phenomenological representation of the hysteretic behavior of reinforced concrete members.

Several lumped plasticity constitutive models have been proposed to date (Fig. 1.2). Such models include cyclic stiffness degradation in flexure and shear, (Clough and Benuska 1966, Takeda et al. 1970, Brancaleoni et al. 1983), pinching under reversal, (Banon et al. 1981, Brancaleoni et al. 1983) and fixed end rotations at the beam-column joint interface due to bar pull-out (Otani 1974, Filippou and Issa 1988). Typically, axial-flexural coupling is neglected. Nonlinear rate constitutive representations have also been generalized from the basic endochronic theory formulation in Ozdemir (1981) to provide continuous hysteretic relations for the nonlinear springs. An extensive discussion of the mathematical functions that are appropriate for such models is given by Iwan (1978). A critical issue for these models is the selection of parameters for representing the experimental hysteretic behavior of reinforced concrete members. Two basic problems are encountered: (a) the model parameters depend not only on the section characteristics but, also, on the load and deformation history, thus limiting the generality of the approach, and, (b) a consistent and rational method for the selection of model parameters requires special algorithms for ensuring a least squares fit between analytical results and experimental data. Such an algorithm is used by Ciampi and Nicoletti (1986) in a formal system identification method for the selection of parameters for the moment-curvature relation proposed by Brancaleoni et al. (1983).

The dependence of flexural strength on the axial load under uniaxial and biaxial bending conditions has been explicitly included in the modeling of beam-columns and structural walls. In most lumped plasticity models the axial force-bending moment interaction is described by a yield surface for the stress resultants and an associated flow rule according to the tenets of classical plasticity theory (Prager and Hodge 1951). The response is assumed to be linear for stress states that fall within the yield surface in which case the flexural and axial stiffness of the member are uncoupled and independent of the end loads. With the introduction of multiple yield and loading surfaces and corresponding hardening rules

multilinear constitutive representations that include cracking and cyclic stiffness degradation are possible for the springs, as originally suggested by Takayanagi and Schnobrich (1979).

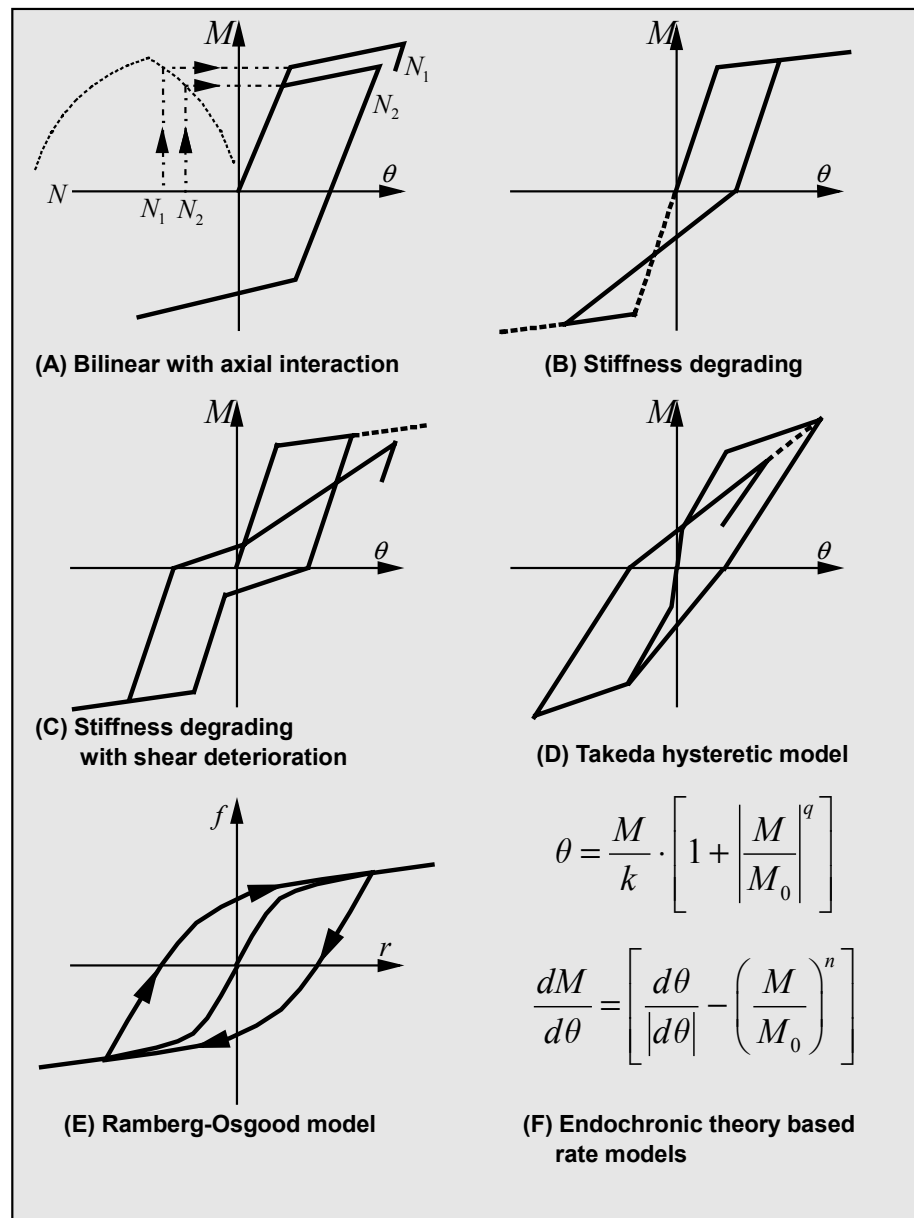


FIGURE 1.2 - PROPOSED CONSTITUTIVE MODELS FOR NONLINEAR SPRINGS

A lumped model is a simplification of the actual behavior that involves the gradual spread of inelastic deformations into the member as a function of loading history. This modeling deficiency was recognized in several correlation studies, particularly, those related to large resisting elements of flexural wall-frame structures, as described in Charney and Bertero (1982) and Bertero et al. (1984). The basic advantage of the lumped model is its

simplicity that reduces storage requirements and computational cost and improves the numerical stability of the computations. Most lumped models, however, oversimplify certain important aspects of the hysteretic behavior of reinforced concrete members and are, therefore, limited in applicability. One such limitation derives from restrictive a priori assumptions for the determination of the spring parameters. Parametric and theoretical studies of girders under monotonic loading presented by Anagnostopoulos (1981) demonstrate a strong dependence between model parameters and the imposed loading pattern and level of inelastic deformation. Neither factor is likely to remain constant during the dynamic response. The problem is further accentuated by the fluctuation of the axial force in the columns. Because of this history dependence, damage predictions at the global, but particularly at the local level, may be grossly inaccurate. Such information can only be obtained with more refined models capable of describing the hysteretic behavior of the section as a function of axial load. Another limitation of most lumped plasticity models proposed to date is their inability to describe adequately the deformation softening behavior of reinforced concrete members. Such deformation softening can be observed as the reduction in lateral resistance of an axially loaded cantilever column under monotonically increasing lateral tip displacement. Again more advanced models are needed in this case.

The generalization of the rigid plastic theory concepts by Prager et al. (1951) to reinforced concrete column stress and strain resultant variables, such as bending moment and rotation, axial force and extension, limits the applicability of these models to well detailed members with large inelastic deformation capacity at the critical regions. For a reinforced concrete column section, the yield surface of the stress resultants is actually a function of a reference strain that couples the corresponding displacement components. This contradicts classical plasticity theory which does not account for deformation softening and assumes that the section deformability is unlimited.

To overcome some of the limitations of classical plasticity theory in the description of the interaction between axial force and bending moments Lai et al. (1984) proposed a fiber hinge model that consists of a linear elastic element extending over the entire length of the reinforced concrete member and has one inelastic element at each end, as shown in Fig. 1.3. Each inelastic element is made up of one inelastic spring at each section corner that represents the longitudinal reinforcing steel and a central concrete spring that is effective in compression only. The five spring discretization of the end sections is capable of simulating the axial force-biaxial bending moment interaction in reinforced concrete members in a more rational way than is possible by classical plasticity theory. In Lai's model, the force-

deformation relation for the effective steel springs follows Takeda's model, but the parameters that define the envelope are established from equilibrium considerations.

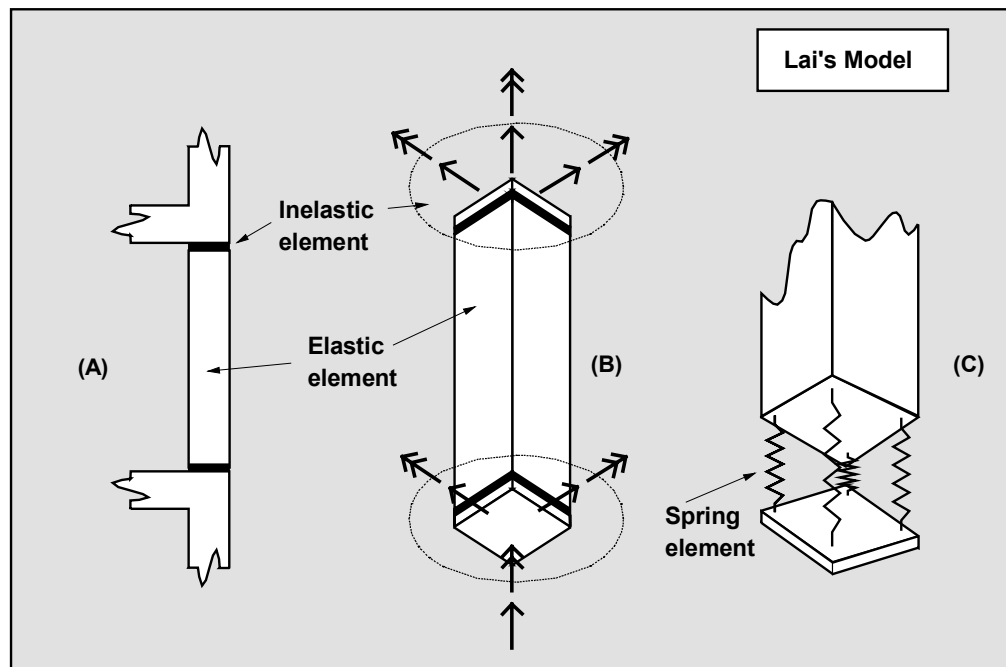


FIGURE 1.3 - LAI'S MODEL: DEGRADING INELASTIC ELEMENT FOR REINFORCED CONCRETE BEAM-COLUMNS UNDER BIAXIAL BENDING AND AXIAL LOAD:
(A) MEMBER IN FRAME; (B) MEMBER MODEL; (C) INELASTIC ELEMENT

1.2.2 Distributed Nonlinearity Models

A more accurate description of the inelastic behavior of reinforced concrete members is possible with distributed nonlinearity models. In contrast to lumped plasticity models, material nonlinearity can take place at any element section and the element behavior is derived by weighted integration of the section response. In practice, since the element integrals are evaluated numerically, only the behavior of selected sections at the integration points is monitored. Either the element deformations or the element forces are the primary unknowns of the model and these are obtained by suitable interpolation functions from the global element displacements or forces, respectively. Discrete cracks are represented as "smeared" over a finite length rather than treated explicitly. The constitutive behavior of the cross section is either formulated in accordance with classical plasticity theory in terms of stress and strain resultants or is explicitly derived by discretization of the cross section into fibers, as is the case in the spread plasticity fiber models. A common assumption of these

models is that plane sections remain plane, such that the strains are linearly distributed over the cross section.

Earlier beam-column models neglect the coupling between axial force and bending moment and, typically, consist of two cantilever elements that are connected at the fixed point of contraflexure of the member, as shown in Fig. 1.4 which refers to the model introduced by Otani (1974). In the derivation of the cantilever stiffness independent hysteresis rules are used for the end moment-free end displacement and for the end moment-free end rotation relation. To overcome some of the numerical difficulties in the element formulation, such as the lack of symmetry of the stiffness matrix, Otani assumed that the inelastic deformations are lumped in two equivalent springs at the ends of the member, thus sacrificing the generality of the model. The global behavior of Otani's model is derived by integration of the curvatures along the two cantilever components. The main limitation of this and similar models is the assumption of a fixed point of contraflexure in the element.

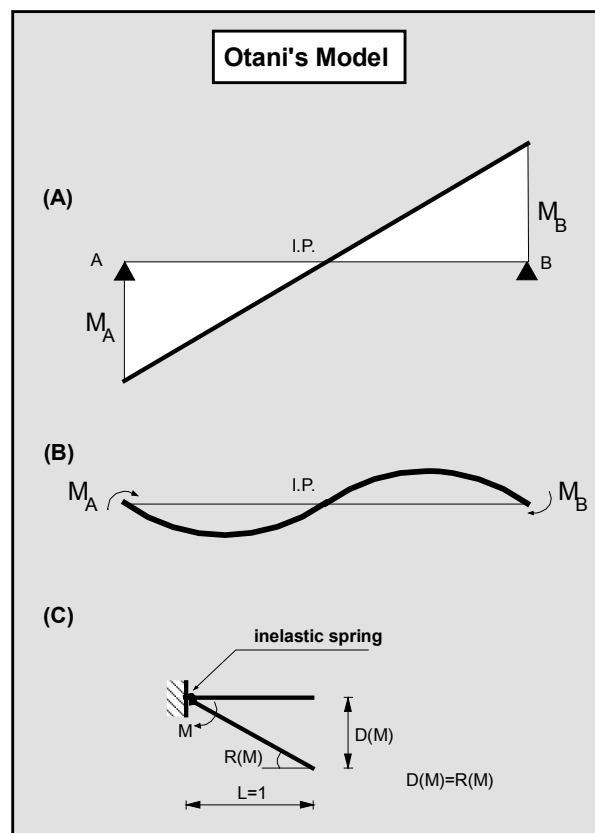


FIGURE 1.4 - OTANI'S MODEL: A) MOMENT DISTRIBUTION
 B) ELEMENT DEFORMATION
 C) EQUIVALENT INELASTIC ROTATIONAL SPRINGS

In the model introduced by Soleimani et al. (1979) a zone of inelastic deformations gradually spreads from the beam-column interface into the member as a function of loading history. The rest of the beam remains elastic. The fixed-end rotations at the beam-column interface are modeled through point hinges inserted at the ends of the member. These are related to the curvature at the corresponding end section through an "effective length" factor which remains constant during the entire response history. A very similar model was developed by Meyer et al. (1983). The flexibility coefficients of the model are identical to those proposed by Soleimani. A slightly different way of calculating the stiffness of the plastic zone during reloading is proposed and Takeda's model is used to describe the hysteretic moment-curvature relation. Fixed-end rotations are not taken into account in the study. The original model was later extended by Roufaiel and Meyer (1987) to include the effect of shear and axial forces on the flexural hysteretic behavior based on a set of empirical rules. The variation of axial loads due to overturning moments is not accounted for. Darvall and Mendis (1985) propose a similar but simpler model with end inelastic deformations defined through a trilinear moment-curvature relation. Once formed the end hinges may remain perfectly plastic or exhibit plastic softening or hardening. Perfectly plastic hinges are concentrated at a point, while softening and hardening hinges have a user defined, finite, fixed length that is normally assumed to be from $0.75 d$ to d , where d is the effective depth of the cross section.

Takayanagi and Schnobrich (1979) propose to divide the element into a finite number of short longitudinal elements, each represented by a nonlinear rotational spring. The model is shown in Fig. 1.5. The properties of a segment depend on the bending moment at its midpoint and are assumed to be constant over the length of the segment. Static condensation is used to reduce this multi-spring model to a single beam-column element. Even though the nonlinear element behavior is eventually lumped at the end springs, this element belongs to the family of distributed nonlinearity models because it accounts for inelastic deformations that take place along the element. The multiple spring model was first used in the study of the seismic response of coupled shear walls, which exhibit significant variation of axial force. To account for the interaction between axial force and bending moment a three dimensional limit surface was introduced for the rotational springs.

Filippou and Issa (1988) also subdivide the element in different subelements, but follow a different approach. Each subelement describes a single effect, such as inelastic behavior due to bending, shear behavior at the interface or bond-slip behavior at the beam-column joint. The interaction between these effects is then achieved by the combination of subelements. This approach allows the hysteretic law of the individual subelement to be

simpler, while the member still exhibits a complex hysteretic behavior through the interaction of the different subelements.

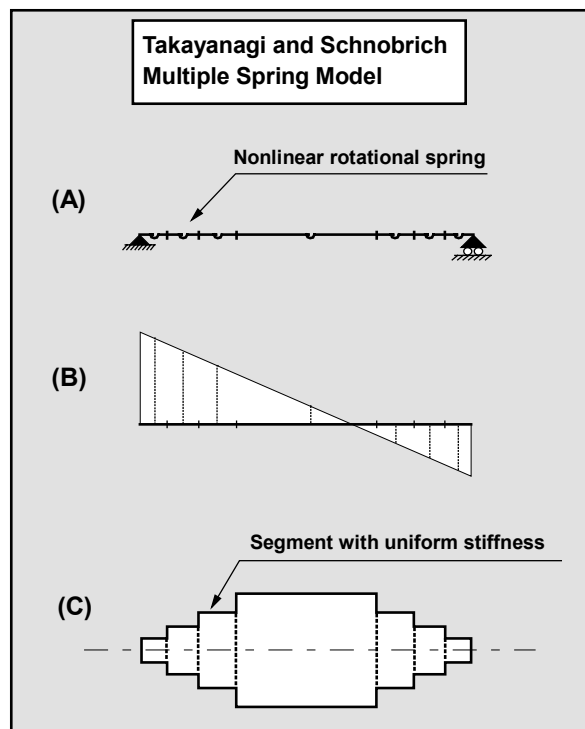


FIGURE 1.5 TAKAYANAGI AND SCHNOBRICH MULTIPLE SPRING MODEL
 (A) ELEMENT MODEL; (B) BENDING MOMENT DIAGRAM;
 (C) SECTION STIFFNESS DISTRIBUTION

The first elements with distributed nonlinearity were formulated with the classical stiffness method using cubic Hermitian polynomials to approximate the deformations along the element. The general three-dimensional element with axial and flexural degrees of freedom is depicted in the local reference system in Fig. 1.6. The element without rigid body modes is shown in Fig. 1.7. For all elements the torsional degrees of freedom are assumed to exhibit linear elastic behavior and to be uncoupled from the axial and flexural degrees of freedom so that they can be omitted in the following presentation. For the sake of brevity the discussion is limited to the case of uniaxial bending about the z -axis, since the extension to the biaxial case is straightforward. Nodal displacements are grouped in vector $\bar{\mathbf{q}}$ for the element with rigid body modes and vector \mathbf{q} for the element without rigid body modes:

$$\bar{\mathbf{q}} = \{\bar{q}_1 \quad \bar{q}_2 \quad \bar{q}_5 \quad \bar{q}_6 \quad \bar{q}_7 \quad \bar{q}_{10}\}^T \quad (1.1)$$

$$\mathbf{q} = \{q_1 \quad q_2 \quad q_5\}^T \quad (1.2)$$

If x denotes the longitudinal axis of the member, the transverse displacement $v(x)$ and the axial displacement $u(x)$ are approximated by

$$\bar{\mathbf{d}}(x) = \begin{Bmatrix} u(x) \\ v(x) \end{Bmatrix} = \mathbf{a}_d(x) \cdot \bar{\mathbf{q}} \quad (1.3)$$

where $\mathbf{a}_d(x)$ is a matrix that contains the cubic interpolation functions for the transverse displacements and the linear interpolation functions for the axial displacements

$$\mathbf{a}_d(x) = \begin{bmatrix} \psi_1(x) & 0 & 0 & \psi_2(x) & 0 & 0 \\ 0 & \phi_1(x) & \phi_2(x) & 0 & \phi_3(x) & \phi_4(x) \end{bmatrix} \quad (1.4)$$

with

$$\begin{aligned} \psi_1(x) &= 1 - \frac{x}{L} & \psi_2(x) &= \frac{x}{L} \\ \phi_1(x) &= 2\frac{x^3}{L^3} - 3\frac{x^2}{L^2} + 1 & \phi_2(x) &= \frac{x^3}{L^2} - 2\frac{x^2}{L} + x \\ \phi_3(x) &= -2\frac{x^3}{L^3} + 3\frac{x^2}{L^2} & \phi_4(x) &= \frac{x^3}{L^2} - \frac{x^2}{L} \end{aligned}$$

The above interpolation functions can be readily extended to the biaxial bending case.

In the derivation of the stiffness matrix of beam and beam-column elements by the principle of virtual work the generalized deformations of the problem are the axial strain $\varepsilon(x)$ and the curvature about the z -axis $\chi_z(x)$. Under the assumptions that displacements are small and plane sections remain plane the section deformations $\mathbf{d}(x)$ are related to the nodal displacements by

$$\mathbf{d}(x) = \begin{Bmatrix} \varepsilon(x) \\ \chi_z(x) \end{Bmatrix} = \begin{Bmatrix} u'(x) \\ v''(x) \end{Bmatrix} = \bar{\mathbf{a}}(x) \cdot \bar{\mathbf{q}} \quad (1.5)$$

where $\bar{\mathbf{a}}(x)$ is derived from the displacement interpolation functions according to

$$\bar{\mathbf{a}}(x) = \begin{bmatrix} \psi_1'(x) & 0 & 0 & \psi_2'(x) & 0 & 0 \\ 0 & \phi_1''(x) & \phi_2''(x) & 0 & \phi_3''(x) & \phi_4''(x) \end{bmatrix} \quad (1.6)$$

Using the principle of virtual displacements or the principle of minimum potential energy the element stiffness matrix $\bar{\mathbf{K}}$ is the integral of section stiffnesses $\mathbf{k}(x)$

$$\bar{\mathbf{K}} = \int_0^L \bar{\mathbf{a}}^T(x) \cdot \mathbf{k}(x) \cdot \bar{\mathbf{a}}(x) \cdot dx \quad (1.7)$$

where the section stiffness $\mathbf{k}(x)$ relates the section forces $\mathbf{D}(x)$ with the corresponding deformations $\mathbf{d}(x)$

$$\mathbf{D}(x) = \mathbf{k}(x) \cdot \mathbf{d}(x) \quad (1.8)$$

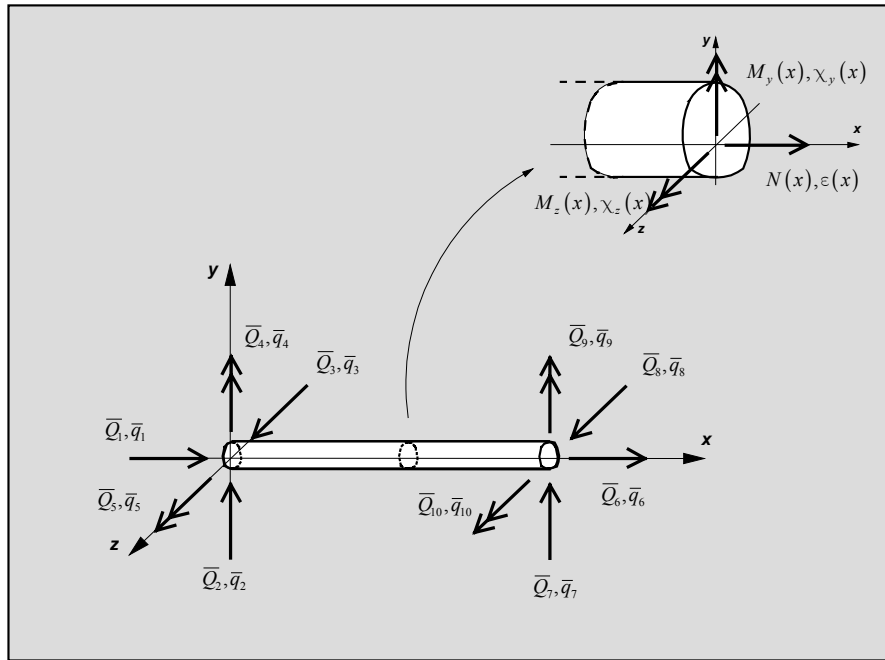


FIGURE 1.6 BEAM ELEMENT WITH RIGID BODY MODES IN LOCAL REFERENCE SYSTEM

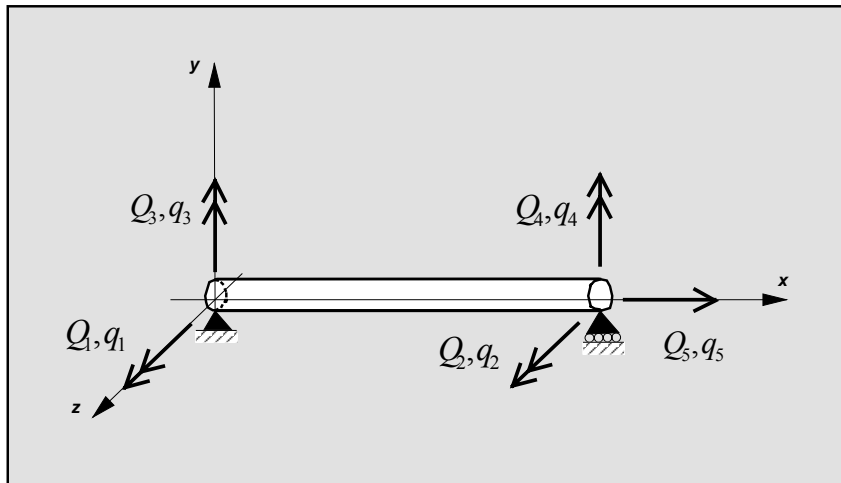


FIGURE 1.7 BEAM ELEMENT WITHOUT RIGID BODY MODES IN LOCAL REFERENCE SYSTEM

The section forces are the generalized stresses of the problem, i.e. the axial force $N(x)$ and the bending moment $M_z(x)$ at section x . Thus:

$$\mathbf{D}(x) = \begin{Bmatrix} N(x) \\ M_z(x) \end{Bmatrix} \quad (1.9)$$

The application of the virtual displacement principle yields the element resisting forces $\bar{\mathbf{Q}}_R$ as the integral of the section resisting forces $\mathbf{D}_R(x)$

$$\bar{\mathbf{Q}}_R = \int_0^L \bar{\mathbf{a}}^T(x) \cdot \mathbf{D}_R(x) \cdot dx \quad (1.10)$$

Elements based on this classical finite element displacement approach are proposed, among others, by Helleland and Scordelis (1981) and Mari and Scordelis (1984). The formulation has been extended by Bazant and Bhat (1977) to include the effect of shear by means of multi-axial constitutive laws based on the endochronic theory. In this model the section is subdivided into horizontal layers but each layer is allowed to crack at a different angle that is derived from the interaction of normal and shear stress in the layer.

The main shortcoming of stiffness-based elements is their inability to describe the behavior of the member near its ultimate resistance and after the onset of strain softening, since they are plagued by numerical instability problems for reasons to be discussed in detail later in this section.

Since the curvature distribution in a member that has yielded at the ends is not well represented by cubic Hermitian interpolation functions, computational economy with improved representation of internal deformations is achieved by the combined approximation of, both, the section deformations, which are the basic unknowns of the problem, and the section flexibilities. Menegotto and Pinto (1977) interpolate both variables based on the values at a few monitored sections and include the axial force-bending moment interaction. The section flexibilities are assumed to vary linearly between monitored sections, which is equivalent to a hyperbolic stiffness variation. This improvement in accuracy makes the approach computationally attractive, since fewer sections need to be monitored and, hence, the number of variables that need to be computed and stored is smaller than in stiffness models of comparable level of discretization.

Further improvement in element accuracy is achieved by the introduction of variable displacement interpolation functions. A major limitation of the classical displacement approach is the assumption of cubic interpolation functions, which result in a linear curvature distribution along the element. This assumption leads to satisfactory results under linear or nearly linear response. However, when the reinforced concrete member undergoes significant yielding at the ends, the curvature distribution becomes highly nonlinear in the inelastic

region. This requires the use of a very fine discretization in the inelastic regions of stiffness-based elements. Mahasuverachai (1982) was the first to propose the use of flexibility-dependent shape functions that are continuously updated during the analysis as inelastic deformations spread into the member. In his study deformation increments rather than total deformations are approximated. The section deformation increments are written as

$$\Delta \mathbf{d}(x) = \mathbf{f}(x) \cdot \mathbf{b}(x) \cdot \mathbf{F}^{-1} \cdot \Delta \mathbf{q} = \mathbf{a}(x) \cdot \Delta \mathbf{q} \quad (1.11)$$

where Δ denotes the increment of the corresponding vector. This new formulation is, however, applied to the development of pipeline elements where the source of nonlinearity is geometric rather than material.

Recent efforts to develop more robust and reliable reinforced-concrete frame elements have shown two parallel trends. First, deviating from the original classical stiffness method, researchers have focused attention on flexibility-dependent shape functions and, more recently, on flexibility-based formulations that permit a more accurate description of the force distribution within the element. Secondly, the elements are subdivided into longitudinal fibers, which has two inherent advantages: a) the reinforced concrete section behavior is derived from the uniaxial stress-strain behavior of the fibers and three-dimensional effects, such as concrete confinement by transverse steel can be incorporated into the uniaxial stress-strain relation; and, b) the interaction between bending moment and axial force can be described in a rational way.

The flexibility approach is based on force interpolation functions within the element. Typically, the element is analyzed without including the rigid body modes. In this case the end rotations relative to the chord and the axial differential displacement are the element generalized deformations, or simply, element deformations. The element forces and deformations without the rigid body modes are shown in Fig. 1.7. Under the assumption of small deformations and small displacements the element deformations \mathbf{q} are related to the element displacements $\bar{\mathbf{q}}$ in Fig. 1.6 by the compatibility matrix. In the uniaxial bending case the vector of element forces without rigid body modes is

$$\mathbf{Q} = \{Q_1 \quad Q_2 \quad Q_3\}^T \quad (1.12)$$

It is common to assume that the bending moment distribution inside the element is linear and that the axial force distribution is constant. In vector notation:

$$\mathbf{D}(x) = \mathbf{b}(x) \cdot \mathbf{Q} \quad (1.13)$$

where $\mathbf{b}(x)$ is a matrix containing the force interpolation functions

$$\mathbf{b}(x) = \begin{bmatrix} 0 & 0 & 1 \\ \left(\frac{x}{L}-1\right) & \left(\frac{x}{L}\right) & 0 \end{bmatrix} \quad (1.14)$$

The application of the virtual force principle yields the element flexibility

$$\mathbf{F} = \int_0^L \mathbf{b}^T(x) \cdot \mathbf{f}(x) \cdot \mathbf{b}(x) \cdot dx \quad (1.15)$$

where $\mathbf{f}(x)$ is the section flexibility matrix, such that:

$$\mathbf{d}(x) = \mathbf{f}(x) \cdot \mathbf{D}(x) \quad (1.16)$$

The advantage of this formulation stems from the realization that, irrespective of the state of the element, the force interpolation functions in Eqs. (1.13) and (1.14) satisfy the element equilibrium in a strict sense, as long as no element loads are applied. In other words, whatever material nonlinearities take place at the section level and even as the element starts softening when deformed beyond its ultimate resistance, the assumed internal force distributions are exact.

A critical issue in flexibility-based elements is the implementation in an existing finite element program. Computer programs are typically based on the direct stiffness method of analysis. In this case the solution of the global system of equilibrium equations for the given loads yields the unknown structural displacements. After the element displacements are extracted from the structural displacements the phase of element state determination starts. During this phase the resisting forces and the stiffness matrix need to be determined for the given element displacements. The element state determination requires a special procedure in a flexibility-based element, since the element resisting forces cannot be derived by integration of the section resisting forces according to Eq. (1.10). An interesting state determination procedure for a flexibility-based finite element is proposed in Ciampi and Carlesimo (1986) and is discussed at length in Spacone et al. (1992). The section moment-curvature relation of this model is based on the endochronic theory presented in Brancaleoni et al. (1983). The element state determination is based on the section deformation residuals that result from the numerical integration of the section constitutive relation. The interaction between axial force and bending moment is not included in the latter model.

1.2.3 Fiber Models

The most promising models for the nonlinear analysis of reinforced concrete members are, presently, flexibility-based fiber elements. In these models the element is subdivided into longitudinal fibers, as shown in Fig. 1.8. The geometric characteristics of the fiber are its location in the local y, z reference system and the fiber area A_{fib} . The constitutive relation of the section is not specified explicitly, but is derived by integration of the response of the fibers, which follow the uniaxial stress-strain relation of the particular material, as shown in Fig. 1.8. The elements proposed to date are limited to small displacements and deformations

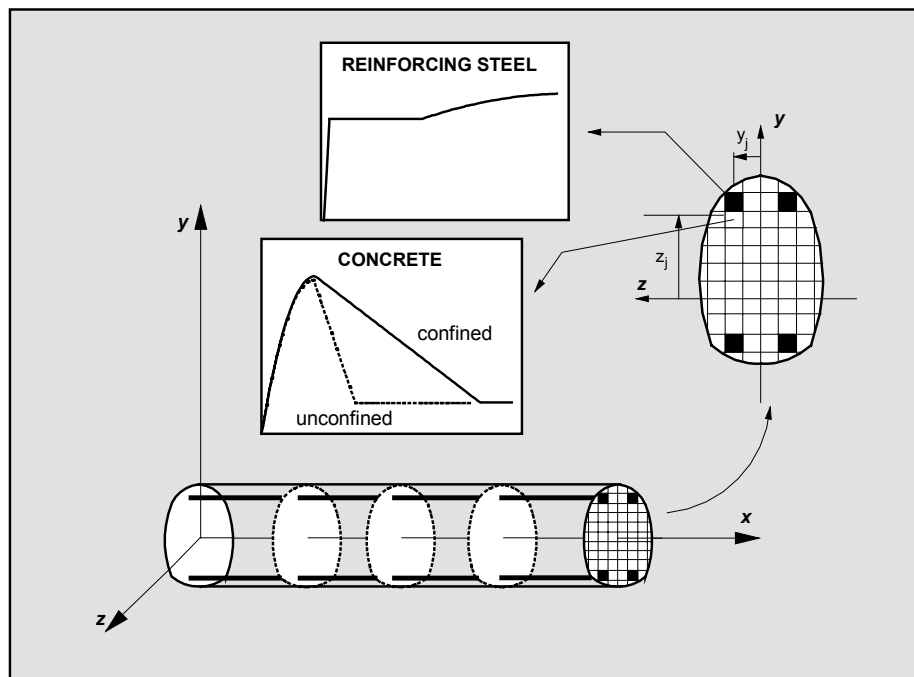


FIGURE 1.8 FIBER ELEMENT: DISTRIBUTION OF CONTROL SECTIONS AND SECTION SUBDIVISION INTO FIBERS

and assume that plane sections remain plane. Two new tasks appear in the formulation of flexibility-based fiber elements: a) the element state determination, which involves the determination of the resisting forces for the given element displacements, and, b) the determination of the section flexibility $f(x)$ that is required in the calculation of the element flexibility F according to Eq. (1.15).

The basic assumption in a flexibility-based model is the internal force distribution in the element, which is expressed in Eq. (1.13) by the force interpolation functions $b(x)$. In a consistent state determination process the section forces are determined from the element

forces according to Eq. (1.13), followed by the computation of the corresponding fiber stresses based on equilibrium. The fiber strains and flexibilities are determined from the fiber stress-strain relations and the section deformations as well as the section flexibility are computed by applying the virtual force principle. The determination of fiber stresses from section forces is, however, a statically indeterminate problem for a section with more than two fibers: the fiber stresses cannot be determined from the axial force and bending moment at the section, since there are only two equilibrium equations in the uniaxial bending case for three or more unknown stresses. One possible solution is to assume a stress distribution within the section, but the problem is, then, only postponed to the fiber state determination phase of the algorithm, since fiber stress-strain relations are typically expressed as explicit functions of strain. The solution adopted in proposed models is to linearize the section constitutive relation and compute the section deformations from the new section forces and the section flexibility from the previous step. Fiber stresses and stiffnesses are then determined from the fiber stress-strain relations. The section resisting forces are computed from the fiber stress distribution and the section stiffness $\mathbf{k}(x)$ is assembled from the fiber stiffnesses. In the uniaxial bending case $\mathbf{k}(x)$ takes the form

$$\mathbf{k}(x) = \begin{bmatrix} \sum_{ifib=1}^{n(x)} E_{ifib} \cdot A_{ifib} & -\sum_{ifib=1}^{n(x)} E_{ifib} \cdot A_{ifib} \cdot y_{ifib} \\ -\sum_{ifib=1}^{n(x)} E_{ifib} \cdot A_{ifib} \cdot y_{ifib} & \sum_{ifib=1}^{n(x)} E_{ifib} \cdot A_{ifib} \cdot y_{ifib}^2 \end{bmatrix} \quad (1.17)$$

The section stiffness is then inverted to yield the section flexibility $\mathbf{f}(x) = \mathbf{k}^{-1}(x)$. The new element flexibility \mathbf{F} is computed from Eq. (1.15) and is then inverted to obtain the element stiffness $\mathbf{K} = \mathbf{F}^{-1}$. The remaining problem is the determination of the element resisting forces from the section resisting forces along the element. Presently, this is the main challenge in the development of flexibility-based fiber elements.

The first flexibility-based fiber element was proposed by Kaba and Mahin (1984). It follows the outline of the flexibility approach presented above using the force interpolation functions $\mathbf{b}(x)$ in Eq. (1.14) in the determination of the element flexibility matrix. Only uniaxial bending is taken into account in this model. In the state determination phase of the nonlinear analysis the section deformations are computed from the element deformations with the flexibility-dependent deformation shape functions in Eq. (1.11). Due to the nonlinear behavior of the section, $\mathbf{f}(x)$, \mathbf{F} and, consequently, $\mathbf{a}(x)$ change during the element deformation history. The section deformations are then used to determine the fiber strains based on the plane section assumption and the corresponding fiber stresses and stiffnesses are

established from the fiber stress-strain relation. Subsequently, the section stiffness $\mathbf{k}(x)$ and the corresponding resisting forces $\mathbf{D}_R(x)$ are determined by application of the principle of virtual work at the section. The section stiffness is inverted to yield the section flexibility $\mathbf{f}(x)$. Finally, the element flexibility matrix \mathbf{F} is determined with Eq. (1.15) and the increment of the element resisting forces $\Delta\mathbf{Q}_R$ is established with the virtual displacement principle,

$$\Delta\mathbf{Q}_R = \int_0^L \mathbf{a}^T(x) \cdot \Delta\mathbf{D}_R(x) \cdot dx = \mathbf{F}^{-1} \cdot \int_0^L \mathbf{b}^T(x) \cdot \mathbf{f}(x) \cdot \Delta\mathbf{D}_R(x) \cdot dx \quad (1.18)$$

The integrals over the element length are evaluated by subdividing the element into equally spaced slices and assuming a linear flexibility distribution between the slices. This model yields very promising results, but is plagued by convergence problems and is unable to describe element softening. The element formulation is actually based on a mixed approach, since it uses both deformation and force interpolation functions. Unfortunately, the element lacks theoretical clarity and contains several inconsistencies that cause the numerical problems. The first inconsistency appears in the determination of the element flexibility matrix that is based on compatibility considerations and the application of the virtual force principle, while the determination of the element resisting forces is based on equilibrium considerations and the application of the virtual displacement principle. The second inconsistency appears in the state determination process which violates the equilibrium within the element, since the distribution of the section resisting forces $\mathbf{D}_R(x)$ does not satisfy the equilibrium conditions in Eqs. (1.13) and (1.14). Consequently, the resulting bending moment distribution is not linear and the axial force distribution is not uniform, as required by the force interpolation functions $\mathbf{b}(x)$.

Zeris and Mahin (1988 and 1991) discuss the improvement of the original Kaba-Mahin model and extend the formulation to the biaxial case. The main improvement concerns the element state determination. Once the main program determines the nodal displacement increments $\Delta\bar{\mathbf{q}}$, the element updating sequence consists of the following steps: a) Eq (1.11) is applied at the end sections of the element to determine the section deformation increments $\Delta\mathbf{d}(0)$ and $\Delta\mathbf{d}(L)$; b) the corresponding bending moments and axial forces at the end sections are established by means of a modified event-to-event advancement method developed by Zeris (1986); c) the deformations at interior sections of the element are updated with an iterative procedure so as to produce section resisting forces that conform to the assumed force distribution in the element.

An interesting analysis of the softening behavior of a cantilever beam is discussed in Zeris and Mahin (1988) and is reproduced in Fig. 1.9. When a cantilever is displaced beyond

the point of ultimate resistance, section 1 at the fixed base of the cantilever loses load carrying capacity and starts softening. Sections 2 through 5 along the height of the cantilever unload elastically in order to satisfy the internal equilibrium. Stiffness-based elements fail to trace the real behavior of the member, because of the assumption of a linear curvature distribution. The assumed curvature distribution deviates significantly from the actual distribution during element softening, as the sharp jump in the curvature value near the fixed end attests in Fig. 1.9. In this case the column has to be subdivided into several elements, but convergence problems are still encountered. Early flexibility elements, such as that described by Kaba and Mahin (1984), are also unable to trace the softening behavior of the member correctly, because equilibrium is not enforced along the element.

Even though the element proposed by Zeris and Mahin shows satisfactory performance, the element state determination procedure is not very clear and is derived from ad hoc corrections of the Kaba-Mahin model rather than from a general theory.

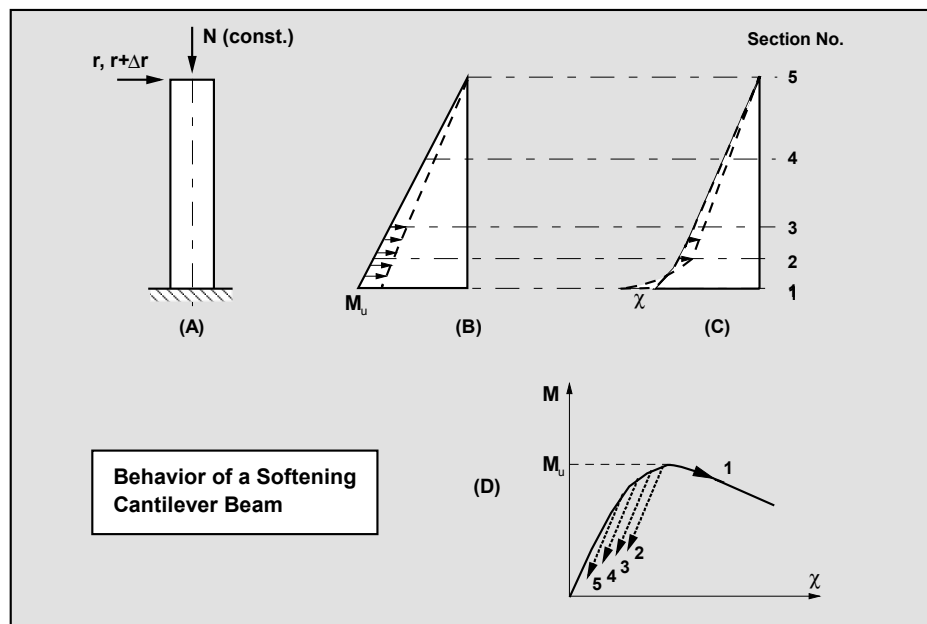


FIGURE 1.9 BEHAVIOR OF SOFTENING CANTILEVER MODEL

(A) MEMBER AND LOADING; (B) MOMENT DISTRIBUTION

(C) CURVATURE DISTRIBUTION; (D) MOMENT-CURVATURE RELATION

1.3 Objectives and Scope

In the literature survey great attention was devoted to fiber beam-column elements because of their ability to combine a relatively accurate description of the section behavior with the simplicity of a frame element. Three dimensional effects, such as confinement of the

concrete by transverse and longitudinal steel, can be included in the uniaxial material behavior of the fibers. The interaction between bending moment and axial force can also be established in a rational manner by integration of the uniaxial behavior of the fibers. This effect is normally ignored in seismic resistant design and analysis because of the computational complexities involved. Recent earthquakes and several experimental studies, however, have demonstrated that the interaction between bending moment and axial force influences the hysteretic behavior of reinforced concrete members, especially, corner columns in frames and slender walls in coupled-wall systems. Fiber models proposed to date fail to offer a clear and reliable nonlinear algorithm for their implementation in the nonlinear dynamic analysis of reinforced concrete structures that might experience considerable local damage and partial loss of load carrying capacity.

The present study proposes a new fiber beam-column finite element along with a consistent nonlinear solution algorithm that is particularly suitable for the analysis of the highly nonlinear hysteretic behavior of softening members, such as reinforced concrete columns under varying axial load. The element formulation is cast in the framework of the mixed method, but can be equally derived with a flexibility approach. The proposed element state determination is based on a nonlinear iterative algorithm that always maintains equilibrium and compatibility within the element and that eventually converges to a state that satisfies the section constitutive relations within a specified tolerance.

The main objectives of this study are:

- to present a formal mixed method framework for the formulation of a beam-column element using force interpolation functions and flexibility-dependent deformation shape functions;
 - to introduce an innovative and numerically robust state determination procedure for flexibility-based beam-column elements. This procedure is based on an iterative process for the determination of resisting forces from the given element deformations that always maintains equilibrium and compatibility within the element. Even though the procedure is discussed in the present study in the context of a fiber beam-column model, it is equally applicable to any nonlinear constitutive relation for the section;
 - to discuss important numerical aspects of the element implementation in a general purpose analysis program, with emphasis on the aspects that relate to the implementation of the element state determination procedure;
 - to extend the element formulation to include the application of element loads. This rather important topic has received scant attention in seismic response studies of
-

reinforced concrete buildings. It is especially relevant for the extension of the proposed model to prestressed concrete structures;

- to illustrate with a series of examples the ability of the proposed model to describe the hysteretic behavior of reinforced concrete members. The response sensitivity to the number of control sections in the element and the effect of the selected tolerance on the accuracy of the results is discussed in a few parameter studies.

Following the review of previous relevant studies in this chapter, Chapter 2 presents the mixed formulation of the beam-column element and illustrates the proposed nonlinear solution algorithm for the element state determination. Chapter 3 extends the formulation to the case of a fiber beam-column element and discusses material models for the nonlinear stress-strain relation of the fibers. In Chapter 4 issues related to the numerical implementation of the nonlinear solution algorithm are discussed along with the associated convergence criteria. A consistent method for the application of element loads in flexibility based finite elements is also presented in this chapter. The response sensitivity to the number of control sections in the element and the effect of the convergence tolerance on the accuracy of the results is discussed in a few parameter studies at the beginning of Chapter 5. The validity of the proposed model is then established by comparing the analytical results with information from experimental studies. The conclusions of this study and directions for future research are presented in Chapter 6.

CHAPTER 2

FORMULATION OF BEAM-COLUMN ELEMENT

2.1 General

This chapter presents the general formulation of a beam-column finite element based on the flexibility method. The presentation is cast in the more general form of a mixed method for two reasons: (a) this approach illustrates better the state-determination process used in the nonlinear analysis algorithm, and, (b) it yields in a direct way the flexibility dependent deformation shape functions of the element that reduce the general mixed method formulation to the flexibility method used in this study. In addition, the generality of the mixed method allows the exploration of alternative deformation shape functions in future studies.

In keeping with the generality of the presentation the force-deformation relation is not specialized at the section level. This is deferred to the following chapter where the section force-deformation relation is derived from a fiber discretization of the cross section. A different approach which uses the theory of classical plasticity to derive a hysteretic model of the section force-deformation relation is presented by Spacone et al. (1992).

The proposed beam-column element is based on the assumption that deformations are small and that plane sections remain plane during the loading history. The formulation of the element is based on the mixed method: the description of the force distribution within the element by interpolation functions that satisfy equilibrium is the starting point of the formulation. Based on the concepts of the mixed method it is shown that the selection of flexibility dependent shape functions for the deformation field of the element results in considerable simplification of the final equations. With this particular selection of deformation shape functions the general mixed method reduces to the special case of the flexibility method. The mixed method formalism is, nonetheless, very useful in understanding the proposed procedure for the element state determination.

The proposed formulation offers several advantages over previous models:

- Equilibrium and compatibility are always satisfied along the element: equilibrium is satisfied by the selection of force interpolation functions and compatibility is satisfied

by integrating the section deformations to obtain the corresponding element deformations and end displacements. An iterative solution is then used to satisfy the nonlinear section force-deformation relation within the specified tolerance.

- The softening response of reinforced concrete members, which are either poorly reinforced or are subjected to high axial forces, can be described without computational difficulties.

In the first part of the chapter, after the definition of generalized element forces and corresponding element deformations, the mixed method formulation of the element is presented. The second part focuses on the element state determination process and the step-by-step calculation of the element resisting forces that correspond to given element deformations. These derivations are made without reference to a specific section model. This is deferred to Chapter 3, where the nonlinear procedure is specialized to a fiber section model.

2.2 Definition of Generalized Forces and Deformations

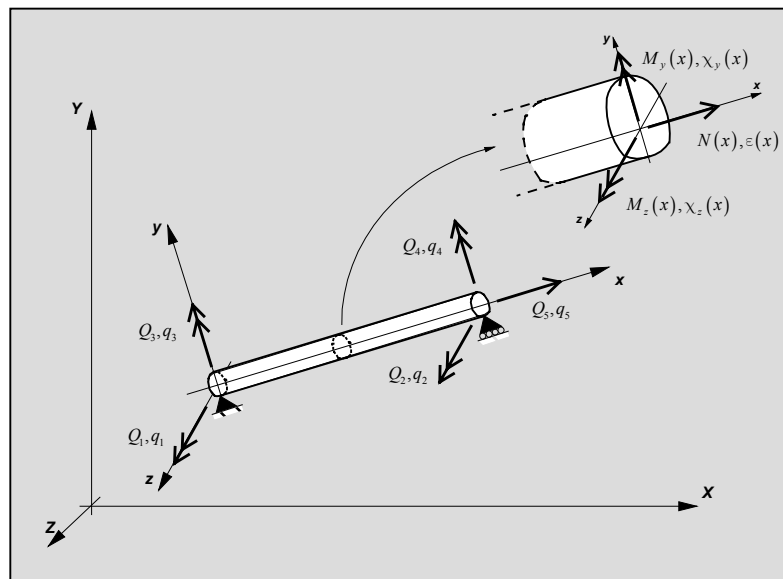


FIGURE 2.1 GENERALIZED FORCES AND DEFORMATIONS
AT THE ELEMENT AND SECTION LEVEL

The beam-column finite element is schematically shown in Fig. 2.1. The reference frame for the element is the local coordinate system x, y, z , while X, Y, Z denotes the global reference system. The longitudinal axis x is the union of geometric centroids of each section.

The following convention is followed for the notation of forces, displacements and deformations: forces are represented by uppercase letters and corresponding deformations or displacements are denoted by the same letter in lowercase. Normal letters denote scalar quantities, while boldface letters denote vectors and matrices.

Fig. 2.1 shows the element forces with the corresponding deformations. Rigid body modes are not included in Fig. 2.1. Since the present formulation is based on linear geometry, rigid body modes can be incorporated with a simple geometric transformation. The element has 5 degrees of freedom: one axial extension, q_5 , and two rotations relative to the chord at each end node, (q_1, q_3) and (q_2, q_4) , respectively. For the sake of clarity these are called element generalized deformations or simply element deformations in the following discussion. Q_1 through Q_5 indicate the corresponding generalized forces: one axial force, Q_5 , and two bending moments at each end node Q_1, Q_3 and Q_2, Q_4 , respectively. The end rotations and corresponding moments refer to two arbitrary, orthogonal axes y and z . The element generalized forces and deformations are grouped in the following vectors:

$$\text{Element force vector} \quad \mathbf{Q} = \left. \begin{array}{c} Q_1 \\ Q_2 \\ Q_3 \\ Q_4 \\ Q_5 \end{array} \right\} \quad (2.1)$$

$$\text{Element deformation vector} \quad \mathbf{q} = \left. \begin{array}{c} q_1 \\ q_2 \\ q_3 \\ q_4 \\ q_5 \end{array} \right\} \quad (2.2)$$

Fig. 2.1 also shows the generalized forces and deformations at a section of the element. Section deformations are represented by three strain resultants: the axial strain $\varepsilon(x)$ along the longitudinal axis and two curvatures $\chi_z(x)$ and $\chi_y(x)$ about two arbitrary, orthogonal axes z and y , respectively. The corresponding force resultants are the axial force $N(x)$ and two bending moments $M_z(x)$ and $M_y(x)$. The section generalized forces and deformations are grouped in the following vectors:

$$\text{Section force vector} \quad \mathbf{D}(x) = \begin{Bmatrix} M_z(x) \\ M_y(x) \\ N(x) \end{Bmatrix} = \begin{Bmatrix} D_1(x) \\ D_2(x) \\ D_3(x) \end{Bmatrix} \quad (2.3)$$

$$\text{Section deformation vector} \quad \mathbf{d}(x) = \begin{Bmatrix} \chi_z(x) \\ \chi_y(x) \\ \varepsilon(x) \end{Bmatrix} = \begin{Bmatrix} d_1(x) \\ d_2(x) \\ d_3(x) \end{Bmatrix} \quad (2.4)$$

The element formulation can be readily extended to include the torsional degrees of freedom, as long as these are uncoupled from the present degrees of freedom and are governed by linear elastic behavior. The focus of the present study is the element in Fig. 2.1, which describes the nonlinear behavior of frame members under arbitrary cyclic load histories of biaxial bending and axial load.

2.3 Beam-Column Element Formulation

In the following the mixed finite element method is used to formulate the beam-column element. At this stage no reference is made to specific interpolation functions. It is shown, however, that, if flexibility dependent deformation shape functions are selected, then the mixed method simplifies to the flexibility method. The nonlinear section force-deformation relation is also kept general. The force interpolation functions and the section force-deformation relations are specialized in the next chapter for a fiber discretization of the cross section of the beam-column element.

The derivation follows the two-field mixed method which uses the integral form of equilibrium and section force-deformation relations to derive the matrix relation between element generalized forces and corresponding deformations. In order to arrive at a linear relation, the section force-deformation relation is linearized about the present state. An iterative algorithm is, then, used to satisfy the nonlinear section force-deformation relation within the required tolerance.

In the two-field mixed method (Zienkiewicz and Taylor 1989) independent shape functions are used for approximating the force and deformation fields along the element. Denoting with Δ increments of the corresponding quantities, the two fields are written

$$\Delta \mathbf{d}^i(x) = \mathbf{a}(x) \cdot \Delta \mathbf{q}^i \quad (2.5)$$

$$\mathbf{D}^i(x) = \mathbf{b}(x) \cdot \mathbf{Q}^i \quad \text{and} \quad \Delta \mathbf{D}^i(x) = \mathbf{b}(x) \cdot \Delta \mathbf{Q}^i \quad (2.6)$$

where matrices $\mathbf{a}(x)$ and $\mathbf{b}(x)$ are the deformation and force interpolation matrices,

respectively. Superscript i indicates the i -th iteration of the Newton-Raphson (N-R) iteration loop, which is performed at the structure degrees of freedom until equilibrium between applied loads and internal resisting forces is satisfied (Zienkiewicz and Taylor 1989). The use of the superscript in the element formulation becomes necessary because of the special form of the deformation interpolation functions, which are flexibility dependent.

In the mixed method formulation the integral forms of equilibrium and section force-deformation relations are expressed first. These are then combined to obtain the relation between element force and deformation increments.

The weighted integral form of the linearized section force-deformation relation is

$$\int_0^L \delta \mathbf{D}^T(x) \cdot [\Delta \mathbf{d}^i(x) - \mathbf{f}^{i-1}(x) \cdot \Delta \mathbf{D}^i(x)] dx = 0 \quad (2.7)$$

The section force-deformation relation appears in the flexibility form

$$\Delta \mathbf{d}^i(x) = \mathbf{f}^{i-1}(x) \cdot \Delta \mathbf{D}^i(x)$$

so that the resulting element flexibility matrix is symmetric, as discussed by Zienkiewicz and Taylor (1989). The superscript $i-1$ indicates that at the i -th Newton-Raphson iteration the section flexibility at the end of the previous iteration is used. Substituting Eqs. (2.5) and (2.6) in Eq. (2.7) results in

$$\delta \mathbf{Q}^T \cdot \int_0^L \mathbf{b}^T(x) \cdot [\mathbf{a}(x) \cdot \Delta \mathbf{q}^i - \mathbf{f}^{i-1}(x) \cdot \mathbf{b}(x) \cdot \Delta \mathbf{Q}^i] dx = 0 \quad (2.8)$$

Since Eq. (2.8) must hold for any $\delta \mathbf{Q}^T$, it follows that

$$\left[\int_0^L \mathbf{b}^T(x) \cdot \mathbf{a}(x) \cdot dx \right] \cdot \Delta \mathbf{q}^i - \left[\int_0^L \mathbf{b}^T(x) \cdot \mathbf{f}^{i-1}(x) \cdot \mathbf{b}(x) \cdot dx \right] \cdot \Delta \mathbf{Q}^i = \mathbf{0} \quad (2.9)$$

The expressions in square brackets represent the following matrices:

$$\mathbf{F}^{i-1} = \left[\int_0^L \mathbf{b}^T(x) \cdot \mathbf{f}^{i-1}(x) \cdot \mathbf{b}(x) \cdot dx \right] \quad (2.10)$$

$$\mathbf{T} = \left[\int_0^L \mathbf{b}^T(x) \cdot \mathbf{a}(x) \cdot dx \right] \quad (2.11)$$

where \mathbf{F} is the element flexibility matrix and \mathbf{T} is a matrix that only depends on the interpolation function matrices. Using Eqs. (2.10) and (2.11) Eq. (2.9) can be written in the form

$$\mathbf{T} \cdot \Delta \mathbf{q}^i - \mathbf{F}^{i-1} \cdot \Delta \mathbf{Q}^i = \mathbf{0} \quad (2.12)$$

or equivalently

$$\mathbf{T} \cdot \Delta \mathbf{q}^i = \mathbf{F}^{i-1} \cdot \Delta \mathbf{Q}^i \quad (2.13)$$

This is the matrix expression of the integral form of the linearized section force-deformation relation.

In the next step the equilibrium of the beam element is satisfied. In the classical two-field mixed method the integral form of the equilibrium equation is derived from the virtual displacement principle

$$\int_0^L \delta \mathbf{d}^T(x) \cdot [\mathbf{D}^{i-1}(x) + \Delta \mathbf{D}^i(x)] \cdot dx = \delta \mathbf{q}^T \cdot \mathbf{P}^i \quad (2.14)$$

where \mathbf{P}^i is the vector of applied loads that are in equilibrium with the internal forces $\mathbf{D}^{i-1}(x) + \Delta \mathbf{D}^i(x)$. Eqs. (2.5) and (2.6) are substituted in Eq. (2.14) to yield

$$\delta \mathbf{q}^T \cdot \left[\int_0^L \mathbf{a}^T(x) \cdot [\mathbf{b}(x) \cdot \mathbf{Q}^{i-1} + \mathbf{b}(x) \cdot \Delta \mathbf{Q}^i] \cdot dx \right] = \delta \mathbf{q}^T \cdot \mathbf{P}^i \quad (2.15)$$

Observing that Eq. (2.15) must hold for arbitrary $\delta \mathbf{q}^T$, it follows that

$$\left[\int_0^L \mathbf{a}^T(x) \cdot \mathbf{b}(x) \cdot dx \right] \cdot \mathbf{Q}^{i-1} + \left[\int_0^L \mathbf{a}^T(x) \cdot \mathbf{b}(x) \cdot dx \right] \cdot \Delta \mathbf{Q}^i = \mathbf{P}^i \quad (2.16)$$

If the notation introduced in Eq. (2.11) is used, Eq. (2.16) can be written in matrix form

$$\mathbf{T}^T \cdot \mathbf{Q}^{i-1} + \mathbf{T}^T \cdot \Delta \mathbf{Q}^i = \mathbf{P}^i \quad (2.17)$$

This is the matrix expression of the integral form of the element equilibrium equations. The rearrangement and combination of Eqs. (2.12) and (2.17) results in

$$\begin{bmatrix} -\mathbf{F}^{i-1} & \mathbf{T} \\ \mathbf{T}^T & \mathbf{0} \end{bmatrix} \cdot \begin{Bmatrix} \Delta \mathbf{Q}^i \\ \Delta \mathbf{q}^i \end{Bmatrix} = \begin{Bmatrix} \mathbf{0} \\ \mathbf{P}^i - \mathbf{T}^T \cdot \mathbf{Q}^{i-1} \end{Bmatrix} \quad (2.18)$$

If the first equation in Eq. (2.18) is solved for $\Delta \mathbf{Q}^i$ and the result is substituted in the second equation, the following expression results

$$\mathbf{T}^T \cdot [\mathbf{F}^{i-1}]^{-1} \cdot \mathbf{T} \cdot \Delta \mathbf{q}^i = \mathbf{P}^i - \mathbf{T}^T \cdot \mathbf{Q}^{i-1} \quad (2.19)$$

So far, the specific selection of force and deformation interpolation functions $\mathbf{b}(x)$ and $\mathbf{a}(x)$, respectively, has not been addressed. In keeping with the generality of the formulation the selection of the force interpolation functions $\mathbf{b}(x)$ is deferred to the following chapter. Even

though in a mixed finite element method the deformation interpolation functions $\mathbf{a}(x)$ are completely independent of $\mathbf{b}(x)$, Eq. (2.11) reveals that a special choice of the deformation shape functions $\mathbf{a}(x)$ results in considerable simplification. With this simplification in mind $\mathbf{a}(x)$ are selected as flexibility dependent shape functions according to the following expression

$$\mathbf{a}(x) = \mathbf{f}^{i-1}(x) \cdot \mathbf{b}(x) \cdot [\mathbf{F}^{i-1}]^{-1} \quad (2.20)$$

These interpolation functions, thus, relate the section deformations with the corresponding element deformations according to

$$\Delta \mathbf{d}^i(x) = \mathbf{f}^{i-1}(x) \cdot \mathbf{b}(x) \cdot [\mathbf{F}^{i-1}]^{-1} \cdot \Delta \mathbf{q}^i \quad (2.21)$$

\mathbf{F}^{i-1} is the tangent element flexibility matrix at the end of the previous Newton-Raphson iteration. This special selection of the deformation shape functions reduces matrix \mathbf{T} in Eq. (2.11) to a 3x3 identity matrix \mathbf{I} . This can be readily proven by substituting Eq. (2.20) in Eq. (2.11):

$$\mathbf{T} = \left[\int_0^L \mathbf{b}^T(x) \cdot \mathbf{a}(x) \cdot dx \right] = \left[\int_0^L \mathbf{b}^T(x) \cdot \mathbf{f}^{i-1}(x) \cdot \mathbf{b}(x) \cdot dx \right] \cdot [\mathbf{F}^{i-1}]^{-1} = \mathbf{I} \quad (2.22)$$

With this choice of the deformation shape functions $\mathbf{a}(x)$ Eq. (2.19) becomes

$$[\mathbf{F}^{i-1}]^{-1} \cdot \Delta \mathbf{q}^i = \mathbf{P} - \mathbf{Q}^{i-1} \quad (2.23)$$

At the same time this choice of functions $\mathbf{a}(x)$ reduces the general mixed method to the flexibility method. The final matrix equation, Eq. (2.23), expresses the linearized relation between the applied unbalanced forces $\mathbf{P} - \mathbf{Q}^{i-1}$ and the corresponding deformation increments $\Delta \mathbf{q}^i$ at the element level. The element stiffness matrix is written in the form $[\mathbf{F}]^{-1}$ to indicate that it is obtained by inverting the element flexibility matrix. The linear equation system in Eq. (2.23) is different from that obtained by the classical stiffness method in two respects: (a) the element stiffness matrix is obtained by inverting the element flexibility matrix, as in the flexibility method, and, (b) the state determination phase of the nonlinear analysis is different, as will be described in detail in the following section.

Even though the classical flexibility method yields the same system of linearized equations in Eq. (2.23), the above derivation was based on the two-field mixed method for the following reasons: (a) the mixed method formulation yields directly the expression for the flexibility dependent deformation shape functions $\mathbf{a}(x)$ in Eq. (2.20), (b) it reveals the consistent implementation of the state determination process, and, (c) it is more general in

scope allowing alternative deformation shape functions to be explored in future studies.

Since $\mathbf{a}(x)$ is not independent of $\mathbf{b}(x)$ and changes during the iterative solution process, as is apparent from Eq. (2.20), the proposed method corresponds to the classical flexibility method. Moreover, this procedure reduces to the stiffness method for the case that the section constitutive relation is perfectly linear. In other words, the independence between the two fields is not intrinsic in the definition of the shape functions, but derives from the material nonlinearity of the section force-deformation relation.

2.4 State Determination

Most studies to date concerned with the analysis of reinforced concrete frame structures are based on finite element models that are derived with the stiffness method. Recent studies have focused on the advantages of flexibility based models (Zeris and Mahin 1988), but have failed to give a clear and consistent method of calculating the resisting forces from the given element deformations. This problem arises when the formulation of a finite element is based on the application of the virtual force principle. While the element is flexibility-dependent, the computer program into which it is inserted is based on the direct stiffness method of analysis. In this case the solution of the global equilibrium equations yields the displacements of the structural degrees of freedom. During the phase of state determination the resisting forces of all elements in the structure need to be determined. Since in a flexibility based element there are no deformation shape functions to relate the deformation field inside the element to the end displacements (or element deformations) this process is not straightforward and is not well developed in flexibility based models proposed to date. This fact has led to some confusion in the numerical implementation of previous models. The description of the consistent state determination process in this study benefits from the derivation of the governing equations by the two-field mixed method.

In a nonlinear structural analysis program each load step corresponds to the application of an external load increment to the structure. The corresponding structural displacement increments are determined and the element deformations are extracted for each element. The process of finding the resisting forces that correspond to the given element deformations is known as state determination. The state determination process is made up of two nested phases: a) *the element state determination*, when the element resisting forces are determined for the given end deformations, and b) *the structure state determination*, when the element resisting forces are assembled to the structure resisting force vector. The resisting forces are then compared with the total applied loads and the difference, if any, yields the unbalanced

forces which are then applied to the structure in an iterative solution process until external loads and internal resisting forces agree within a specified tolerance.

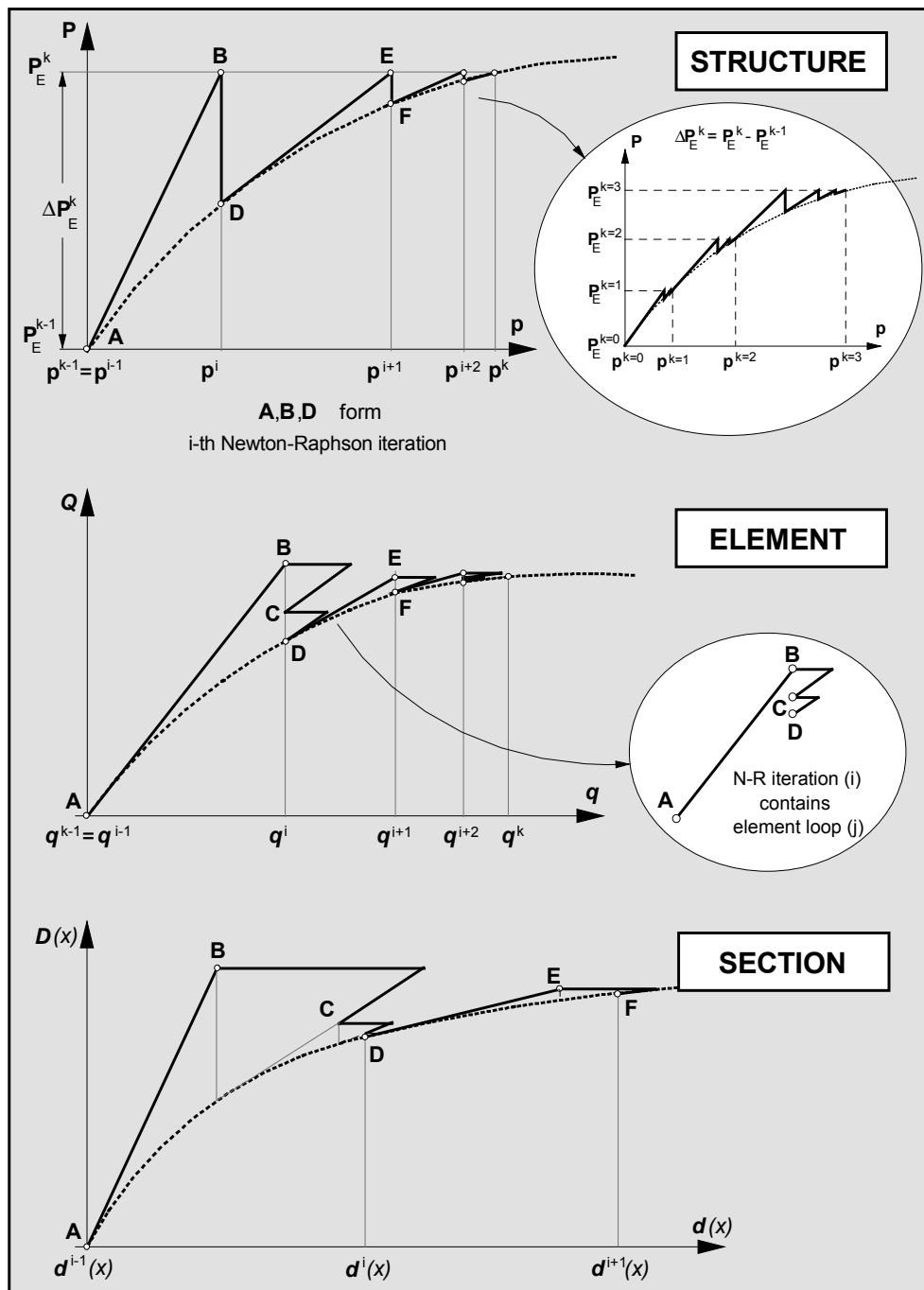


FIGURE 2.2 SCHEMATIC ILLUSTRATION OF STATE DETERMINATION AT THE STRUCTURE, ELEMENT AND SECTION LEVEL: k DENOTES THE LOAD STEP, i THE STRUCTURE NEWTON-RAPHSON ITERATION AND j THE ITERATION FOR THE ELEMENT STATE DETERMINATION

In the present study the nonlinear algorithm consists of three distinct nested processes, which are illustrated in Fig. 2.2. The two outermost processes denoted by indices k and i involve structural degrees of freedom and correspond to classical nonlinear analysis procedures. The innermost process denoted by index j is applied within each element and corresponds to the element state determination. Fig. 2.2. shows the evolution of the structure, element and section states during one load increment $\Delta \mathbf{P}_E^k$ that requires several Newton-Raphson iterations i .

In summary, the superscripts of the nested iterations are defined as follows:

- k denotes the applied load step. The external load is imposed in a sequence of load increments $\Delta \mathbf{P}_E^k$. At load step k the total external load is equal to $\mathbf{P}_E^k = \mathbf{P}_E^{k-1} + \Delta \mathbf{P}_E^k$ with $k=1, \dots, nstep$ and $\mathbf{P}_E^0 = 0$;
- i denotes the Newton-Raphson iteration scheme at the structure level, i.e. the structure state determination process. This iteration loop yields the structural displacements \mathbf{p}^k that correspond to applied loads \mathbf{P}_E^k ;
- j denotes the iteration scheme at the element level, i.e. the element state determination process. This iteration loop is necessary for the determination of the element resisting forces that correspond to element deformations \mathbf{q}^i during the i -th Newton-Raphson iteration.

The processes denoted by indices k and i are common in nonlinear analysis programs and will not be discussed further. The iteration process denoted by the index j , on the other hand, is special to the beam-column element formulation developed in this study and will be described in detail. It should be pointed out that any suitable nonlinear solution algorithm can be used for the iteration process denoted by index i . In this study the Newton-Raphson method is used. The selection of this method for iteration loop i does not affect the strategy for iteration loop j , which has as its goal the determination of the element resisting forces for the given element deformations.

In a finite element that is based on the stiffness method of analysis the section deformations are obtained directly from the element end deformations by deformation interpolation functions. The corresponding section resisting forces are determined subsequently from the section force-deformation relation. The weighted integral of the *section resisting forces* over the element length yields the *element resisting forces* and completes the process of element state determination.

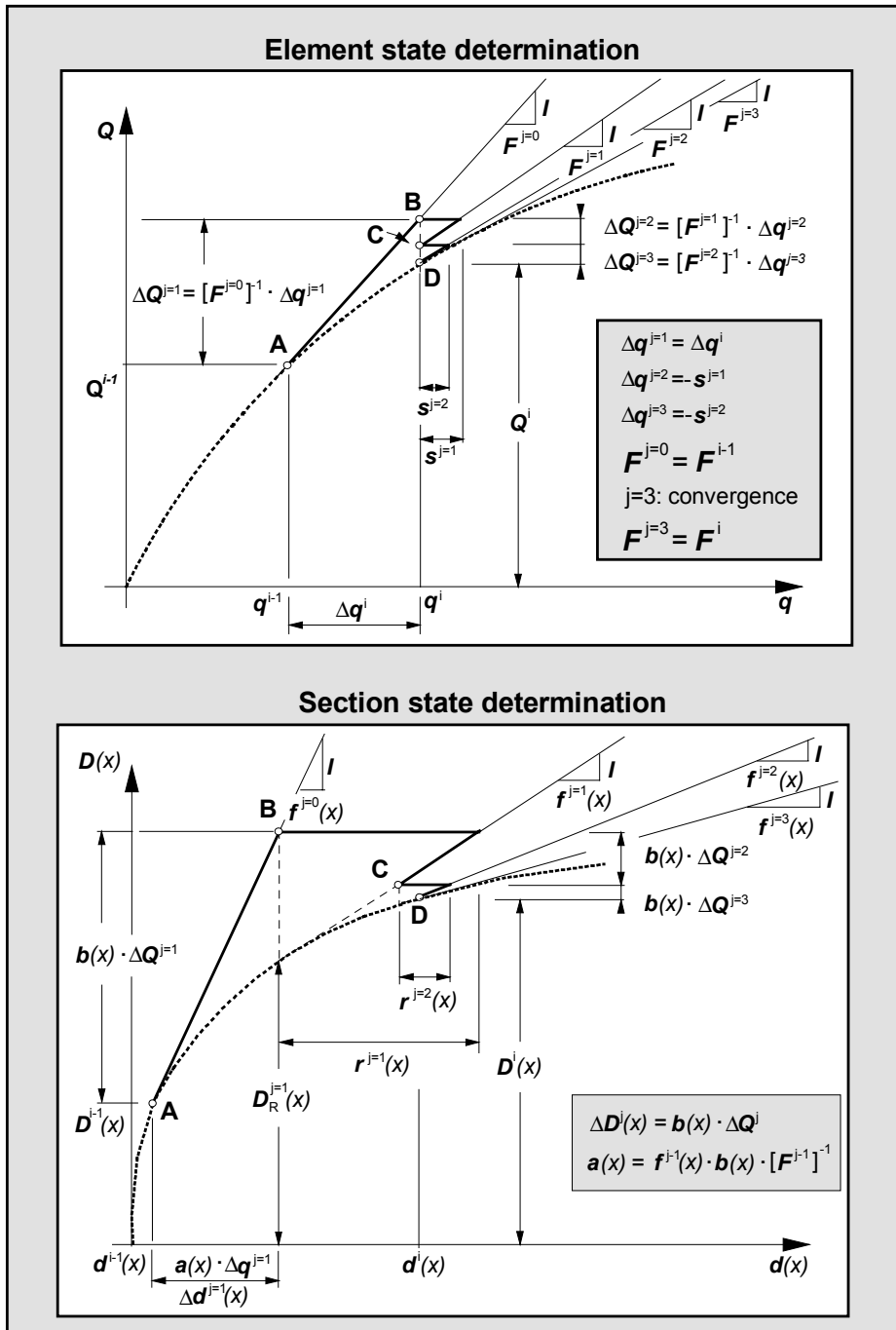


FIGURE 2.3 ELEMENT AND SECTION STATE DETERMINATION FOR FLEXIBILITY-BASED ELEMENT: COMPUTATION OF ELEMENT RESISTING FORCES Q^i CORRESPONDING TO ELEMENT DEFORMATIONS q^i

In a flexibility-based finite element the first step is the determination of the element forces from the current element deformations using the stiffness matrix at the end of the last iteration. The force interpolation functions yield the forces along the element. The first

problem is, then, the determination of the section deformations from the given section forces, since the nonlinear section force-deformation relation is commonly expressed as an explicit function of section deformations. The second problem arises from the fact that changes in the section stiffness produce a new element stiffness matrix which, in turn, changes the element forces for the given deformations.

These problems are solved in the present study by a special nonlinear solution method. In this method residual element deformations are determined at each iteration. Deformation compatibility at the structural level requires that these residual deformations be corrected. This is accomplished at the element level by applying corrective element forces based on the current stiffness matrix. The corresponding section forces are determined from the force interpolation functions so that equilibrium is always satisfied along the element. These section forces cannot change during the section state determination in order to maintain equilibrium along the element. Consequently, the linear approximation of the section force-deformation relation about the present state results in residual section deformations. These are then integrated along the element to obtain new residual element deformations and the whole process is repeated until convergence occurs. It is important to stress that *compatibility of element deformations and equilibrium along the element are always satisfied in this process.*

The nonlinear solution procedure for the element state determination is schematically illustrated in Fig. 2.3 for one Newton-Raphson iteration i . In Fig. 2.3 convergence in loop j is reached in three iterations. The consistent notation between Figs. 2.2 and 2.3 highlights the relation between the corresponding states of the structure, the element and the section, which are denoted by uppercase Roman letters.

At the i -th Newton-Raphson iteration it is necessary to determine the element resisting forces for the current element deformations

$$\mathbf{q}^i = \mathbf{q}^{i-1} + \Delta \mathbf{q}^i$$

To this end an iterative process denoted by index j is introduced inside the i -th Newton-Raphson iteration. The first iteration corresponds to $j=1$. The initial state of the element, represented by point **A** and $j=0$ in Fig. 2.3, corresponds to the state at the end of the last iteration of loop j for the $(i-1)$ Newton-Raphson iteration. With the initial element tangent stiffness matrix

$$[\mathbf{F}^{j=0}]^{-1} = [\mathbf{F}^{i-1}]^{-1}$$

and the given element deformation increments

$$\Delta \mathbf{q}^{j+1} = \Delta \mathbf{q}^j$$

the corresponding element force increments are:

$$\Delta \mathbf{Q}^{j+1} = [\mathbf{F}^{j+1}]^{-1} \cdot \Delta \mathbf{q}^{j+1}$$

The section force increments can now be determined from the force interpolation functions:

$$\Delta \mathbf{D}^{j+1}(x) = \mathbf{b}(x) \cdot \Delta \mathbf{Q}^{j+1}$$

With the section flexibility matrix at the end of the previous Newton-Raphson iteration

$$\mathbf{f}^{j+1}(x) = \mathbf{f}^j(x)$$

the linearization of the section force-deformation relation yields the section deformation increments $\Delta \mathbf{d}^{j+1}(x)$:

$$\Delta \mathbf{d}^{j+1}(x) = \mathbf{f}^{j+1}(x) \cdot \Delta \mathbf{D}^{j+1}(x)$$

The section deformations are updated to the state that corresponds to point **B** in Fig. 2.3:

$$\mathbf{d}^{j+1}(x) = \mathbf{d}^j(x) + \Delta \mathbf{d}^{j+1}(x)$$

According to the section force-deformation relation, which is here assumed to be explicitly known for simplicity's sake, section deformations $\mathbf{d}^{j+1}(x)$ correspond to resisting forces $\mathbf{D}_R^{j+1}(x)$ and a new tangent flexibility matrix $\mathbf{f}^{j+1}(x)$ (Fig. 2.3). In a finite element based on the stiffness method the section resisting forces $\mathbf{D}_R^{j+1}(x)$ would be directly transformed to element resisting forces \mathbf{Q}^{j+1} thus violating the equilibrium along the element in a strict sense. Since this is undesirable, a new nonlinear solution method is proposed in this study. In this approach the section unbalanced forces are first determined

$$\mathbf{D}_U^{j+1}(x) = \mathbf{D}^{j+1}(x) - \mathbf{D}_R^{j+1}(x)$$

and are then transformed to residual section deformations $\mathbf{r}^{j+1}(x)$

$$\mathbf{r}^{j+1}(x) = \mathbf{f}^{j+1}(x) \cdot \mathbf{D}_U^{j+1}(x) \quad (2.24)$$

The residual section deformations are thus the linear approximation to the deformation error made in the linearization of the section force-deformation relation (Fig. 2.3). While any suitable flexibility matrix can be used in calculating the residual deformations, the tangent flexibility matrix used in this study offers the fastest convergence rate.

The residual section deformations are integrated along the element based on the virtual force principle to obtain the residual element deformations:

$$\mathbf{s}^{j=1} = \int_0^L \mathbf{b}^T(x) \cdot \mathbf{r}^{j=1}(x) \cdot dx \quad (2.25)$$

At this point the first iteration $j=1$ of the corresponding iteration loop is complete. The final element and section states for $j=1$ correspond to point **B** in Fig. 2.3. The residual section deformations $\mathbf{r}^{j=1}(x)$ and the residual element deformations $\mathbf{s}^{j=1}$ are determined in the first iteration, but the corresponding deformation vectors are not updated. Instead, they are the starting point of the remaining steps within iteration loop j . The presence of residual element deformations $\mathbf{s}^{j=1}$ violates compatibility, since elements sharing a common node would now have different end displacements. In order to restore the inter-element compatibility corrective forces equal to $-\mathbf{F}^{j=1}]^{-1} \cdot \mathbf{s}^{j=1}$ must be applied at the ends of the element, where $\mathbf{F}^{j=1}$ is the updated element tangent flexibility matrix determined by integration of the section flexibility matrices according to Eq. (2.10). A corresponding force increment $-\mathbf{b}(x) \cdot \mathbf{F}^{j=1}]^{-1} \cdot \mathbf{s}^{j=1}$ is applied at all control sections inducing a deformation increment $-\mathbf{f}^{j=1}(x) \cdot \mathbf{b}(x) \cdot \mathbf{F}^{j=1}]^{-1} \cdot \mathbf{s}^{j=1}$. Thus, in the second iteration $j=2$ the state of the element and of the sections within the element change as follows: the element forces are updated to the value

$$\mathbf{Q}^{j=2} = \mathbf{Q}^{j=1} + \Delta \mathbf{Q}^{j=2}$$

where

$$\Delta \mathbf{Q}^{j=2} = -\mathbf{F}^{j=1}]^{-1} \cdot \mathbf{s}^{j=1}$$

and the section forces and deformations are updated to the values

$$\mathbf{D}^{j=2}(x) = \mathbf{D}^{j=1}(x) + \Delta \mathbf{D}^{j=2}(x)$$

and

$$\mathbf{d}^{j=2}(x) = \mathbf{d}^{j=1}(x) + \Delta \mathbf{d}^{j=2}(x)$$

where

$$\Delta \mathbf{D}^{j=2}(x) = -\mathbf{b}(x) \cdot \mathbf{F}^{j=1}]^{-1} \cdot \mathbf{s}^{j=1}$$

$$\Delta \mathbf{d}^{j=2}(x) = \mathbf{r}^{j=1}(x) - \mathbf{f}^{j=1}(x) \cdot \mathbf{b}(x) \cdot \mathbf{F}^{j=1}]^{-1} \cdot \mathbf{s}^{j=1}$$

The state of the element and the sections within the element at the end of the second iteration $j=2$ corresponds to point **C** in Fig. 2.3. The new tangent flexibility matrices $\mathbf{f}^{j=2}(x)$ and the new residual section deformations

$$\mathbf{r}^{j=2}(x) = \mathbf{f}^{j=2}(x) \cdot \mathbf{D}_U^{j=2}(x)$$

are computed for all sections. The residual section deformations are then integrated to obtain the residual element deformations $\mathbf{s}^{j=2}$ and the new element tangent flexibility matrix $\mathbf{F}^{j=2}$ is determined by integration of the section flexibility matrices $\mathbf{f}^{j=2}(x)$ according to Eq. (2.10). This completes the second iteration within loop j .

The third and subsequent iterations follow exactly the same scheme. Convergence is achieved when the selected convergence criterion is satisfied, as discussed in more detail in Chapter 4. With the conclusion of iteration loop j the element resisting forces for the given deformations \mathbf{q}^i are established, as represented by point \mathbf{D} in Figs. 2.2 and 2.3. The Newton-Raphson iteration process can now proceed with step $i+1$.

It is important to point out that during iteration loop j the element deformations \mathbf{q}^i do not change except in the first iteration $j=1$, when increments $\Delta\mathbf{q}^{j=1} = \Delta\mathbf{q}^i$ are added to the element deformations \mathbf{q}^{i-1} at the end of the previous Newton-Raphson iteration. These deformation increments result from the application of corrective loads $\Delta\mathbf{P}_E^i$ at the structural degrees of freedom during the Newton-Raphson iteration process. For $j>1$ only the element forces change until the nonlinear solution procedure converges to the element resisting forces \mathbf{Q}^i which correspond to element deformations \mathbf{q}^i . This is illustrated at the top of Fig. 2.3 where points \mathbf{B} , \mathbf{C} and \mathbf{D} , which represent the state of the element at the end of subsequent iterations in loop j , lie on the same vertical line, while the corresponding points at the control sections of the element do not, as shown in the bottom of Fig. 2.3. This feature of the proposed nonlinear solution procedure ensures displacement compatibility at the element ends.

The proposed nonlinear analysis method offers several advantages. Equilibrium along the element is always strictly satisfied, since section forces are derived from element forces by the force interpolation functions according to Eq. (2.6). Compatibility is also satisfied, not only at the element ends, but also along the element. In fact, in the expression for the section deformation corrections

$$\Delta\mathbf{d}^j(x) = \mathbf{r}^{j-1}(x) - \mathbf{f}^{j-1}(x) \cdot \mathbf{b}(x) \cdot [\mathbf{F}^{j-1}]^{-1} \cdot \mathbf{s}^{j-1}$$

the second term satisfies Eqs. (2.20) and (2.21), which express the relation between section and element deformations by means of shape functions $\mathbf{a}(x)$. The residual section deformations $\mathbf{r}^{j-1}(x)$, however, do not strictly satisfy this compatibility condition. It is possible to satisfy this requirement by integrating the residual deformations $\mathbf{r}^{j-1}(x)$ to obtain \mathbf{s}^{j-1} and then using the deformation shape functions $\mathbf{a}(x)$ to calculate the section

deformation increments as $\mathbf{a}(x) \cdot \mathbf{s}^{j-1}$. Since this is, however, rather inefficient from a computational standpoint, the small compatibility error in the calculation of residual section deformations $\mathbf{r}^{j-1}(x)$ is neglected in this study.

While equilibrium and compatibility are satisfied along the element during each iteration of loop j , the section force-deformation relation and, consequently, the element force-deformation relation is only satisfied within a specified tolerance when convergence is achieved at point **D** in Fig. 2.3. In other words, during subsequent iterations the element forces approach the value that corresponds to the imposed element deformations, while maintaining equilibrium and compatibility along the element at all times. This approximation of the force-deformation relation in the proposed nonlinear analysis method is preferable to the approximation of either the equilibrium or the compatibility conditions of the element, particularly when considering the uncertainty in the definition of constitutive relations for reinforced concrete structures.

2.5 Summary of Nonlinear Solution Algorithm

After the description of the element state determination process in the previous section a step-by-step summary of the computations is presented below. The summary focuses on a single iteration i at the structural degrees of freedom, because the innovative aspect of the present study is the process of element state determination. The rest of the nonlinear solution algorithm follows well established methods, such as the Newton-Raphson method selected in this study. Alternative solution strategies can be implemented without additional effort, since these are independent of the element state determination. The relation of the Newton-Raphson iteration to the nonlinear solution of the entire structure is illustrated at the top of Fig. 2.2, which also shows the relation between the overall solution strategy and the element state determination process with corresponding states denoted by uppercase Roman letters. Fig. 2.3 shows in detail the evolution of the state determination process for an element and corresponds to steps **(4)** through **(13)** in the following summary. The flow chart of computations for the entire solution algorithm is shown in Fig. 2.4, while the flow chart of computations for the element state determination is shown in Fig. 2.5.

The i -th Newton-Raphson iteration is organized as follows:

- (1)** *Solve the global system of equations and update the structural displacements.*

At the i -th Newton-Raphson iteration the structure stiffness matrix \mathbf{K}_s^{i-1} at the end of the previous iteration $i-1$ is used to compute the displacement increments $\Delta \mathbf{p}^i$ for the

given load increments $\Delta \mathbf{P}_E^i$ which represent the unbalanced forces from the previous iteration.

$$\mathbf{K}_s^{i-1} \cdot \Delta \mathbf{p}^i = \Delta \mathbf{P}_E^i \quad (2.26)$$

$$\mathbf{p}^i = \mathbf{p}^{i-1} + \Delta \mathbf{p}^i \quad (2.27)$$

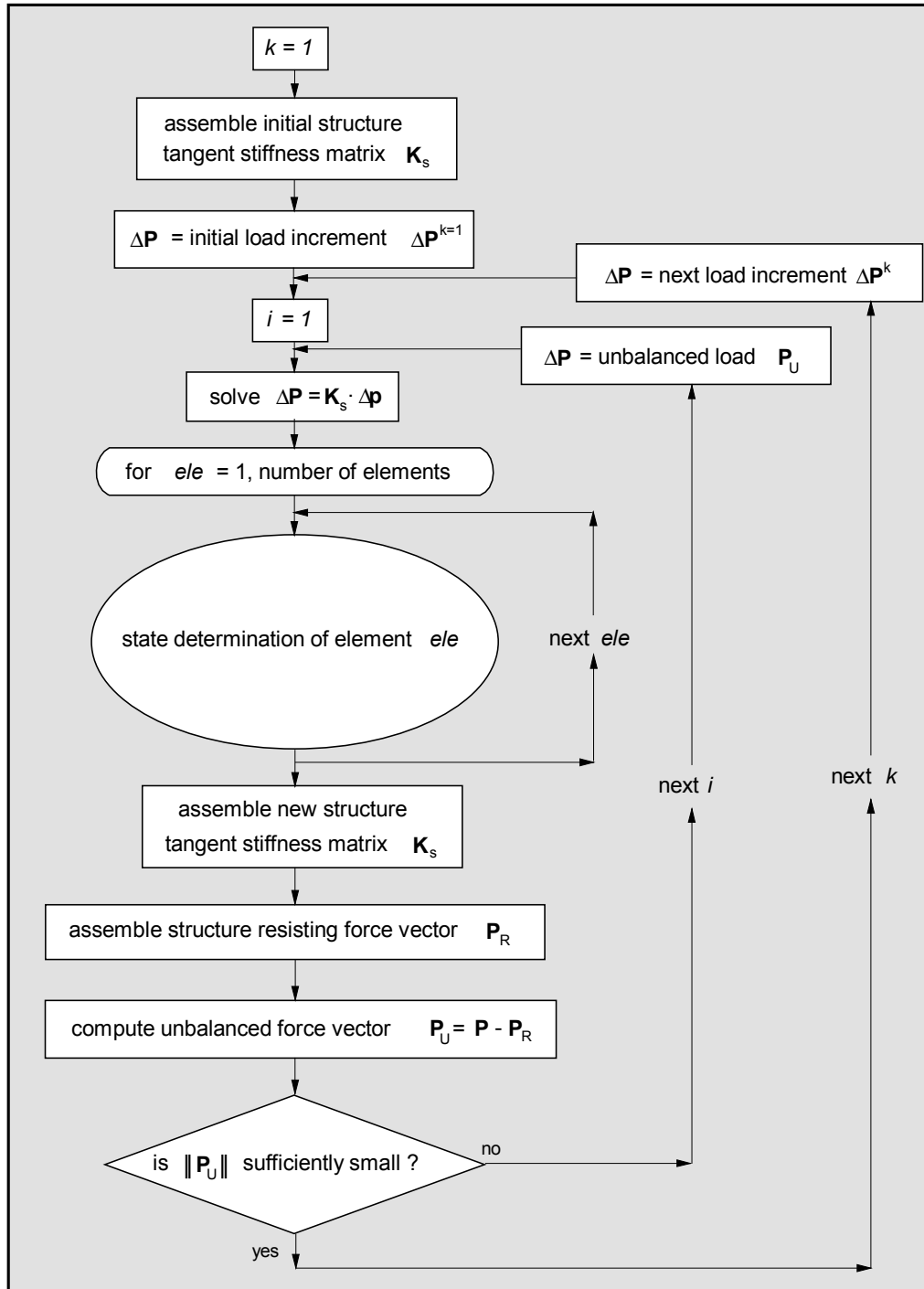


FIGURE 2.4 FLOW CHART OF STRUCTURE STATE DETERMINATION

- (2) *Calculate the element deformation increments and update the element deformations.*

Using matrix \mathbf{L}_{ele} , which relates structural displacements with element deformations, the element deformation increments $\Delta \mathbf{q}^i$ are determined:

$$\Delta \mathbf{q}^i = \mathbf{L}_{ele} \cdot \Delta \mathbf{p}^i \quad (2.28)$$

$$\mathbf{q}^i = \mathbf{q}^{i-1} + \Delta \mathbf{q}^i \quad (2.29)$$

Note that matrix \mathbf{L}_{ele} is the combination of two transformations: in the first transformation the element displacements in the global reference system \mathbf{p} are transformed to the displacements $\bar{\mathbf{q}}$ in the element local reference system. In the second transformation the element displacements $\bar{\mathbf{q}}$ are transformed to element deformations \mathbf{q} by elimination of the rigid-body modes.

As discussed in Section 2.4, the new element deformations \mathbf{q}^i do not change until the following $(i+1)$ Newton-Raphson iteration. The remaining operations of the nonlinear solution algorithm make up the element state determination process which establishes the element resisting forces for the given element deformations \mathbf{q}^i .

- (3) *Start the element state determination. Loop over all elements in the structure.*

The state determination of each element is performed in loop j . The index of the first iteration is $j=1$.

- (4) *Determine the element force increments.*

The element force increments $\Delta \mathbf{Q}^j$ are determined with the element stiffness matrix \mathbf{K}^{j-1} at the end of the previous iteration in loop j

$$\Delta \mathbf{Q}^j = \mathbf{K}^{j-1} \cdot \Delta \mathbf{q}^j \quad (2.30)$$

When $j=1$, $\mathbf{K}^0 = \mathbf{K}^{i-1}$ and $\Delta \mathbf{q}^1 = \Delta \mathbf{q}^i$ where $i-1$ corresponds to the state of the element at the end of the last Newton-Raphson iteration. When $j>1$ $\Delta \mathbf{q}^j$ is equal to the residual element deformations of the previous iteration, as determined in Step (13).

- (5) *Update the element forces.*

$$\mathbf{Q}^j = \mathbf{Q}^{j-1} + \Delta \mathbf{Q}^j \quad (2.31)$$

When $j=1$, $\mathbf{Q}^0 = \mathbf{Q}^{i-1}$ where $i-1$ corresponds to the state at the end of the last Newton-Raphson iteration.

- (6) *Determine the section force increments. Steps (6) through (11) are performed for all control sections (integration points) of the element.*

The section force increments $\Delta \mathbf{D}^j(x)$ are determined from the force interpolation functions $\mathbf{b}(x)$. Subsequently, the section forces $\mathbf{D}(x)$ are updated.

$$\Delta \mathbf{D}^j(x) = \mathbf{b}(x) \cdot \Delta \mathbf{Q}^j \quad (2.32)$$

$$\mathbf{D}^j(x) = \mathbf{D}^{j-1}(x) + \Delta \mathbf{D}^j(x) \quad (2.33)$$

(7) *Determine the section deformation increments.*

The section deformation increments $\Delta \mathbf{d}^j(x)$ are determined by adding the residual section deformations from the previous iteration $\mathbf{r}^{j-1}(x)$ to the deformation increments caused by the section force increments $\Delta \mathbf{D}^j(x)$. The latter are determined with the section flexibility matrix $\mathbf{f}^{j-1}(x)$ at the end of the previous iteration in loop j .

$$\Delta \mathbf{d}^j(x) = \mathbf{r}^{j-1}(x) + \mathbf{f}^{j-1}(x) \cdot \Delta \mathbf{D}^j(x) \quad (2.34)$$

$$\mathbf{d}^j(x) = \mathbf{d}^{j-1}(x) + \Delta \mathbf{d}^j(x) \quad (2.35)$$

When $j=1$, $\mathbf{r}^0(x) = \mathbf{0}$.

(8) *Determine the tangent stiffness and flexibility matrices of the section.*

Assuming for simplicity that the section force-deformation relation is known explicitly, the tangent stiffness matrix $\mathbf{k}^j(x)$ is updated for the new section deformations $\mathbf{d}^j(x)$. This stiffness matrix $\mathbf{k}^j(x)$ is then inverted to obtain the new tangent flexibility matrix $\mathbf{f}^j(x)$ of the section.

$$\mathbf{f}^j(x) = [\mathbf{k}^j(x)]^{-1} \quad (2.36)$$

(9) *Determine the section resisting forces.*

The resisting forces $\mathbf{D}_R^j(x)$ are determined for the current deformations $\mathbf{d}^j(x)$ from the section force-deformation relation.

(10) *Determine the unbalanced forces at the section.*

The section unbalanced forces $\mathbf{D}_U^j(x)$ are the difference between the applied forces $\mathbf{D}^j(x)$ and the resisting forces $\mathbf{D}_R^j(x)$.

$$\mathbf{D}_U^j(x) = \mathbf{D}^j(x) - \mathbf{D}_R^j(x) \quad (2.37)$$

(11) *Determine the residual section deformations.*

The section unbalanced forces and the new section flexibility yield the residual section deformations $\mathbf{r}^j(x)$

$$\mathbf{r}^j(x) = \mathbf{f}^j(x) \cdot \mathbf{D}_U^j(x) \quad (2.38)$$

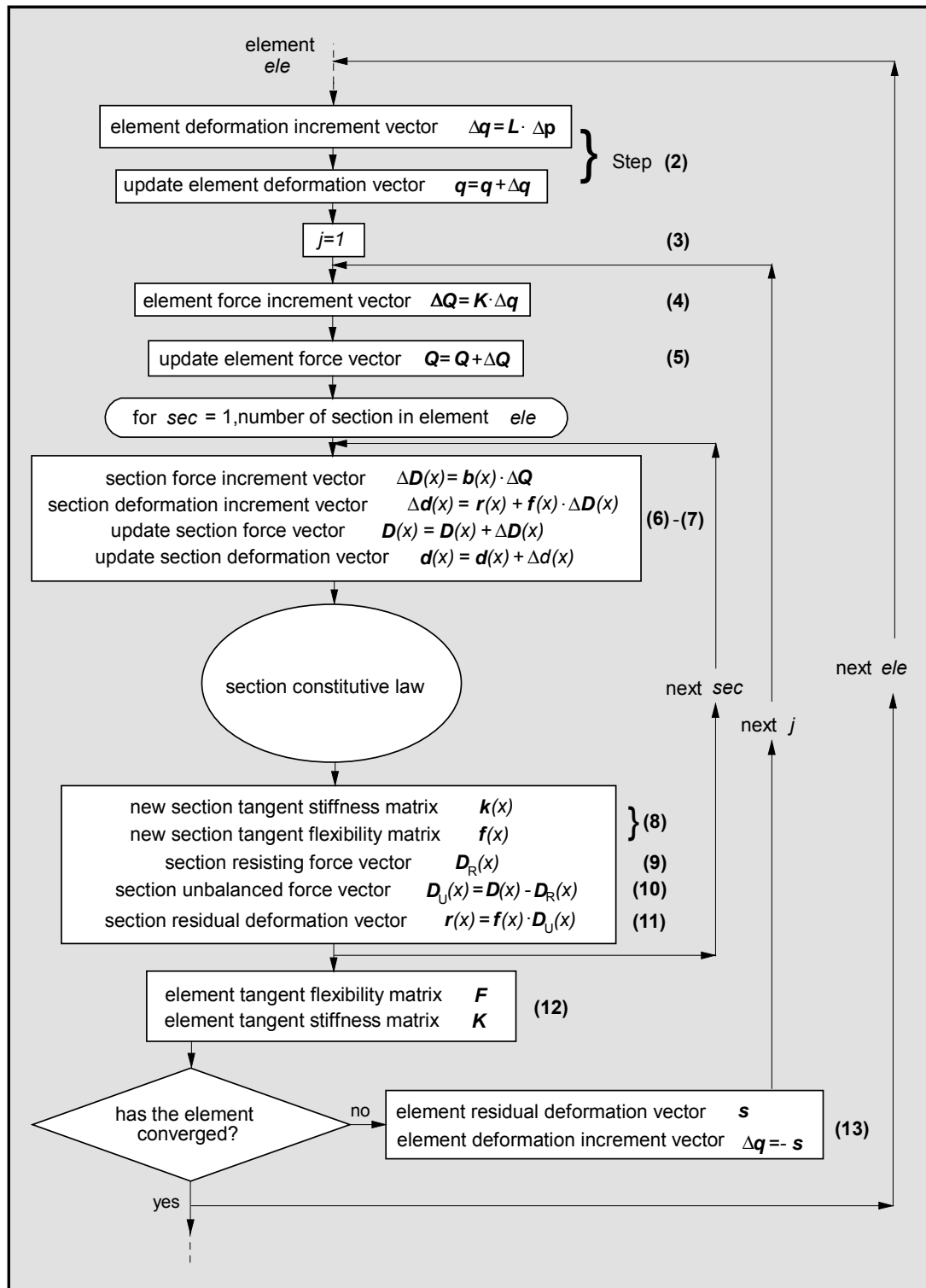


FIGURE 2.5 FLOW CHART OF ELEMENT STATE DETERMINATION: THE SECTION CONSTITUTIVE RELATION IS ASSUMED TO BE EXPLICITLY KNOWN

(12) *Determine the element flexibility and stiffness matrices.*

The element flexibility matrix \mathbf{F}^j is formed by integration of the section flexibility matrices $\mathbf{f}^j(x)$. This matrix is then inverted to obtain the element tangent stiffness matrix \mathbf{K}^j .

$$\mathbf{F}^j = \left[\int_0^L \mathbf{b}^T(x) \cdot \mathbf{f}^j(x) \cdot \mathbf{b}(x) \cdot dx \right] \quad (2.39)$$

$$\mathbf{K}^j = [\mathbf{F}^j]^{-1} \quad (2.40)$$

(13) *Check for element convergence.*

- a) If the unbalanced forces at all element sections are sufficiently small, the element is considered to have converged. After setting $\mathbf{Q}^i = \mathbf{Q}^j$ and $\mathbf{K}^i = \mathbf{K}^j$ the process continues with step **(14)**.
- b) If some sections have not converged, the residual element deformations \mathbf{s}^j are determined by integration of the residual section deformations $\mathbf{r}^j(x)$.

$$\mathbf{s}^j = \left[\int_0^L \mathbf{b}^T(x) \cdot \mathbf{r}^j(x) \cdot dx \right] \quad (2.41)$$

At this point j is incremented to $j+1$ and a new iteration begins in loop j . In this case $\Delta \mathbf{q}^j$ in Eq. (2.30) is replaced with $\Delta \mathbf{q}^{j+1}$ which is set equal to $-\mathbf{s}^j$

$$\Delta \mathbf{q}^{j+1} = -\mathbf{s}^j \quad (2.42)$$

and steps **(4)** through **(13)** are repeated until convergence is achieved at all sections of the element.

(14) *Determine the resisting forces and the new stiffness matrix of the entire structure.*

When all elements have converged, the i -th step of the Newton-Raphson iteration is complete. The element force vectors are assembled to form the updated structure resisting forces

$$\mathbf{P}_R^i = \sum_{ele=1}^n \mathbf{L}_{ele}^T \cdot (\mathbf{Q}^i)_{ele} \quad (2.43)$$

where n is the total number of beam-column elements in the structure and the subscript ele is added as a summation index. The new structure stiffness matrix is formed by assembling the current element stiffness matrices

$$\mathbf{K}_s^i = \sum_{ele=1}^n \mathbf{L}_{ele}^T \cdot (\mathbf{K}^i)_{ele} \cdot \mathbf{L}_{ele} \quad (2.44)$$

At this point the structure resisting forces \mathbf{P}_R^i are compared with the total applied loads. If the difference $\Delta \mathbf{P}_U^i$, which is the structure unbalanced force vector, is not within the specified tolerance, i is incremented to $i+1$ and the next Newton-Raphson iteration begins. Steps **(1)** through **(14)** are repeated after replacing $\Delta \mathbf{P}_E^i$ with $\Delta \mathbf{P}_E^{i+1} = \Delta \mathbf{P}_U^i$ until convergence takes place at the structure degrees of freedom.

A graphical overview of the entire nonlinear analysis procedure is presented in Figs. 2.4 and 2.5. Fig. 2.4 provides an overview of the entire process with the nesting of the individual iteration loops and does not differ from conventional nonlinear analysis schemes. The new features of the algorithm are introduced in the element state determination phase, which is singled out for presentation in Fig. 2.5. Since all integrations along the element in Eqs. (2.39) and (2.41) need to be performed numerically, an additional iteration loop over all control sections of the element is introduced in this diagram. The actual numerical implementation is deferred to Chapter 4.

In the interest of clarity the above presentation of the nonlinear analysis procedure refers to an explicit section deformation relation. The following chapter addresses the implementation of this algorithm in the context of a fiber beam-column element. In the latter case the section force-deformation relation is not explicitly known, but is derived from the stress-strain relation of the fibers that the section is divided into.

CHAPTER 3

REINFORCED CONCRETE FIBER BEAM-COLUMN ELEMENT

3.1 General

In the previous chapter a beam-column element was formulated based on the flexibility method of analysis. For clarity of presentation the section force-deformation relation was assumed explicitly known, but no further details about the constitutive model were discussed in order to demonstrate the general character of the proposed method. In this chapter the proposed method is specialized to a beam-column element composed of longitudinal fibers for which the section force-deformation relation is established by integration of the uniaxial stress-strain behavior of the fibers.

The element is based on the assumption that plane sections remain plane and normal to the reference axis during the deformation history. This leads to a simple geometric relation between section generalized deformations and fiber strains. The nonlinear character of the element derives entirely from the nonlinear fiber stress-strain relations (material nonlinearity). The element formulation is based on the formal framework of the mixed method, as described in the previous chapter. The deformation interpolation matrix has the same flexibility dependent form as discussed in Chapter 2, while the force interpolation matrix is selected to represent linear bending moment and constant axial force distribution along the element. This form is exact when no element loads are present. The latter case is dealt with in Chapter 4, where a procedure is proposed for the consistent inclusion of element loads in the context of the flexibility method.

The fiber element state determination is identical to the procedure presented at length in Chapter 2. In the fiber beam-column element, however, the section force-deformation relation is only implicitly known as a function of the stress-strain relation and the deformation history of the fibers. Correspondingly, a few steps need to be added to the procedure in Section 2.5 for the section state determination, which determines the section force and new tangent stiffness matrix for the given section deformations.

Following a definition of new variables that the discretization of the cross section into fibers introduces, the material models for describing the hysteretic behavior of the fibers are

discussed. Subsequently, the element state determination for the fiber section model is presented in detail and the chapter concludes with a brief summary of the entire nonlinear analysis algorithm, with highlights of the new steps that are introduced by the fiber discretization of the cross section.

3.2 Model Assumptions

The formulation of the fiber beam-column element is based on the assumption of linear geometry. Plane sections remain plane and normal to the longitudinal axis during the element deformation history. While this hypothesis is acceptable for small deformations of elements composed of homogeneous materials, it does not properly account for phenomena which are characteristic of reinforced concrete elements, such as cracking and bond-slip. The effect of cracking and tension stiffening can be included in the model by an appropriate modification of the stress-strain relation of reinforcing steel or concrete according to the smeared crack concept of finite element analysis. This effect is only significant in the pre-yield phase of response and can be neglected in studies which focus on the hysteretic behavior under large inelastic deformation reversals. By contrast, the contribution of bond-slip to the element deformations increases with the magnitude and number of loading cycles. The inclusion of bond-slip deformations in an element that is based on section behavior is a challenging problem, which is beyond the scope of the present study. Shear effects are also neglected, which is a reasonable approximation for medium to large span to depth ratios of the member.

From the assumption that plane sections remain plane and normal to the longitudinal axis, all fiber strains and stresses act parallel to this axis. Since the reference axis is fixed, this implies that the geometric centroids of the sections form a straight line that coincides with the reference axis. If an element does not comply with this hypothesis, it should be divided into subelements that connect the centroids of the selected sections.

The accuracy of the element response and, consequently, that of the entire structure are affected by the mesh selection, that is the number of sections used in the discretization of a given member, and by the number of fibers in a section. A large number of fibers certainly gives better results, but computational cost increases with it, since the history variables necessary to track the hysteretic behavior of each fiber must be stored at each iteration. The selection of the optimum number and location of fibers and the optimum number of integration points along the element axis is beyond the scope of this study.

3.3 Generalized Forces and Deformations

The fiber beam-column element is shown in Fig. 3.1 in the local reference system x, y, z . It is divided into a discrete number of cross sections. These are located at the control points of the numerical integration scheme used in the element formulation. In this study the Gauss-Lobato integration scheme is used, since it allows for two integration points to coincide with the end sections of the element, where significant inelastic deformations typically take place. More details on the integration scheme are provided in Chapter 4. Each section is subdivided into $n(x)$ fibers. n is a function of x to account for the fact that the longitudinal reinforcement can vary along the element. For the sake of clarity the dependence of n on x is not explicitly carried through the equations in the remainder of this chapter.

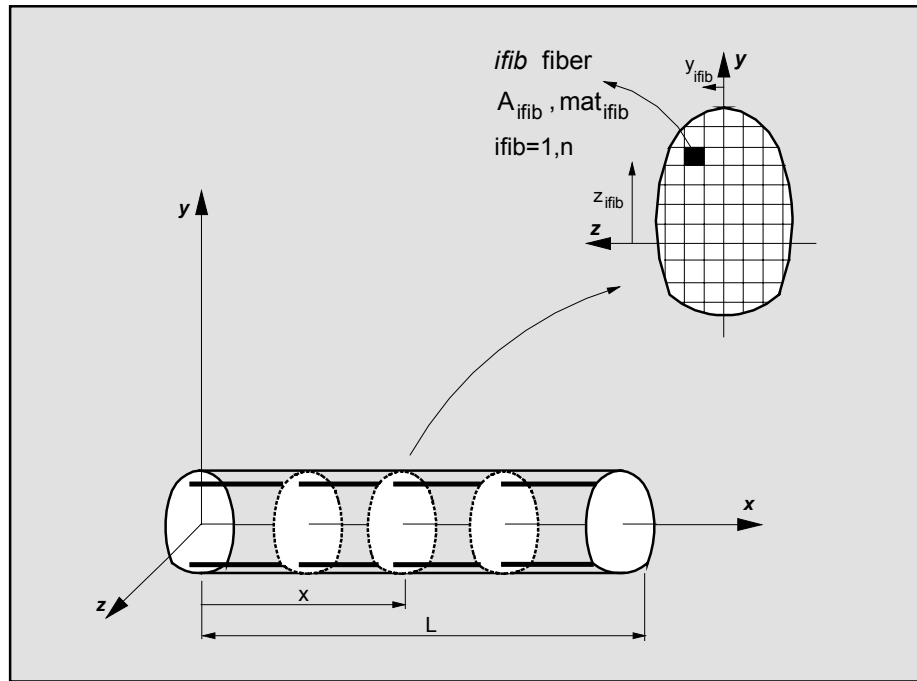


FIGURE 3.1 FIBER BEAM-COLUMN ELEMENT IN THE LOCAL REFERENCE SYSTEM:
SUBDIVISION OF CROSS SECTION INTO FIBERS

The generalized element forces and deformations and the corresponding section forces and deformations are those defined in Section 2.2 and shown in Fig. 2.1. These are grouped in the following vectors:

$$\text{Element force vector} \quad \mathbf{Q} = \{Q_1 \quad Q_2 \quad Q_3 \quad Q_4 \quad Q_5\}^T \quad (3.1)$$

$$\text{Element deformation vector} \quad \mathbf{q} = \{q_1 \quad q_2 \quad q_3 \quad q_4 \quad q_5\}^T \quad (3.2)$$

$$\text{Section force vector} \quad \mathbf{D}(x) = \begin{Bmatrix} M_z(x) \\ M_y(x) \\ N(x) \end{Bmatrix} \quad (3.3)$$

$$\text{Section deformation vector} \quad \mathbf{d}(x) = \begin{Bmatrix} \chi_z(x) \\ \chi_y(x) \\ \varepsilon(x) \end{Bmatrix} \quad (3.4)$$

Two more vectors are introduced to describe the state of the fibers at each section. These contain the strains and stresses of the fibers and are written in the following form

$$\text{Fiber strain vector} \quad \mathbf{e}(x) = \begin{Bmatrix} \varepsilon_1(x, y_1, z_1) \\ \vdots \\ \varepsilon_{ifib}(x, y_{ifib}, z_{ifib}) \\ \vdots \\ \varepsilon_n(x, y_n, z_n) \end{Bmatrix} \quad (3.5)$$

$$\text{Fiber stress vector} \quad \mathbf{E}(x) = \begin{Bmatrix} \sigma_1(x, y_1, z_1) \\ \vdots \\ \sigma_{ifib}(x, y_{ifib}, z_{ifib}) \\ \vdots \\ \sigma_n(x, y_n, z_n) \end{Bmatrix} \quad (3.6)$$

In the fiber state vectors x describes the position of the section along the longitudinal reference axis and y_{ifib}, z_{ifib} refer to the fiber position in the cross section, as shown in Fig 3.1. Following the hypothesis that plane sections remain plane and normal to the longitudinal axis, the fiber strain vector and the section deformation vector are related by the simple matrix relation

$$\mathbf{e}(x) = \mathbf{l}(x) \cdot \mathbf{d}(x) \quad (3.7)$$

where $\mathbf{l}(x)$ is a linear geometric matrix as follows

$$\mathbf{l}(x) = \begin{bmatrix} -y_1 & z_1 & 1 \\ \vdots & \vdots & \vdots \\ -y_{ifib} & z_{ifib} & 1 \\ \vdots & \vdots & \vdots \\ -y_n & z_n & 1 \end{bmatrix} \quad (3.8)$$

More complex forms of the compatibility matrix $\mathbf{l}(x)$ could be used to account for the effects of shear and bond-slip, but this is beyond the scope of this study.

3.4 Fiber Constitutive Models

The nonlinear behavior of the proposed fiber beam-column element derives entirely from the nonlinear behavior of the fibers. Thus, the validity of the analytical results depends on the accuracy of the fiber material models. Since the present study is limited to the hysteretic behavior of reinforced concrete members and the effect of bond-slip is neglected, only two material models are required: one for concrete and one for reinforcing steel. The element formulation simplifies the task of material model selection to uniaxial behavior, which is thoroughly studied and well established to date. Three-dimensional effects on material behavior can be included into the uniaxial model by appropriate modification of the parameters that define the monotonic envelope. This is important in the case of concrete, where confinement by transverse and longitudinal reinforcement has a significant effect on the stress-strain behavior.

The models used in the present study are those discussed in Filippou et al. (1983). While the reinforcing steel model in Filippou et al. (1983) remains one of the most accurate and convenient to use, many improved confined concrete models have been proposed in the last ten years (Mander et al. 1988, Sheikh and Yeh 1990). Still, the model used in this study offers a good compromise between simplicity and accuracy and remains an excellent choice for the hysteretic behavior of concrete. Comparisons between analytical and experimental results in Chapter 5 demonstrate that for RC beam-column elements under small axial loads the concrete material model shows satisfactory accuracy. In any case the modular program architecture that underlies the proposed beam-column element allows for the easy exchange of material models and a more extensive material library will be developed in the near future.

It is important to note that both stress-strain models are explicit functions of strain. This is a significant feature of the material models in connection with the proposed fiber model, where fiber strains are determined from section deformations according to Eq. (3.7). The stress determination only involves a function evaluation based on the current fiber stress and strain and the given strain increment. This reduces the computational effort considerably relative to material models that are not explicit functions of strain, such as the well-known Ramberg-Osgood steel model.

3.4.1 Steel Stress-Strain Relation

The reinforcing steel stress-strain behavior is described by the nonlinear model of Menegotto and Pinto (1973), as modified by Filippou et al. (1983) to include isotropic strain

hardening. The model is computationally efficient and agrees very well with experimental results from cyclic tests on reinforcing steel bars.

The model, as presented in Menegotto and Pinto (1973) takes on the form

$$\sigma^* = b \cdot \varepsilon^* + \frac{(1-b) \cdot \varepsilon^*}{(1 + \varepsilon^{*R})^{1/R}} \quad (3.9)$$

where

$$\varepsilon^* = \frac{\varepsilon - \varepsilon_r}{\varepsilon_0 - \varepsilon_r} \quad (3.10)$$

and

$$\sigma^* = \frac{\sigma - \sigma_r}{\sigma_0 - \sigma_r} \quad (3.11)$$

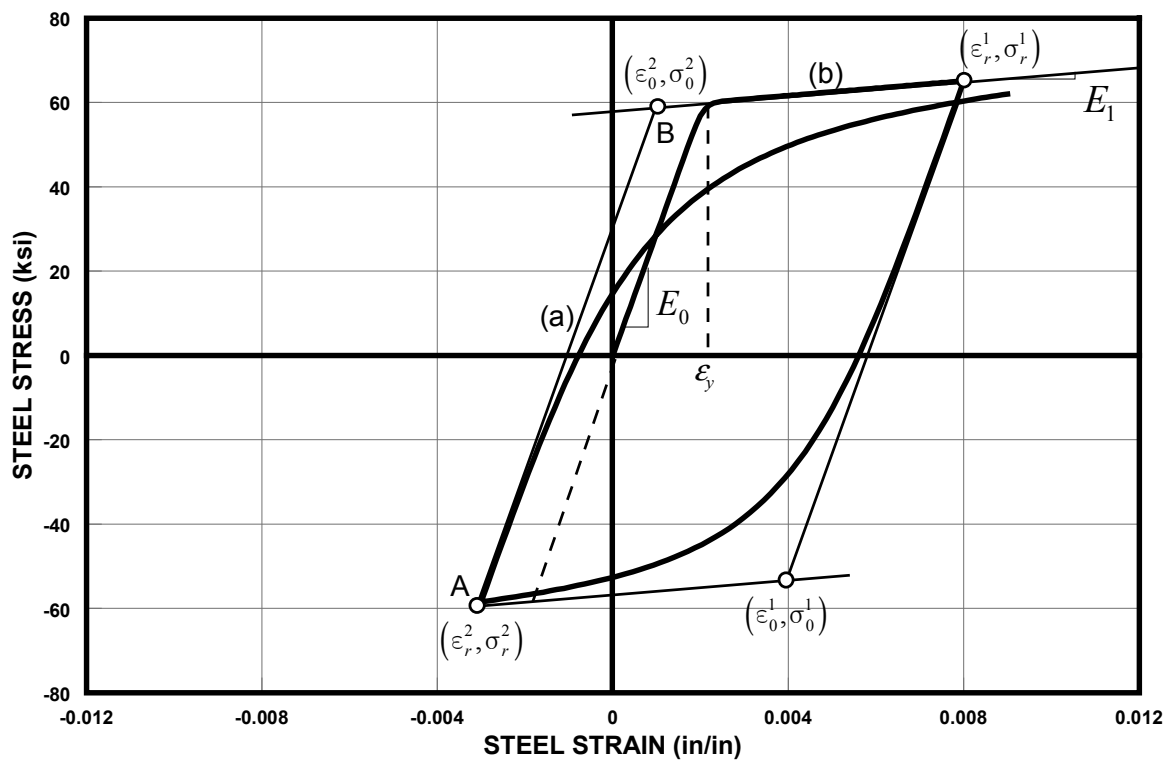


FIGURE 3.2 MENEGOTTO-PINTO STEEL MODEL

Eq. (3.9) represents a curved transition from a straight line asymptote with slope E_0 to another asymptote with slope E_1 (lines (a) and (b), respectively, in Fig. 3.2). σ_0 and ε_0 are the stress and strain at the point where the two asymptotes of the branch under consideration meet (point B in Fig. 3.2); similarly, σ_r and ε_r are the stress and strain at the point where the

last strain reversal with stress of equal sign took place (point A in Fig. 3.2); b is the strain hardening ratio, that is the ratio between slope E_1 and E_0 and R is a parameter that influences the shape of the transition curve and allows a good representation of the Bauschinger effect. As indicated in Fig. 3.2, $(\varepsilon_0, \sigma_0)$ and $(\varepsilon_r, \sigma_r)$ are updated after each strain reversal.

R is considered dependent on the strain difference between the current asymptote intersection point (point A in Fig. 3.3) and the previous load reversal point with maximum or minimum strain depending on whether the corresponding steel stress is positive or negative (point B in Fig. 3.3). The expression for R takes the form suggested in Menegotto and Pinto (1973)

$$R = R_0 - \frac{a_1 \cdot \xi}{a_2 + \xi} \quad (3.12)$$

where ξ is updated following a strain reversal. R_0 is the value of the parameter R during first loading and a_1, a_2 are experimentally determined parameters to be defined together with R_0 . The definition of ξ remains valid in case that reloading occurs after partial unloading.

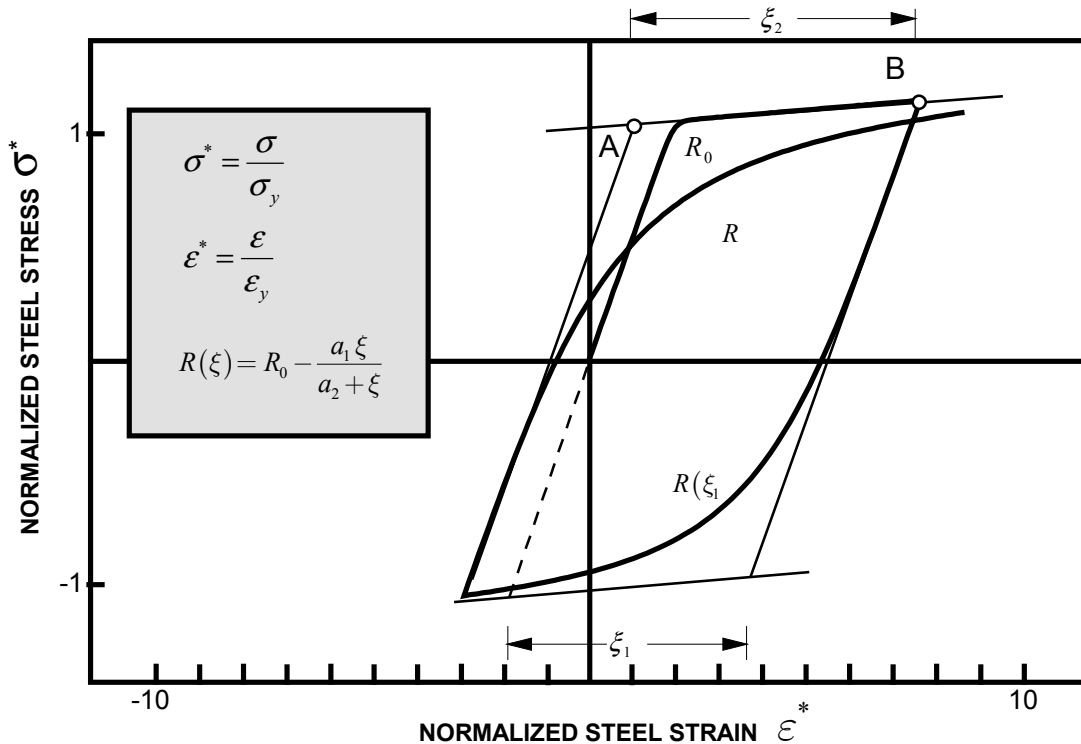


FIGURE 3.3 DEFINITION OF CURVATURE PARAMETER R IN MENEGOTTO -PINTO STEEL MODEL

Some clarification is needed in connection with the set of rules for unloading and reloading which complement Eqs. (3.10) and (3.11), allowing for a generalized load history. If the analytical model had a memory extending over all previous branches of the stress-strain history, it would follow the previous reloading branch, as soon as the new reloading curve reached it. This would require that the model store all necessary information to retrace all previous reloading curves which were left incomplete. This is clearly impractical from a computational standpoint. Memory of the past stress-strain history is, therefore, limited to a predefined number of controlling curves, which in the present model include,

1. the monotonic envelope,
2. the ascending upper branch curve originating at the reversal point with smallest ε value,
3. the descending lower branch curve originating at the reversal point with largest ε value,
4. the current curve originating at the most recent reversal point.

Due to the above restrictions reloading after partial unloading does not rejoin the original reloading curve after reaching the point from which unloading started, but, instead, continues on the new reloading curve until reaching the envelope. However, the discrepancy between the analytical model and the actual behavior is typically very small, as discussed in detail by Filippou et al. (1983).

The above implementation of the model corresponds to its simplest form, as proposed in Menegotto and Pinto (1973): elastic and yield asymptotes are assumed to be straight lines, the position of the limiting asymptotes corresponding to the yield surface is assumed to be fixed at all times and the slope E_0 remains constant (Fig. 3.2).

In spite of the simplicity in formulation, the model is capable of reproducing well experimental results. Its major drawback stems from its failure to allow for isotropic hardening. To account for this effect Filippou et al. (1983) proposed a stress shift in the linear yield asymptote as a function of the maximum plastic strain as follows:

$$\frac{\sigma_{st}}{\sigma_y} = a_3 \cdot \left(\frac{\varepsilon_{max}}{\varepsilon_y} - a_4 \right) \quad (3.13)$$

where ε_{max} is the absolute maximum strain at the instant of strain reversal, ε_y , σ_y are, respectively, the strain and stress at yield, and a_3 and a_4 are experimentally determined parameters. The model used in this study was implemented without the isotropic strain hardening option. For this case the parameter values are: $R_0 = 20$, $a_1 = 18.5$, $a_2 = 0.15$,

$a_3 = 0.$, $a_4 = 0$. With the exception of the last two parameters the values used are those in the original model of Menegotto and Pinto (1973).

3.4.2 Concrete Stress-Strain Relation

In order to compute the concrete stress in each layer, a material law describing the concrete stress-strain relation under arbitrary cyclic strain histories is needed. There is some uncertainty as to the influence of the concrete model on the overall behavior of RC members subjected to bending and small values of axial force. Some investigators have concluded that a crude concrete model suffices to accurately predict experimental results. This might be true in the case of monotonic loading and cyclic loading that is restricted to small excitations. It is not true, however, in the case of severe cyclic loading. The results of this study indicate that the strength deterioration of RC members under large cyclic excitations depends largely on the capacity of confined concrete to sustain stresses in the strain range beyond the maximum strength. This requires the use of a refined concrete model.

The model implemented in this study is summarized below:

The monotonic envelope curve of concrete in compression follows the model of Kent and Park (1973) that was later extended by Scott et al. (1982). Even though more accurate and complete models have been published since, the so-called modified Kent and Park model offers a good balance between simplicity and accuracy.

In the modified Kent and Park model the monotonic concrete stress-strain relation in compression is described by three regions:

$$\varepsilon_c \leq \varepsilon_0 \quad \sigma_c = K f'_c \left[2 \left(\frac{\varepsilon_c}{\varepsilon_0} \right) - \left(\frac{\varepsilon_c}{\varepsilon_0} \right)^2 \right] \quad (3.14)$$

$$\varepsilon_0 \leq \varepsilon_c \leq \varepsilon_u \quad \sigma_c = K f'_c \left[1 - Z (\varepsilon_c - \varepsilon_0) \right] \geq 0.2 K f'_c \quad (3.15)$$

where

$$\varepsilon_0 = 0.002K \quad (3.16)$$

$$K = 1 + \frac{\rho_s f_{yh}}{f'_c} \quad (3.17)$$

$$Z = \frac{0.5}{\frac{3 + 0.29 f'_c}{145 f'_c - 1000} + 0.75 \rho_s \sqrt{\frac{h'}{s_h}} - 0.002K}$$

ε_0 is the concrete strain at maximum stress, K is a factor which accounts for the strength increase due to confinement, Z is the strain softening slope, f'_c is the concrete compressive cylinder strength in MPa (1 MPa = 145 psi), f_{yh} is the yield strength of stirrups in MPa, ρ_s is the ratio of the volume of hoop reinforcement to the volume of concrete core measured to outside of stirrups, h' is the width of concrete core measured to outside of stirrups, and s_h is the center to center spacing of stirrups or hoop sets.

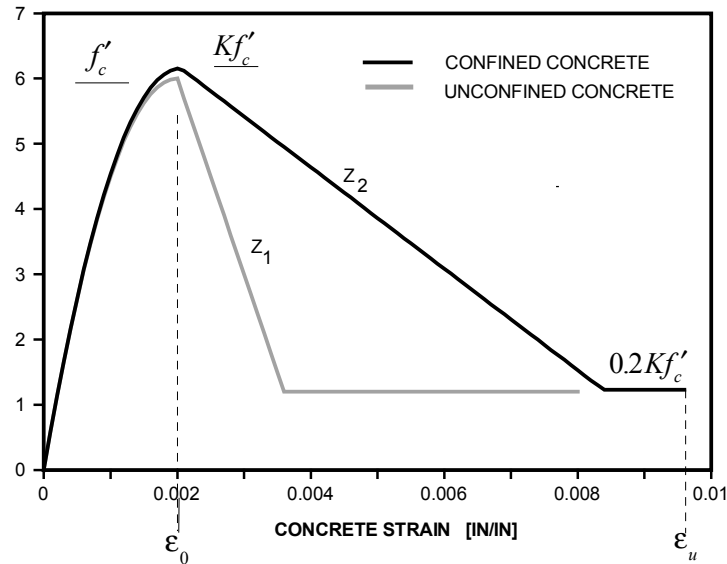


FIGURE 3.4 STRESS-STRAIN RELATION FOR CONFINED AND UNCONFINED CONCRETE

In the case of *concrete confined by stirrup-ties*, Scott et al. suggest that ε_u be determined conservatively from the following equation:

$$\varepsilon_u = 0.004 + 0.9\rho_s \left(f_{yh}/300 \right) \quad (3.18)$$

To account for crushing of *concrete cover* the strength in a cover layer is reduced to $0.2f'_c$ once the compressive strain exceeds the value of ε_u , which in this study is set equal to 0.005.

The tensile strength of concrete is neglected in the model, since it only influences the response of a RC section during cycles prior to yielding.

The following rules govern the hysteretic behavior of the concrete stress-strain relation (Fig. 3.5):

1. Unloading from a point on the envelope curve takes place along a straight line connecting the point ε_r at which unloading starts to a point ε_p on the strain axis given by the equations

$$\frac{\varepsilon_p}{\varepsilon_0} = 0.145 \cdot \left(\frac{\varepsilon_r}{\varepsilon_0} \right)^2 + 0.13 \cdot \left(\frac{\varepsilon_r}{\varepsilon_0} \right) \quad \text{for} \quad \left(\frac{\varepsilon_r}{\varepsilon_0} \right) < 2 \quad (3.19)$$

$$\frac{\varepsilon_p}{\varepsilon_0} = 0.707 \cdot \left(\frac{\varepsilon_r}{\varepsilon_0} - 2 \right) + 0.834 \quad \text{for} \quad \left(\frac{\varepsilon_r}{\varepsilon_0} \right) \geq 2 \quad (3.20)$$

where ε_0 is the strain level corresponding to the maximum stress in compression.

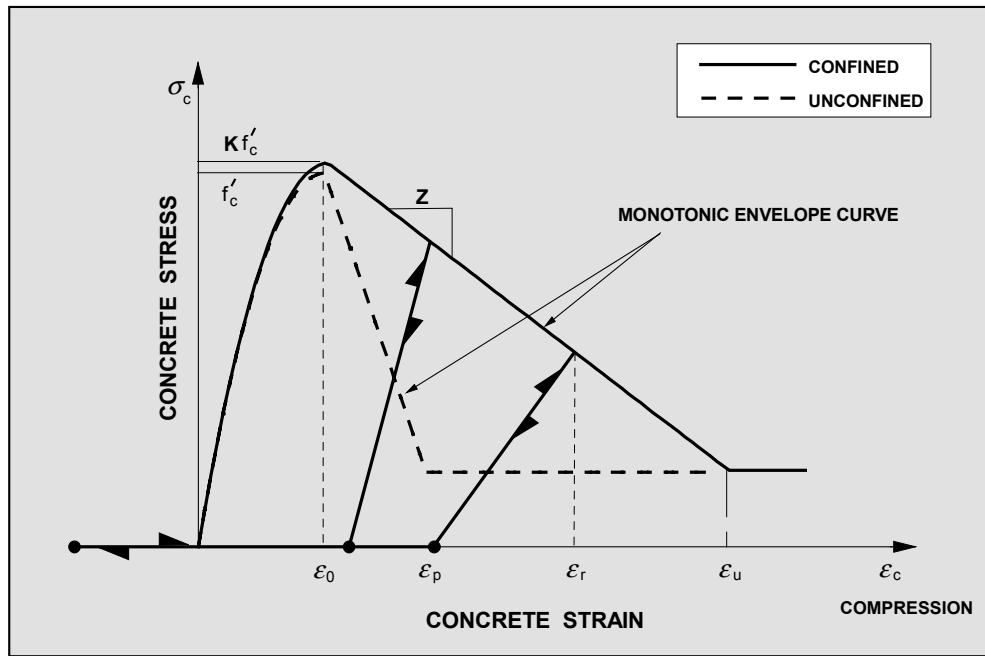


FIGURE 3.5 HYSTERETIC CONCRETE STRESS-STRAIN RELATION

Eq. (3.19) was proposed by Karsan and Jirsa (1969) and relates the normalized strains on the envelope with the strains at the completion of unloading through a quadratic formula. Since Eq. (3.19) exhibits unreasonable behavior under high compressive strain conditions, Eq. (3.20) is added to the model so that the unloading modulus of elasticity remains positive under high compressive strains.

2. The concrete stress is equal to zero for strains smaller than the strain at complete unloading (open crack) since the tensile resistance is neglected in this study (Fig. 3.5).
3. On reloading in compression the stress is zero as long as the strain is smaller than the strain at complete unloading (open crack). Once the concrete strain becomes larger than that value, reloading continues along the previous unloading path (Fig. 3.5). In reality unloading and reloading follow nonlinear paths which together form a hysteresis loop.

This was neglected here for reasons of simplicity, since it has a minor influence on the hysteretic response of the member.

The proposed hysteretic behavior of concrete in compression does not account for the cyclic damage of concrete. The importance of this effect on the hysteretic behavior of RC members merits further study, but is beyond the scope of the present report.

3.5 Fiber Beam-Column Element Formulation

The fiber beam-column element is formulated within the same framework of the mixed finite element method used in Section 2.3. The element deformation field is represented by the flexibility dependent shape functions defined in Eqs. (2.20) and (2.21). The force field is selected so that the two bending moment fields $M_z(x)$ and $M_y(x)$ in Fig. 2.1 are linear and the axial force field $N(x)$ is constant. This selection results in a matrix for the force interpolation functions given by

$$\mathbf{b}(x) = \begin{bmatrix} \left(\frac{x}{L} - 1\right) & \left(\frac{x}{L}\right) & 0 & 0 & 0 \\ 0 & 0 & \left(\frac{x}{L} - 1\right) & \left(\frac{x}{L}\right) & 0 \\ 0 & 0 & 0 & 0 & 1 \end{bmatrix} \quad (3.21)$$

where $\mathbf{b}(x)$ relates the force distribution $\mathbf{D}(x)$ along the element to the element generalized force vector \mathbf{Q} according to

$$\mathbf{D}^i(x) = \mathbf{b}(x) \cdot \mathbf{Q}^i \quad \text{and} \quad \Delta \mathbf{D}^i(x) = \mathbf{b}(x) \cdot \Delta \mathbf{Q}^i \quad (3.22)$$

The bending moment and axial force fields are exact when no element loads are present. Element loads can be included in the initial stage of the analysis by modifying the corresponding bending moment and axial force distributions, so that they are exact for the particular loading case. This case and its numerical implementation will be presented in more detail in Chapter 4.

The final matrix equation relating the applied unbalanced element forces $\mathbf{P} - \mathbf{Q}^{i-1}$ to the unknown element deformation increments $\Delta \mathbf{q}^i$ is equivalent to Eq. (2.23)

$$\left[\mathbf{F}^{i-1} \right]^{-1} \cdot \Delta \mathbf{q}^i = \mathbf{P} - \mathbf{Q}^{i-1} \quad (3.23)$$

where the superscripts denote the corresponding Newton-Raphson iteration.

The element state determination follows the steps presented in Section 2.4. Since the section force-deformation relation is no longer explicit but depends on the stress-strain behavior of the fibers some additional steps become necessary. When the section force-deformation relation is explicitly known the new tangent stiffness of the section $\mathbf{k}^j(x)$ can be directly computed for the given section forces $\mathbf{D}^j(x)$ and deformations $\mathbf{d}^j(x)$, as described in Sections 2.4 and 2.5. In the case of the fiber model the geometric matrix $\mathbf{I}(x)$ in Eq. (3.8) is first used to obtain the fiber strain increments for the given deformation increments $\Delta\mathbf{d}^j(x)$ following the hypothesis that plane sections remain plane and normal to the longitudinal axis

$$\Delta\mathbf{e}^j(x) = \mathbf{I}(x) \cdot \Delta\mathbf{d}^j(x)$$

The fiber strains are then updated to the new value

$$\mathbf{e}^j(x) = \mathbf{e}^{j-1}(x) + \Delta\mathbf{e}^j(x)$$

The new stress σ_{ifib}^j and tangent modulus E_{ifib}^j of all fibers are determined from the appropriate fiber stress-strain relation: the fiber stresses are then grouped in vector \mathbf{E}^j and the tangent moduli are written in a diagonal matrix \mathbf{E}_{tan}^j . By calling \mathbf{A} a diagonal matrix with entries the areas A_{ifib} of all fibers and using the section compatibility matrix $\mathbf{I}(x)$ of Eq. (3.8) well established structural analysis concepts yield the new section tangent stiffness matrix

$$\mathbf{k}^j(x) = \mathbf{I}^T(x) \cdot (\mathbf{E}_{tan}^j \mathbf{A}) \cdot \mathbf{I}(x) \quad (3.24)$$

which after carrying out the multiplication results in

$$\mathbf{k}^j(x) = \begin{bmatrix} \sum_{ifib=1}^{n(x)} E_{ifib}^j \cdot A_{ifib} \cdot y_{ifib}^2 & \sum_{ifib=1}^{n(x)} E_{ifib}^j \cdot A_{ifib} \cdot y_{ifib} \cdot z_{ifib} & -\sum_{ifib=1}^{n(x)} E_{ifib}^j \cdot A_{ifib} \cdot y_{ifib} \\ \sum_{ifib=1}^{n(x)} E_{ifib}^j \cdot A_{ifib} \cdot y_{ifib} \cdot z_{ifib} & \sum_{ifib=1}^{n(x)} E_{ifib}^j \cdot A_{ifib} \cdot z_{ifib}^2 & \sum_{ifib=1}^{n(x)} E_{ifib}^j \cdot A_{ifib} \cdot z_{ifib} \\ -\sum_{ifib=1}^{n(x)} E_{ifib}^j \cdot A_{ifib} \cdot y_{ifib} & \sum_{ifib=1}^{n(x)} E_{ifib}^j \cdot A_{ifib} \cdot z_{ifib} & \sum_{ifib=1}^{n(x)} E_{ifib}^j \cdot A_{ifib} \end{bmatrix}$$

The new section tangent stiffness matrix $\mathbf{k}^j(x)$ is then inverted to obtain the new section tangent flexibility matrix $\mathbf{f}^j(x)$. Similarly, the section resisting forces $\mathbf{D}_R^j(x)$ cannot be obtained directly from the section force-deformation relation as in Chapter 2, but are determined by summation of the axial force and biaxial bending contribution of all fibers as follows

$$\mathbf{D}_R^j(x) = \mathbf{I}^T(x) \cdot \mathbf{A} \cdot \mathbf{E}^j \quad (3.25)$$

or, after carrying out the multiplications

$$\mathbf{D}_R^j(x) = \left\{ \begin{array}{l} - \sum_{ifib=1}^n \sigma_{ifib}^j \cdot A_{ifib} \cdot y_{ifib} \\ \sum_{ifib=1}^n \sigma_{ifib}^j \cdot A_{ifib} \cdot z_{ifib} \\ \sum_{ifib=1}^n \sigma_{ifib}^j \cdot A_{ifib} \end{array} \right\}$$

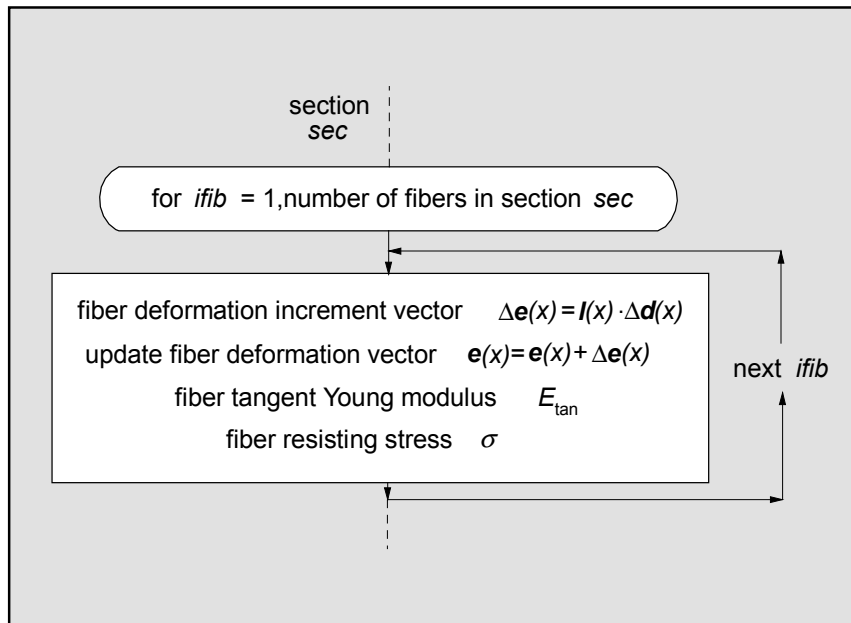


FIGURE 3.6 FLOW CHART OF THE SECTION FIBER STATE DETERMINATION

It is important to point out that all section matrices and vectors are computed with respect to a fixed section reference system which coincides with element axes y and z . This choice simplifies the computational effort. The origin of this reference system $(x, 0, 0)$, shown in Fig. 2.1, does not necessarily have to coincide with the neutral axis of the section. Since the position of the neutral axis changes during the analysis, using the neutral axis as reference would require the determination of its position at each element iteration, as discussed by Zeris and Mahin (1991). The section flexibility matrix and the section deformation vectors need to be transformed to the element coordinate system before determining the element flexibility matrix and the residual element deformations by integration. Similarly, the section forces calculated by the force interpolation functions refer to the element system and should be transformed to the local reference system before proceeding with the section state determination. To simplify these transformations between element and section variables and

noting that the selection of a section reference system is arbitrary, it is expedient to select a readily available reference system for the section such as the y and z axes. Consequently, the neutral axis at a section need never be computed.

The steps relevant to the fiber state determination are illustrated in Fig. 3.6. The flow chart of the element state determination in Fig. 2.5 is now completed by introducing the chart of Fig. 3.6 into the box denoted by *section constitutive law* in Fig. 2.5. The rest of the element state determination procedure agrees with the steps described in Sections 2.4 and 2.5. The complete element state determination is summarized in the following section, with no further comments regarding the steps that were already discussed in Chapter 2 and only minor comments concerning the steps for the section state determination.

3.6 Summary of the Fiber Beam-Column Element State Determination

During the structure state determination, each Newton-Raphson iteration i is organized as follows:

- (1) *Solve the global system of equations and update the structure displacements.*

$$\mathbf{K}_s^{i-1} \cdot \Delta \mathbf{p}^i = \Delta \mathbf{P}_E^i \quad (3.26)$$

$$\mathbf{p}^i = \mathbf{p}^{i-1} + \Delta \mathbf{p}^i \quad (3.27)$$

- (2) *Compute the element deformation increments and update the element deformations.*

$$\Delta \mathbf{q}^i = \mathbf{L}_{ele} \cdot \Delta \mathbf{p}^i \quad (3.28)$$

$$\mathbf{q}^i = \mathbf{q}^{i-1} + \Delta \mathbf{q}^i \quad (3.29)$$

- (3) *Start the fiber beam-column element state determination.*

Set $j=1$

- (4) *Compute the element force increments.*

$$\Delta \mathbf{Q}^j = \mathbf{K}^{j-1} \cdot \Delta \mathbf{q}^j \quad (3.30)$$

- (5) *Update the element forces.*

$$\mathbf{Q}^j = \mathbf{Q}^{j-1} + \Delta \mathbf{Q}^j \quad (3.31)$$

- (6) *Compute the section force increments.*

$$\Delta \mathbf{D}^j(x) = \mathbf{b}(x) \cdot \Delta \mathbf{Q}^j \quad (3.32)$$

$$\mathbf{D}^j(x) = \mathbf{D}^{j-1}(x) + \Delta \mathbf{D}^j(x) \quad (3.33)$$

(7) *Compute the section deformation increments.*

$$\Delta \mathbf{d}^j(x) = \mathbf{f}^{j-1}(x) \cdot \Delta \mathbf{D}^j(x) + \mathbf{r}^{j-1}(x) \quad (3.34)$$

$$\mathbf{d}^j(x) = \mathbf{d}^{j-1}(x) + \Delta \mathbf{d}^j(x) \quad (3.35)$$

(8) *Compute the fiber deformation increments.*

Following the assumption that plane sections remain plane and normal to the reference longitudinal axis and that no bond-slip takes place, the section compatibility matrix $\mathbf{I}(x)$ is used to obtain the fiber strain increments $\Delta \mathbf{e}^j(x)$ from the section deformation increments $\Delta \mathbf{d}^j(x)$. The fiber strains are then updated

$$\Delta \mathbf{e}(x) = \mathbf{I}(x) \cdot \Delta \mathbf{d}(x) \quad (3.36)$$

$$\mathbf{e}^j(x) = \mathbf{e}^{j-1}(x) + \Delta \mathbf{e}^j(x) \quad (3.37)$$

(9) *Compute fiber stresses and tangent moduli.*

Using the fiber material models in Section 3.4, the stresses $\sigma_{ifib}^j(x, y_i, z_i)$ and tangent moduli $E_{ifib}^j(x)$ of all fibers are computed from the stresses σ_{ifib}^{j-1} and strains ε_{ifib}^{j-1} at the previous step $j-1$ and the current fiber deformation increments $\Delta \varepsilon_{ifib}^j$

(10) *Compute the section tangent stiffness and flexibility matrices.*

Using the tangent moduli $E_{ifib}^j(x)$ of all fibers the new section tangent stiffness matrix $\mathbf{k}^j(x)$ is computed:

$$\mathbf{k}^j(x) = \begin{bmatrix} \sum_{ifib=1}^n E_{ifib}^j \cdot A_{ifib} \cdot y_{ifib}^2 & \sum_{ifib=1}^n E_{ifib}^j \cdot A_{ifib} \cdot y_{ifib} \cdot z_{ifib} & -\sum_{ifib=1}^n E_{ifib}^j \cdot A_{ifib} \cdot y_{ifib} \\ \sum_{ifib=1}^n E_{ifib}^j \cdot A_{ifib} \cdot y_{ifib} \cdot z_{ifib} & \sum_{ifib=1}^n E_{ifib}^j \cdot A_{ifib} \cdot z_{ifib}^2 & \sum_{ifib=1}^n E_{ifib}^j \cdot A_{ifib} \cdot z_{ifib} \\ -\sum_{ifib=1}^n E_{ifib}^j \cdot A_{ifib} \cdot y_{ifib} & \sum_{ifib=1}^n E_{ifib}^j \cdot A_{ifib} \cdot z_{ifib} & \sum_{ifib=1}^n E_{ifib}^j \cdot A_{ifib} \end{bmatrix} \quad (3.38)$$

where n is the total number of fibers at the section and A_{ifib} is the fiber area. The stiffness matrix is then inverted to obtain the new section flexibility matrix $\mathbf{f}^j(x)$.

$$\mathbf{f}^j(x) = [\mathbf{k}^j(x)]^{-1} \quad (3.39)$$

(11) *Compute the section resisting forces.*

The section resisting forces $\mathbf{D}_R^j(x)$ are computed by summation of the axial force and biaxial bending moment contributions of all fibers

$$\mathbf{D}_R^j(x) = \begin{Bmatrix} -\sum_{ifib=1}^n \sigma_{ifib}^j \cdot A_{ifib} \cdot y_{ifib} \\ \sum_{ifib=1}^n \sigma_{ifib}^j \cdot A_{ifib} \cdot z_{ifib} \\ \sum_{ifib=1}^n \sigma_{ifib}^j \cdot A_{ifib} \end{Bmatrix} \quad (3.40)$$

From here on the element state determination is identical to Section 2.5.

(12) *Compute the section unbalanced forces.*

$$\mathbf{D}_U^j(x) = \mathbf{D}^j(x) - \mathbf{D}_R^j(x) \quad (3.41)$$

(13) *Compute the residual section deformations.*

$$\mathbf{r}^j(x) = \mathbf{f}^j(x) \cdot \mathbf{D}_U^j(x) \quad (3.42)$$

(14) *Compute the element flexibility and stiffness matrices.*

$$\mathbf{F}^j = \left[\int_0^L \mathbf{b}^T(x) \cdot \mathbf{f}^j(x) \cdot \mathbf{b}(x) \cdot dx \right] \quad (3.43)$$

$$\mathbf{K}^j = [\mathbf{F}^j]^{-1} \quad (3.44)$$

(15) *Check for element convergence*

- a) If the element has converged, set $\mathbf{Q}^i = \mathbf{Q}^j$ and $\mathbf{K}^i = \mathbf{K}^j$, then go to step (16);
- b) If the element has not converged, compute the residual element deformations

$$\mathbf{s}^j = \left[\int_0^L \mathbf{b}^T(x) \cdot \mathbf{r}^j(x) \cdot dx \right] \quad (3.45)$$

then increment j to $j+1$ and set $\Delta \mathbf{q}^{j+1} = -\mathbf{s}^j$. Repeat steps (4) through (15) with $\Delta \mathbf{q}^{j+1}$ until element convergence is reached.

(16) *Compute the structure resisting forces and the new structure stiffness matrix.*

If all elements have converged, the Newton-Raphson iteration i is complete.

$$\mathbf{P}_R^i = \sum_{ele=1}^n \mathbf{L}_{ele}^T \cdot (\mathbf{Q}^i)_{ele} \quad (3.46)$$

$$\mathbf{K}_s^i = \sum_{ele=1}^n \mathbf{L}_{ele}^T \cdot (\mathbf{K}^i)_{ele} \cdot \mathbf{L}_{ele} \quad (3.47)$$

If convergence at the structural level is achieved, apply a new load increment, otherwise continue the Newton-Raphson iteration process.

CHAPTER 4
NUMERICAL IMPLEMENTATION OF BEAM-COLUMN ELEMENT

4.1 General

A discussion of some of the issues involved in the numerical implementation of the fiber beam-column element in a general purpose computer program is presented in this chapter. The element was first implemented in a stand-alone computer program. After successfully testing its performance, the element was adapted to the finite element program FEAP developed by Professor R. L. Taylor at the University of California, Berkeley and described in Zienkiewicz and Taylor (1989 and 1991). The present report focuses on the numerical aspects of the stand alone program and briefly discusses some differences in the numerical strategies between the stand alone program and the implementation in FEAP.

The stand-alone program is a special purpose program for the analysis of frames composed of fiber beam-column elements. The input data contain information concerning the geometry and material properties of the structure as well as information about the applied loads, which include both nodal and element loads. Nodal loads can be constant or time-varying, in which case they are applied in a sequence of steps. Element loads are constant and are applied with the constant nodal loads at the beginning of the analysis.

The nonlinear solution algorithm is divided into three nested loops. The first and outermost loop consists of the sequence of load steps that the applied load is divided into. The second loop consists of the Newton-Raphson solution procedure that is necessary within each load step for determining the structural displacements that result from the total applied load. This loop is also referred to as structure state determination. The third and innermost loop consists of the element iteration process that is necessary within each Newton-Raphson iteration in order to compute the element resisting forces that correspond to given element deformations. This loop is also referred to as element state determination.

In order to better illustrate the three nested loops the notation in the previous chapters is extended so that every variable now carries information about the load step number, the current Newton-Raphson iteration and, when necessary, the current element iteration. This information is represented by three different superscripts on the variable: consistent with the

notation in the two previous chapters, k refers to the load step, i to the Newton-Raphson iteration scheme and j to the element iteration loop. This notation is particularly useful in the numerical implementation of the nonlinear solution algorithm, which is summarized in Appendix A.

After a brief discussion of the notation and the numerical scheme for the integration along the element axis, the problem of defining a convergence criterion, both, at the element and at the structure level is discussed. Different alternatives are explored outlining their advantages and disadvantages. The criteria used in the stand-alone program are based on unbalanced forces, both, at the structure and at the element level, while program FEAP uses an energy criterion at the structure level, so that a corresponding criterion is adopted at the element level.

The procedure for including element loads in the model is presented next. An initial force distribution that is in equilibrium with the applied element loads is assumed first. The corresponding residual element deformations are used to start the element iterations that will ultimately yield the fixed-end moments for the applied element loads. Rigid body modes are then added in order to include the shear forces due to the element loads. The resulting end moments and shear forces do not generally satisfy equilibrium at the structural nodes, because no nodal forces were originally applied to the structure in connection with the element loads. The resulting end moments and shear forces contribute to the unbalanced nodal loads that need to be applied with opposite sign at the structural nodes in order to restore equilibrium. This step concludes the first Newton-Raphson iteration for the element load application. If the element is elastic, no further iterations are required within the element and the resulting end moments constitute the fixed-end moments for the applied element loads. If the element undergoes inelastic behavior under the application of element loads, the iterations of the element state determination phase of the algorithm converge to the fixed-end forces of the element.

Two alternative methods for including the shear forces are presented. One is implemented in the stand alone program and the other is used in program FEAP. A simple example of a linear elastic cantilever with uniformly distributed load is used to illustrate the process of element load application.

A brief discussion of the application of the nonlinear algorithm to the state determination of softening elements concludes the chapter. A simple system of two springs in series is used to illustrate how well the proposed algorithm works for softening elements.

4.2 Preliminary Considerations

The implementation of the fiber beam-column element evolved over two stages. A stand alone computer program was developed first in order to test the element performance. In the second stage the element was implemented in the finite element program FEAP. In this report the computational considerations concerning the general implementation of the element rather than the specific details for the two numerical implementations are discussed.

In both implementations the input data consist of the geometry description and material properties of the structure. From the geometric viewpoint the structure is an assemblage of beam-column elements connected at nodes so that the nodal degrees of freedom, grouped in vector \mathbf{p} , are the basic unknowns of the problem. The element deformations \mathbf{q} are related to the structure degrees of freedom \mathbf{p} through a constant compatibility matrix \mathbf{L}_{ele} . Each element is subdivided into several control sections and each section is composed of a number of fibers. The number of sections and their locations depends on the integration scheme and the desired level of accuracy. The number of fibers in a section depends on the geometric and material properties of the section and on the level of detail sought in the section representation. Each fiber is characterized by its area, material type and position with respect to the section reference system (Fig. 3.1). The origin of this local system is the geometric centroid of the section. The union of the geometric centroids of the section defines the longitudinal axis of the element \mathbf{x} . The material behavior of the element depends entirely on the fiber stress-strain relation of the fibers, which follow the confined and unconfined concrete as well as reinforcing steel models of Section 3.4. Different concrete and steel material types can be specified for the fibers by varying the values of material parameters.

External loads can be applied to the structure in the form of nodal forces or element loads. Incremental static loads can be included in the analysis with the introduction of a fictitious time scale. In general, all constant loads are applied at the beginning of the analysis, while incremental loads are applied in a sequence of steps $k=1, \dots, nk$. Two different methods are used for the application of nodal forces and element loads. Following classical structural analysis methods nodal loads are assembled in the global force vector \mathbf{P}_E . Element loads are included in an element load vector \mathbf{W} and a new method for incorporating these loads within a flexibility-based beam element is described in Section 4.5.

The nonlinear analysis algorithm is organized in four modules corresponding to the different discretization levels of the structure. The four modules refer to structure, elements, sections and fibers. The vectors and matrices that represent the basic variables within each module are summarized in Table 4.1.

During the structural analysis phase each module is called with a set of given data and the module computes and returns the desired variables, as summarized in the flow charts at the end of Chapters 2 and 3. In the structure module the applied force increments constitute the given input data and the solution algorithm returns the incremental and total displacements of the structure, the corresponding resisting forces and the current stiffness matrix. In the element module the total and incremental element deformations represent the input data and the solution algorithm returns the corresponding element resisting forces and the current stiffness matrix. In the section module the output contains the section flexibility $f(x)$ rather than the section stiffness $k(x)$ in order to underline the flexibility-based nature of the algorithm that is proposed for the element state determination. The input and output variables for the four modules are summarized in Table 4.2.

Module	Vectors and Matrices		
	Force/Stress	Displacement/Deformation	Stiffness/Flexibility
Structure	\mathbf{P}	\mathbf{p}	\mathbf{K}
Element	\mathbf{Q}	\mathbf{q}	\mathbf{F}, \mathbf{K}
Section	$\mathbf{D}(x)$	$\mathbf{d}(x)$	$\mathbf{k}(x), \mathbf{f}(x)$
Fiber	$\mathbf{E}(x)$	$\mathbf{e}(x)$	E_{tan}

TABLE 4.1 VECTORS AND MATRICES DEFINING THE STATE OF EACH MODULE

Module	Input	Output
Structure	Applied force increments $\Delta \mathbf{P}_E$	Total displacements \mathbf{p} Displacement increments $\Delta \mathbf{p}$ Resisting forces \mathbf{P}_R Stiffness \mathbf{K}
Element	Total deformations \mathbf{q} Deformation increments $\Delta \mathbf{q}$	Resisting forces \mathbf{Q} Stiffness \mathbf{K}
Section	Force increments $\Delta \mathbf{D}(x)$	Residual deformation $\mathbf{r}(x)$ Flexibility $\mathbf{f}(x)$
Fiber	Total strains $\mathbf{e}(x)$ Strain increments $\Delta \mathbf{e}(x)$	Resisting stresses $\mathbf{E}(x)$ Stiffness E_{tan}

TABLE 4.2 INPUT AND OUTPUT DATA FOR EACH MODULE

The nonlinear solution algorithm is organized in three nested computational loops. Loads are applied in a sequence of load steps, that are indicated by superscript k , so that each load increment is denoted by vector $\Delta \mathbf{P}_E^k$. The total applied load \mathbf{P}_E is equal to the sum of load increments $\Delta \mathbf{P}_E^k$, i.e.

$$\mathbf{P}_E = \sum_{k=1}^{nk} \Delta \mathbf{P}_E^k$$

Because of nonlinear structural behavior, a linearization is introduced about the present state of the structure and an iteration scheme is needed to compute the structure displacements \mathbf{p}^k that result from the imposed forces $\mathbf{P}^k = \mathbf{P}^{k-1} + \Delta \mathbf{P}^k$ at each load step. To this end the Newton-Raphson algorithm is used in the stand alone computer program and in program FEAP, even though alternative strategies are available in the latter and can be implemented easily. Another index i is introduced for the iterations of the Newton-Raphson solution method. Finally, a third iteration loop is needed within each Newton-Raphson iteration in order to determine the element resisting forces for the given element deformations \mathbf{q}^i . Correspondingly, a third superscript j is introduced.

From this discussion it is clear that two nested loops are needed within each load step k in order to obtain a converged solution at the structure degrees of freedom. The solution algorithm is such that, at the converged state, equilibrium and compatibility are strictly satisfied within the elements, while all section states satisfy the section force-deformation relation within the specified tolerance.

A special notation is introduced to trace the evolution of each variable during the nonlinear analysis. Vectors and matrices are denoted by three superscripts corresponding to the three iteration loops. For example, the notation for the element force vector \mathbf{Q} is

$$\left((\mathbf{Q}^k)^i \right)^j$$

where k indicates the load step, i the Newton-Raphson iteration and j the element iteration. It should be pointed out that element, section and fiber variables carry all three superscripts, whereas structure variables do not carry the superscript j , since they do not change during element iterations. For example, the structure displacement vector and the element force vector are written

$$\left(\mathbf{p}^k \right)^i \quad \text{and} \quad \left((\Delta \mathbf{Q}^k)^i \right)^j, \text{ respectively.}$$

The only exception to this rule is the element deformation vector \mathbf{q} , which does not carry the index j because it is not affected by the element iteration loop (Fig. 2.5).

The numerical implementation of the beam-column element in a finite element program follows very closely the procedure outlined in Chapters 2 and 3. In addition, it requires the introduction of an incremental vector for each vector that varies during the iterations. For instance, $(\delta\Delta\mathbf{p}^k)^i$ is the change in the structural displacement increments at the i -th Newton-Raphson iteration, whereas $(\Delta\mathbf{p}^k)^i$ denotes the total structural displacement increment during the k -th load step, which is updated using

$$(\Delta\mathbf{p}^k)^i = (\Delta\mathbf{p}^k)^{i-1} + (\delta\Delta\mathbf{p}^k)^i$$

where $(\Delta\mathbf{p}^k)^{i=0} = \mathbf{0}$. Once convergence is reached at the structure degrees of freedom, the superscript i is dropped and the total displacement increments simply become $\Delta\mathbf{p}^k$, while the total structural displacements are updated to the value

$$\mathbf{p}^k = \mathbf{p}^{k-1} + \Delta\mathbf{p}^k$$

Similarly, $\left((\delta\Delta\mathbf{Q}^k)^i\right)^j$ is the change in the element force increments in the j -th element iteration, and $\left((\Delta\mathbf{Q}^k)^i\right)^j$ is the total element force increment during the i -th Newton-Raphson iteration, which is updated using

$$\left((\Delta\mathbf{Q}^k)^i\right)^j = \left((\Delta\mathbf{Q}^k)^i\right)^{j-1} + \left((\delta\Delta\mathbf{Q}^k)^i\right)^j$$

where $\left((\Delta\mathbf{Q}^k)^i\right)^0 = (\Delta\mathbf{Q}^k)^{i-1}$ and $\left((\Delta\mathbf{Q}^k)^1\right)^0 = \mathbf{0}$. When convergence is reached in the element iterations, the superscript j is dropped and $\left((\Delta\mathbf{Q}^k)^i\right)^j$ becomes $(\Delta\mathbf{Q}^k)^i$. Similarly, when convergence is also reached at the structure degrees of freedom, superscript i is dropped and $(\Delta\mathbf{Q}^k)^i$ becomes $\Delta\mathbf{Q}^k$. At this point the element forces are updated using

$$\mathbf{Q}^k = \mathbf{Q}^{k-1} + \Delta\mathbf{Q}^k$$

with $\mathbf{Q}^0 = \mathbf{0}$.

It should be noted that, the change in vector increments, denoted by symbol $\delta\Delta$, is only used to update the corresponding vector increments and total vectors during the iterations, and, therefore, does not need to be stored.

The summary of the nonlinear solution algorithm was already presented at the end of Chapters 2 and 3 with a notation that did not use all superscripts for the sake of clarity.

Appendix A contains a more detailed summary of the solution algorithm with an outline of the updating procedure and a brief discussion of some implementation issues.

4.3 Numerical Integration

All integrals in the element formulation are evaluated numerically with the Gauss-Lobato integration scheme that is based on the expression

$$I = \int_0^L f(x) \cdot dx = \sum_{h=1}^m w_h \cdot f(x_h) \quad (4.1)$$

where h denotes the monitored section and w_h is the corresponding weight factor. The Gauss-Lobato scheme with m integration points permits the exact integration of polynomials of degree up to $(2m-3)$. This procedure is superior to the classical Gauss integration method, when it is important to include in the integration the end points of the element. Since inelastic behavior in beam-column elements often concentrates at the ends of the member, the monitoring of the end sections of the element offers advantages from the standpoint of accuracy and numerical stability.

4.4 Definition of Tolerance

The nonlinear solution algorithm in this study is based on a set of linear matrix relations that are repeatedly applied until convergence is achieved. Theoretically, this occurs when the applied loads are perfectly balanced by the internal resisting forces of the elements. Numerically, however, such perfect balance is either impossible or too expensive to attain. In a nonlinear solution algorithm it is normally accepted that convergence is reached when some control parameters, such as the unbalanced forces, are smaller than a specified threshold or tolerance. Norms or absolute values of these variables may be selected as control parameters as many studies to date have discussed. Different control parameters are selected for the stand alone program than for the implementation of the element in program FEAP, where the choice of tolerance parameters is limited by the main program.

In the stand-alone program two different iteration algorithms are used: the first is implemented at the structure level and is the well known Newton-Raphson scheme, while the second is used at the element level, as described in the previous chapters. Correspondingly, two convergence controls are needed. In this study the unbalanced forces at the structure degrees of freedom and at the control sections of the element are selected as control parameters. Two types of tolerance are defined: the first is an absolute force bound and the

second is a relative force bound defined as a fraction of the corresponding total applied force. The unbalanced force is compared with the largest of the two bounds. This choice derives from the consideration that the absolute tolerance is too restrictive for large applied loads, while the relative check may be too severe for small loads. Since the stability of the proposed solution algorithm is not affected by the size of the load step increments, the selected convergence criteria are not overly restrictive in the extreme case of very small or very large load steps. In the following the convergence criteria at the element and at the structure level are discussed separately.

(a) *Element convergence.* Convergence at the element level is achieved when all monitored sections have converged. Section convergence is reached when all section force unbalances fall within the absolute or relative tolerance. Three generalized forces, two bending moments $D_1(x_h)$, $D_2(x_h)$ and the axial force $D_3(x_h)$ are defined at each monitored section h , as shown in Fig. 2.1. Two element tolerance values are defined for all elements. These are called:

$$EAT = \textit{Element Absolute Tolerance}$$

$$ERT = \textit{Element Relative Tolerance}$$

ERT and EAT are related to the corresponding structure tolerances SRT and SAT through a scale factor that is selected by the user, as will be discussed later in the section. At every element iteration j three different section tolerance values $SeT_n(x_h)$ are defined:

$$SeT_n(x_h) = \max \left\{ EAT \times L, \left((D_n^k(x_h))^i \right)^j \times ERT \right\} \quad n = 1, 2$$

$$SeT_n(x_h) = \max \left\{ EAT, \left((D_n^k(x_h))^i \right)^j \times ERT \right\} \quad n = 3$$

where L is the element length. In the computer program an element counter EC is introduced to monitor the number of force unbalances that are smaller than the corresponding tolerance. During the element iterations the counter is first initialized to zero and is then incremented by one every time a section force satisfies the section tolerance, i.e.

$$\left((D_{nU}^k(x_h))^i \right)^j \leq SeT_n(x_h) \Rightarrow EC = EC + 1$$

Element convergence is reached when all monitored sections have converged, or, in symbols when

$$EC = 3m \Rightarrow \textit{element convergence}$$

where m is the number of monitored sections in the element. At this point iteration loop j is complete. After all elements converge the element state determination is complete and the program checks for convergence at the structure level.

- (b) *Structure convergence.* Convergence at the structure level is reached when all nodal unbalanced forces are smaller than the corresponding tolerance. The convergence check is similar to that adopted for the element. Absolute and relative tolerances are specified in the input data:

$$SAT = \textit{Structure Absolute Tolerance}$$

$$SRT = \textit{Structure Relative Tolerance}$$

SRT is typically assigned a value of 0.01, while SAT depends on the type of problem to be solved. For each degree of freedom $ndof$ a tolerance measure is computed

$$StT_{ndof} = \max \left\{ SAT, (P_n^k)^i \times SRT \right\} \quad ndof = 1, \dots, maxdof$$

where $maxdof$ is the total number of unconstrained degrees of freedom. A structure counter SC is introduced to monitor the number of converged degrees of freedom. This counter is initialized to zero at the beginning of every Newton-Raphson iteration i and is incremented by one every time a structure unbalance force is smaller than the corresponding tolerance, i.e.

$$(P_{U_{ndof}}^k)^i \leq StT_{ndof} \Rightarrow SC = SC + 1$$

Structure convergence is reached when the counter is equal to the total number of unconstrained degrees of freedom, that is:

$$SC = maxdof \Rightarrow \textit{structure convergence}$$

When the structure converges, the Newton-Raphson loop is complete and the next load increment is applied.

Structure and element tolerances are related by a tolerance factor TF , such that

$$EAT = TF \times SAT$$

$$ERT = TF \times SRT$$

The default value for TF is 1. As TF becomes larger, the number of element iterations j decreases and in the limit tends to 1. Conversely, as TF gets smaller, the number of iterations j increases. When load increments are small, few Newton-Raphson iterations are needed to achieve convergence at the structure level, because only small stiffness changes occur within each load step. There is, therefore, no need to be overly restrictive during the element convergence check and factor TF can be larger than 1 with typical values ranging from 5 to 10. On the other hand, when load increments are large, significant stiffness changes may take place within a load step and several Newton-Raphson iterations are needed to converge to the solution. In this case it is important to trace closely the force-deformation relation at the element level by selecting a TF value close to 1. In other words the TF factor controls the relation between the number of iterations j within each Newton-Raphson iteration i and the total number of Newton-Raphson iterations within a load step.

The convergence criteria in program FEAP are different. At the structure level the work (energy) increment is chosen as the convergence control parameter. Convergence of the Newton-Raphson iteration algorithm is reached when the ratio between the current work increment and the initial work increment is smaller than a specified tolerance. With the adopted notation the structural convergence criterion is:

$$\frac{\left\{ \left[(\Delta \mathbf{P}_E^k)^i \right]^T \cdot (\delta \Delta \mathbf{p}^k)^i \right\}}{\left\{ \left[(\Delta \mathbf{P}_E^k)^1 \right]^T \cdot (\delta \Delta \mathbf{p}^k)^1 \right\}} = \frac{\left\{ \left[(\mathbf{P}_U^k)^{i-1} \right]^T \cdot (\delta \Delta \mathbf{p}^k)^i \right\}}{\left\{ \left[(\Delta \mathbf{P}_E^k)^1 \right]^T \cdot (\delta \Delta \mathbf{p}^k)^1 \right\}} \leq Stol \quad (4.2)$$

Typically, $Stol$ is assigned the value of 10^{-16} by default. This convergence scheme is part of the FEAP program and is completely independent of the present application. More details on the convergence criterion can be found in Zienkiewicz and Taylor (1989 and 1991).

In the implementation of the beam-column element in program FEAP the same convergence criterion is used to check convergence within the element iteration loop. The value of the work increment for the current element iteration j is compared to the work for the first element iteration, i.e. $j=1$. In symbols:

$$\frac{\left\{ \left[\left((\delta \Delta \mathbf{Q}^k)^i \right)^j \right]^T \cdot \left((\delta \Delta \mathbf{q}^k)^i \right)^j \right\}}{\left\{ \left[\left((\delta \Delta \mathbf{Q}^k)^i \right)^1 \right]^T \cdot \left((\delta \Delta \mathbf{q}^k)^i \right)^1 \right\}} = \frac{\left\{ \left[\left((\mathbf{s}^k)^i \right)^{j-1} \right]^T \cdot \left((\mathbf{K}^k)^i \right)^{j-1} \cdot \left((\mathbf{s}^k)^i \right)^{j-1} \right\}}{\left\{ \left[\left((\delta \Delta \mathbf{q}^k)^i \right)^1 \right]^T \cdot \left(\mathbf{K}^k \right)^{i-1} \cdot \left((\delta \Delta \mathbf{q}^k)^i \right)^1 \right\}} \leq Etol \quad (4.3)$$

Typically, $Etol$ is assigned the value of 10^{-16} by default. This criterion has a clear advantage over that used in the stand-alone program, since it controls, both, unbalanced forces and residual deformations. This is quite significant when the element reaches its peak resistance and its stiffness matrix becomes ill-conditioned. In this case the unbalanced forces may be very small while the element residual deformations are still large. Consequently, the element iterations, which are based on residual deformations, should not stop. Energy is the only measure which accounts for, both, unbalanced forces and residual deformations.

Another significant difference between the element convergence criterion in the stand alone program and that in program FEAP is that in the former case element convergence is based on section convergence, while in the latter convergence is entirely based on element forces and deformations, *implicitly assuming that convergence at the element degrees of freedom implies section convergence*. To validate this assumption another convergence criterion was also introduced in the implementation of the element in FEAP. In this third criterion convergence is also checked at the section level by measuring the energy increment rather than the unbalanced forces. In this case convergence is achieved when the following condition is satisfied:

$$\frac{\sum_{i \text{ sec}=1}^{n \text{ sec}} \left\{ \left[\left((\mathbf{r}^k(x_{i \text{ sec}}))^i \right)^j \right]^T \cdot \left((\mathbf{k}^k(x_{i \text{ sec}}))^i \right)^j \cdot \left((\mathbf{r}^k(x_{i \text{ sec}}))^i \right)^j \right\}}{\sum_{i \text{ sec}=1}^{n \text{ sec}} \left\{ \left[\left((\delta \mathbf{d}^k(x_{i \text{ sec}}))^i \right)^1 \right]^T \cdot \left((\mathbf{k}^k(x_{i \text{ sec}}))^i \right)^0 \cdot \left((\delta \mathbf{d}^k(x_{i \text{ sec}}))^i \right)^1 \right\}} \leq Etol \quad (4.4)$$

In the test phase of the element implementation the convergence criteria in Eqs. (4.3) and (4.4) proved equally effective. Consequently, the convergence criterion in Eq. (4.3) that is only based on the energy at the element level is selected in this study, since it leads to shorter calculation times.

4.5 Application of Element Loads

A new method for the application of element loads in the context of a flexibility based beam-column element is presented in this section. In the linear elastic range, both, stiffness and flexibility methods yield identical results, so that well established methods for the calculation of equivalent nodal forces based on displacement shape functions can be used. In the nonlinear range, however, different methods need to be used in the two cases. The method proposed in this study follows the nonlinear solution algorithm for applied nodal loads. In the stand-alone program only uniform loads are included in the element. These are

applied during the first load step corresponding to $k=1$. In program FEAP different element load distributions can be included.

The application of element loads is more complex than that of nodal loads, since it requires the explicit inclusion of rigid-body modes. Rigid-body modes have not been considered so far, because they are not necessary for the element formulation. They are implicitly included in the transformation matrix \mathbf{L}_{ele} in Eqs. (2.28), (2.43) and (2.44), which transforms the element displacements \mathbf{p} from the global reference system to the element deformations \mathbf{q} in the local reference system. Transverse element loads induce shear forces in the element that can only be accounted for by the inclusion of rigid-body modes. The effect of rigid body modes in the application of element loads can be included in different ways. In this section the original implementation in the stand-alone program is described, with a brief discussion of the method used in program FEAP.

The procedure for the application of element loads consists of the following steps. For simplicity the structure is assumed to be at an initial unstressed state, with unstressed elements and sections and no nodal loads present. The bending moment and axial force diagrams that result from the application of element loads on a statically determinate simply supported beam are imposed as incremental forces at the sections of the unstressed element without rigid body modes. These section forces induce section deformations that are integrated along the element to yield the corresponding element deformations. The latter violate the compatibility condition at the structure level that element displacements and deformations be equal to zero for zero external loads. Corrective forces need to be applied at the member ends to restore the element deformations to zero, exactly as is the case in the algorithm of the nonlinear element state determination. For nonlinear element behavior under the applied element loads the iterations continue within the element until convergence is achieved. Upon convergence the element resisting forces are computed and the equilibrium is checked at the structure degrees of freedom. Since no external loads are present, the element resisting forces violate the equilibrium at the structure degrees of freedom and their nodal equivalents must be applied with opposite sign to the structure. These nodal forces are, thus, treated as structure unbalanced loads. From this point on the procedure is identical to the application of nodal loads. For nonlinear behavior under the applied element loads Newton-Raphson iterations are necessary to reach the converged state of the structure. At the end of the initial load step the bending moment distribution in the elements is not linear, since it results from the superposition of the generally nonlinear force distribution for the applied element loads with the linear bending moment distribution due to nodal load corrections. If no nodal loads are applied to the structure in the first load step, the final state of the structure

is one with zero nodal forces but non-zero nodal displacements due to the applied element loads.

Rigid-body modes are important in the application of element loads. The beam-column element without rigid-body modes is shown in Fig. 2.1. When the rigid-body modes are included, five additional degrees of freedom appear, as shown in Fig. 4.1, with the relevant forces $\bar{\mathbf{Q}}$ and displacements $\bar{\mathbf{q}}$ expressed relative to the local reference axis. The rigid-body modes are added before checking convergence within the Newton-Raphson iteration i . From equilibrium considerations \mathbf{Q} is first expanded to $\bar{\mathbf{Q}}$ and then the forces at the additional degrees of freedom due to element loads are added to $\bar{\mathbf{Q}}$. The inclusion of rigid body modes is illustrated with a simple example later in the section.

While the discussion about element loads is limited in this report to the case of a uniform load over the entire element and a single concentrated load at distance x_p from the left support, the proposed method is general and can be readily extended to other load types and distributions. In the uniform load case the element loads are grouped in a vector consisting of the load per unit length in the x , y and z directions:

$$\mathbf{W} = [w_x \quad w_y \quad w_z]^T \quad (4.5)$$

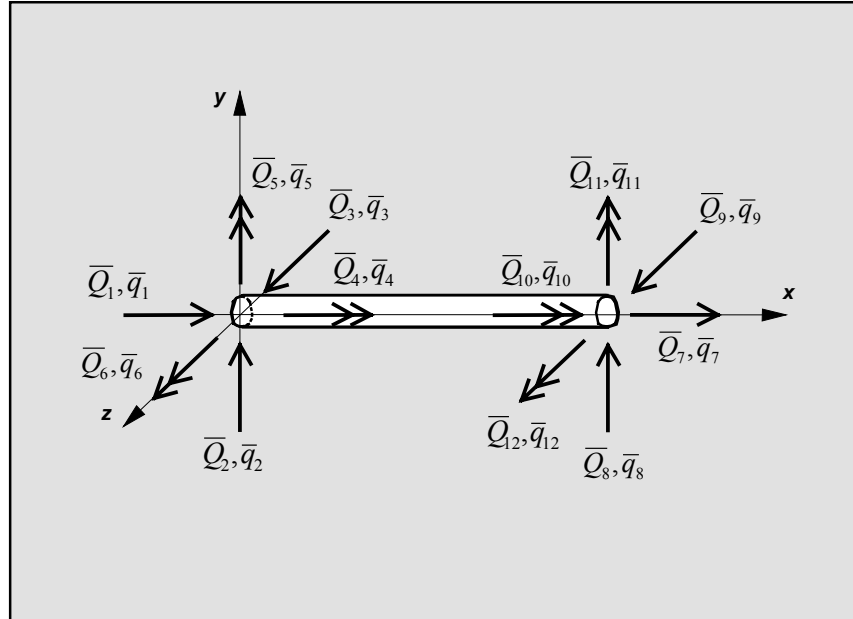


FIGURE 4.1 BEAM-COLUMN ELEMENT WITH RIGID BODY MODES

The sequence of steps for the application of element loads is presented here with the numbering scheme of Appendix A. The inclusion of element loads in the analysis procedure

is accomplished in the first load step, i.e. for $k=1$. For the sake of clarity it is assumed that no other external loads act on the structure in the first load step. A summary of the steps that need to be performed in addition to those in Appendix A for the inclusion of element loads is given below.

(1) *Start of the analysis.*

Set $k=1$.

(2) *Start of Newton-Raphson iterations.*

Set $i=1$.

(3) *Solve the global system of equations and update the structure displacement increments.*

For $k=1$ and $i=1$, there are no external load increments applied to the structure, so that

$$\Delta \mathbf{P}_E^1 = \mathbf{0}$$

$$(\mathbf{P}_U^1)^1 = \mathbf{0}$$

$$(\delta \Delta \mathbf{p}^1)^1 = \mathbf{0}$$

(4) *Compute the element deformation increments.*

The change in the element displacement increments $(\delta \Delta \mathbf{q}^k)^i$ is computed from Eq. (A.3) and the element deformation increments $(\Delta \mathbf{q}^k)^i$ are updated according to Eq. (A.4). For $k=1$ and $i=1$, $(\delta \Delta \mathbf{q}^1)^1 = \mathbf{0}$.

(5) *Start the element state determination. Set $j=1$.*

(6) *Compute the change in the element force increments.*

(7) *Update the element force increments and the element resisting forces.*

(8) *Compute the section force increments.*

In the general case the section force increment $\left((\delta \Delta \mathbf{D}(x)^k)^i \right)^1$ is computed with Eq. (A.9). When $k=1$, $i=1$ and $j=1$, the section force increments due to the applied element loads are computed by

$$\left((\delta \Delta \mathbf{D}^1(x))^1 \right)^1 = \mathbf{b}_g(x) \cdot \mathbf{W} \quad (4.6)$$

where $\mathbf{b}_g(x)$ is a force transformation matrix that relates the applied loads \mathbf{W} to the element forces in a beam without rigid body modes. Details about $\mathbf{b}_g(x)$ are provided later in the section.

(9) *Compute the change in the section deformation increments.*

The change in the section deformation increments $\left(\left(\delta\Delta\mathbf{d}^1(x)\right)^i\right)^j$ is computed according to Eq. (A.12) and the section deformation increments $\left(\left(\Delta\mathbf{d}^1(x)\right)^i\right)^j$ are updated with Eq. (A.13). When $k=1$, $i=1$ and $j=1$, the section deformation increments $\left(\left(\Delta\mathbf{d}^1(x)\right)^1\right)^0$ are not updated so that $\left(\left(\Delta\mathbf{d}^k(x)\right)^1\right)^1 = \mathbf{0}$.

(10) *Compute the fiber deformation increments.*

(11) *Compute the fiber stresses and current tangent moduli.*

(12) *Compute the section tangent stiffness and flexibility matrices.*

(13) *Compute the section resisting forces.*

(14) *Compute the section unbalanced forces.*

(15) *Compute the residual section deformations.*

The residual section deformations $\left(\left(\mathbf{r}^1(x)\right)^i\right)^j$ are computed with Eq. (A.21).

When $k=1$, $i=1$ and $j=1$, the section unbalanced forces are zero and the residual section deformations $\left(\left(\mathbf{r}^1(x)\right)^1\right)^1$ are equal to the section deformation increments $\left(\left(\delta\mathbf{d}^1(x)\right)^1\right)^1$ due to the applied element loads in Eq. (4.6):

$$\left(\left(\mathbf{r}^1(x)\right)^1\right)^1 = \left(\left(\delta\mathbf{d}^1(x)\right)^1\right)^1 \quad (4.7)$$

The section deformations $\left(\left(\delta\Delta\mathbf{d}^k(x)\right)^1\right)^1$ are considered part of the residual section deformations, since they are not compatible with the end deformations of the element that are equal to zero according to step **(4)**.

(16) *Compute the element flexibility and stiffness matrices.*

(17) *Check for element convergence.*

When $i=1$ and $j=1$, the convergence criterion is not satisfied.

- a) *Convergence is achieved*: the rigid body modes are added to the element resisting forces using equilibrium considerations: $(\mathbf{Q}^k)^i \Rightarrow (\bar{\mathbf{Q}}^k)^i$. The effect of element loads is then superimposed

$$(\bar{\mathbf{Q}}^k)^i = (\mathbf{Q}^k)^i + \mathbf{t}_g \cdot \mathbf{W} \quad (4.8)$$

where \mathbf{t}_g is a transformation matrix that depends on the element loads \mathbf{W} and is specified later. *Go to step (18)*.

- b) *Convergence is not achieved*: compute the residual element deformations $\left((\mathbf{s}^k)^i \right)^j$ according to Eq. (A.24), increment j by 1, and *go to step (6)*.

(18) *Compute the structure resisting forces and the new structure stiffness matrix.*

The structure resisting force vector is determined by assembling the element force vectors $(\bar{\mathbf{Q}}^k)^i$ that contain the rigid-body modes.

$$(\mathbf{P}_R^k)^i = \sum_{ele=1}^n (\bar{\mathbf{L}})_{ele}^T \cdot (\bar{\mathbf{Q}}^k)^i \quad (4.9)$$

(19) *Compute the structure unbalance forces.*

(20) *Check for structure convergence.*

(21) *Update force and deformation vectors and complete step $k=1$.*

Since no nodal loads were included in this summary, the analysis consists of just one load step $k=1$. If time varying nodal loads were included, the analysis would involve additional load steps, with only the first step affected by the application of element loads. The discussion was also limited to time independent element loads that are applied during the first load step $k=1$. For time dependent element loads the above procedure should be repeated at every load step k .

The force transformation matrices $\mathbf{b}_g(x)$ and \mathbf{t}_g in Eqs. (4.6) and (4.8), respectively, depend on the element load vector \mathbf{W} . In the uniform load case \mathbf{W} is given by Eq. (4.5) and the transformation matrices are:

$$\mathbf{b}_g(x) = \begin{bmatrix} 0 & \frac{L}{2}x(x-L) & 0 \\ 0 & 0 & \frac{L}{2}x(L-x) \\ L-x & 0 & 0 \end{bmatrix} \quad (4.10)$$

$$\mathbf{t}_g^T = \begin{bmatrix} 0 & 0 & 0 & 0 & 0 & 0 & 0 & 0 & 0 & 0 & -L \\ 0 & 0 & 0 & 0 & 0 & -\frac{L}{2} & -\frac{L}{2} & 0 & 0 & 0 & 0 \\ 0 & 0 & 0 & 0 & 0 & 0 & 0 & -\frac{L}{2} & -\frac{L}{2} & 0 & 0 \end{bmatrix} \quad (4.11)$$

In the case of a concentrated load at a distance x_p from the left node of the beam the element load vector \mathbf{W} contains the load components relative to the three local axes:

$$\mathbf{W} = [P_x \quad P_y \quad P_z]^T \quad (4.12)$$

The corresponding transformation matrices $\mathbf{b}_g(x)$ and \mathbf{t}_g are:

$$\mathbf{b}_g(x) = \begin{bmatrix} 0 & \left(\frac{x_p}{L} - 1\right) \cdot x & 0 \\ 0 & 0 & \left(1 - \frac{x_p}{L}\right) \cdot x \\ 1 & 0 & 0 \end{bmatrix} \quad \text{for } 0 \leq x < x_p \quad (4.13)$$

$$\mathbf{b}_g(x) = \begin{bmatrix} 0 & \left(\frac{x}{L} - 1\right) \cdot x_p & 0 \\ 0 & 0 & \left(1 - \frac{x}{L}\right) \cdot x_p \\ 0 & 0 & 0 \end{bmatrix} \quad \text{for } x_p \leq x \leq L \quad (4.14)$$

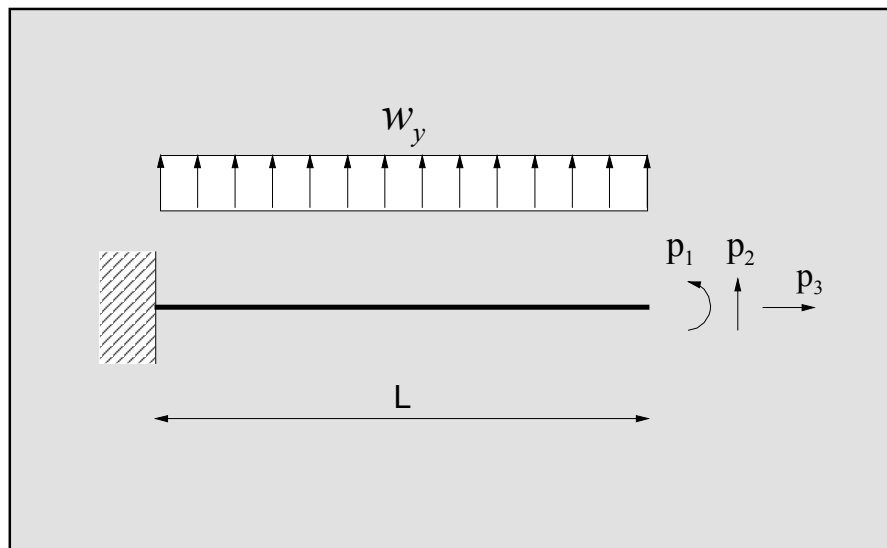


FIGURE 4.2 CANTILEVER WITH UNIFORMLY DISTRIBUTED LOAD

$$\mathbf{t}_g^T = \begin{bmatrix} 0 & 0 & 0 & 0 & 0 & 0 & 0 & 0 & 0 & 0 & -1 \\ 0 & 0 & 0 & 0 & 0 & \left(\frac{x_p}{L}-1\right) & \left(-\frac{x_p}{L}\right) & 0 & 0 & 0 & 0 \\ 0 & 0 & 0 & 0 & 0 & 0 & 0 & \left(\frac{x_p}{L}-1\right) & \left(-\frac{x_p}{L}\right) & 0 & 0 \end{bmatrix} \quad (4.15)$$

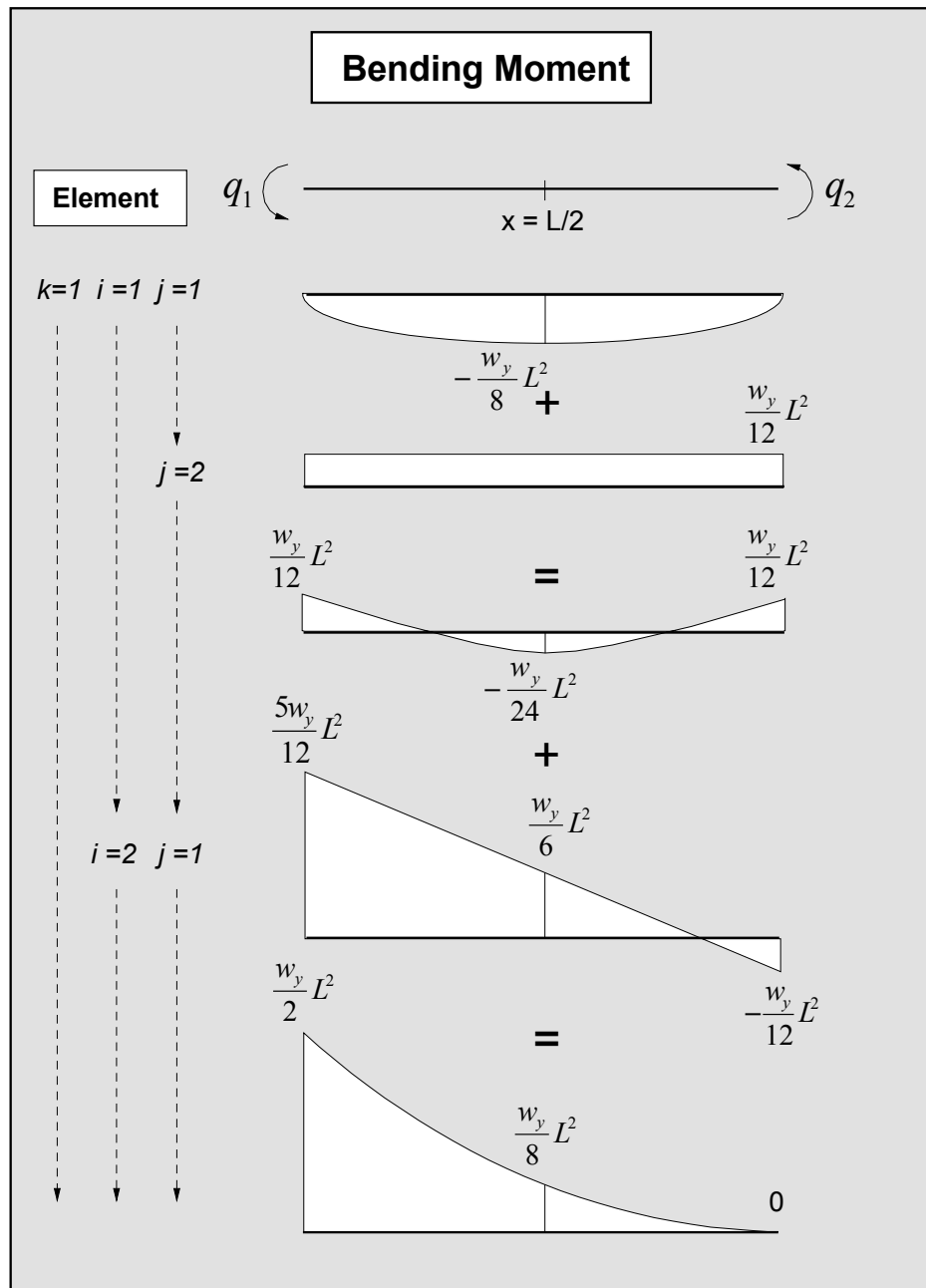


FIGURE 4.3 CANTILEVER WITH UNIFORMLY DISTRIBUTED LOAD:
BENDING MOMENT HISTORY

The procedure for the application of element loads is now illustrated for the case of a linear elastic cantilever in Fig. 4.2 under a uniform load w_y acting in the y direction. The structure has three degrees of freedom at the tip of the cantilever. The element is linear elastic with uniform cross-section and, thus, uniform section stiffness.

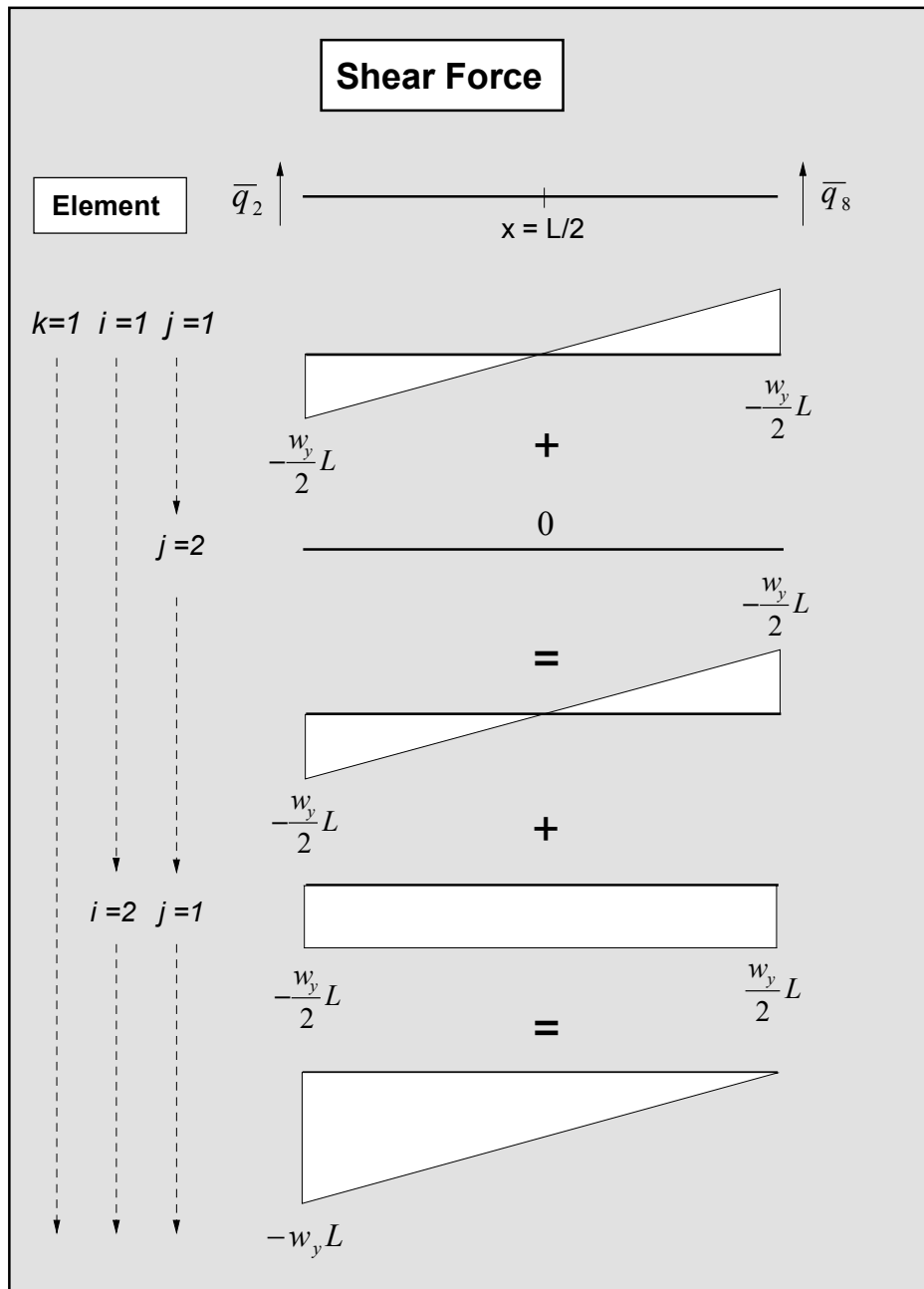


FIGURE 4.4 CANTILEVER WITH UNIFORMLY DISTRIBUTED LOAD:
SHEAR FORCE HISTORY

For the applied loads and for linear elastic behavior the axial displacement p_3 is zero and only two degrees of freedom, p_1 and p_2 , need to be included. Figs. 4.3 and 4.4 show the change of the bending moment and shear force distribution in the element as the iterations for load step $k=1$ progress.

In the very first element iteration, corresponding to $k=1$, $i=1$ and $j=1$, the parabolic bending moment diagram corresponds to a uniform load on a simply supported beam according to Eq. (4.6). The corresponding section deformations are transformed into residual deformations using Eq. (4.7). The section deformations are integrated along the element using Eq. (A.24) to yield the residual element deformations, which become the element deformation increments for the following iteration, corresponding to $k=1$, $i=1$ and $j=2$. The element deformations are transformed into element force increments with Eq. (A.6). For a linear elastic element the element force increments are the well known fixed end moments $w_y L^2 / 12$. At this point the element has converged and its bending moment diagram corresponds to that of a beam that is fixed at both ends. In order to include the rigid body modes according to Eq. (4.8) two vertical forces $w_y L / 2$ are added to the element resisting forces $\bar{\mathbf{Q}}$ and equilibrium is checked at the structure level. Since no external loads are applied to the structure, an unbalanced moment of $w_y L^2 / 12$ and an unbalanced shear force of $w_y L / 2$ now act at the free end of the cantilever. These need to be applied as nodal forces with opposite sign in the next Newton-Raphson iteration corresponding to $k=1$ and $i=2$ in order to restore equilibrium at the structure degrees of freedom. During the first element iteration of the new Newton-Raphson iteration, i.e. for $k=1$, $i=2$ and $j=1$, a linear bending moment distribution is added to the existing moments in the cantilever, as shown in Fig. 4.3. Since the cantilever is linear elastic, element convergence is reached immediately. Because convergence is also reached at the structural level, the analysis is complete. The final bending moment diagram is the well known parabola shown at the bottom of Fig. 4.3. The evolution of all element and structural vectors for this example is given in detail in Appendix B.

The selected example is very simple, since the element is linear elastic and has a uniform cross section. The proposed procedure for the application of element loads is, however, general and can be applied for any material behavior and for any distribution of element loads. In the general case of nonlinear material behavior and non-uniform cross section properties of the element more iterations at the element and structure level are necessary for satisfying the equilibrium and compatibility requirements under the applied element loads.

The same procedure is also used in the implementation of the beam-column element in program FEAP, but the rigid body modes are included in a different way. In the stand alone program, no forces due to element loads are applied at the structure degrees of freedom, so that on convergence no forces act at the structural nodes. In other words the element loads are treated as an initial force distribution. In program FEAP the shear forces that result from the applied element loads when the rigid body modes are included according to Eq. (4.8) are applied as forces at the structure degrees of freedom. The remainder of the process is identical to that described previously, except that Eq. (4.8) is now bypassed. This alternative scheme is more similar to the procedure that is typically followed in a stiffness-based element where element loads are transformed into equivalent nodal loads.

In the implementation of this procedure in program FEAP for the linear elastic cantilever under uniform load the element has non zero end deformations $\left((\delta\Delta\mathbf{Q}^1)^1\right)$ during the first iteration ($k=1$, $i=1$ and $j=1$) caused by a vertical force of $(\mathbf{P}_2^1)^1 = -w_y L/2$. The parabolic bending moment diagram for a simply supported beam under a uniform load is then added to the linear diagram that results from the non zero end deformations $\left((\delta\Delta\mathbf{Q}^1)^1\right)$. This minor change facilitates the implementation of the element load procedure in an existing finite element program.

4.6 Material Softening and Unloading in Reinforced Concrete Members

The nonlinear solution procedure that is proposed in the present study is particularly suitable for modeling the softening behavior of reinforced concrete members. Even though the algorithm is described here with reference to a fiber beam-column element, the procedure can be used in structural members with any continuous nonlinear or piece-wise linear section force-deformation relation. Spacone et al. (1992) discuss the implementation of the method in the context of a differential moment-curvature relation. The method can also be extended to the nonlinear analysis of other types of systems. The extension of the theory to systems made up of several components in series and/or in parallel suitable for the nonlinear analysis of prestressed concrete members with bonded or unbonded, internal or external tendons is the subject of another current study.

In the discussion about softening it is important to underline the distinction between softening of the entire structure and softening of certain members in a stiffening structure. Softening of the entire structure is very difficult to simulate from a numerical standpoint and

the general Newton-Raphson method is not suitable for the task. Special iterative strategies, such as the arc-length method, or ad-hoc procedures, such as displacement control analysis, should be used in this case, but such discussion is beyond the scope of the present study.

The state determination process of the nonlinear analysis of a structure involves the application of end displacements on the structural elements. Consequently, tracing the softening response of elements under displacement control conditions is computationally easier than tracing the softening response of the structure. Even so, element softening is a very challenging numerical problem and there is growing interest in the development of a reliable solution method, especially for the response analysis of reinforced concrete structures under strong ground motions. Element softening plays an important role in the assessment of global and local ductility demands of structures under intense ground shaking when some members might reach their capacity and start experiencing strength softening. While force redistribution might lead to an increase of the lateral load capacity of the structure, the deformation ductility demand of softening members might be so high, that partial or total collapse will take place before the structure reaches its lateral load capacity.

From a theoretical standpoint the flexibility method is ideally suited for modeling the softening behavior of reinforced concrete elements. When an element exhibits strain softening at the end sections, the moments decrease along the element and non-softening sections unload to satisfy equilibrium. Since in the absence of element loads the moment distribution along the element is always linear, this behavior is captured by the flexibility method. Such softening and unloading behavior is much harder to represent with a classical stiffness-based two-node element in which the curvature distribution is assumed linear. In such case several elements are needed to approximate the actual nonlinear curvature distribution and numerical difficulties can, nonetheless, arise as discussed in Section 1.2.3 and Fig. 1.9, which is excerpted from Zeris and Mahin (1988). A comparison of the two types of element formulation is presented in Spacone et al. (1992).

The application of the proposed solution algorithm to the case of a softening element is first discussed from a theoretical standpoint and, subsequently, illustrated with a simple example. For the sake of simplicity superscript k that denotes the current load step is omitted in the following discussion. The discussion starts when the structure is at the beginning of Newton-Raphson iteration i and with the assumption that the stiffness matrices \mathbf{K}^{i-1} of all elements at the end of the last iteration are positive definite. At the start of the new iteration the deformation increments $\Delta \mathbf{q}^i$ are imposed on the elements and the resulting element force increments $(\delta \Delta \mathbf{Q}^i)^j$ are converted to section force increments $(\delta \Delta \mathbf{D}^i(x))^j$ through

force interpolation functions. The section force increments $(\delta\Delta\mathbf{D}^i(x))^j$ cause section deformation increments according to Eq. (A.12) which are added to the previous section deformations to yield the new total deformations $(\mathbf{d}^i(x))^j$. Consider the case that upon completion of the section state determination for the new total deformations $(\mathbf{d}^i(x))^j$ one section exhibits softening, so that its stiffness changes from positive definite $(\mathbf{k}^i(x))^{j-1}$ to negative definite $(\mathbf{k}^i(x))^j$. The unbalanced forces $(\Delta\mathbf{D}_U^i(x))^j$ are positive, while the residual section deformations

$$(\mathbf{r}^i(x))^j = (\mathbf{k}^i(x))^j \cdot (\mathbf{D}_U^i(x))^j$$

are negative. The element stiffness is updated with Eqs. (A.22) and (A.23). Assuming that the entire element stiffness has also changed from positive definite $(\mathbf{K}^i)^{j-1}$ to negative definite $(\mathbf{K}^i)^j$ and that Eq. (A.24) also returns negative residual deformations $(\mathbf{s}^i)^j$ at the element ends, it is concluded from Eq. (A.6) that the new force increments $(\delta\Delta\mathbf{Q}^i)^{j+1}$ are also negative. The element has, thus, detected the fact that, under the new deformations \mathbf{q}^i , it can resist a smaller force than that predicted with the stiffness of the previous converged state. The negative unbalanced forces at the element ends are converted to negative section force increments $(\delta\Delta\mathbf{D}^i(x))^{j+1}$ based on the force interpolation functions and the corresponding section deformation increments $(\delta\Delta\mathbf{d}^i(x))^{j+1}$ are obtained with Eq. (A.12). At the section that exhibited softening in the previous iteration j the sign of the deformation increments depends on the size of the positive increments $(\mathbf{f}^i(x))^j \cdot (\delta\Delta\mathbf{D}^i(x))^{j+1}$ relative to the negative residual deformations $(\mathbf{r}^i(x))^j$. In either case it is important to note that the section resisting force is reduced.

Once the element converges, it is very likely that the current element stiffness matrix is negative definite. The structure stiffness matrix is assembled from all element stiffness matrices and another load increment is applied to the structure. Since the structure stiffness matrix is still positive definite, the structure is capable of resisting a higher load, even though one element is softening. The new deformation increments $\Delta\mathbf{q}^{i+1}$ at the element ends give rise to negative force increments in the softening element as a result of the multiplication of the negative stiffness matrix \mathbf{K}^i with positive deformation increments $\Delta\mathbf{q}^{i+1}$. Thus, the softening element continues to unload, while the hardening members now resist a greater

portion of the applied load increment. At the same time the softening element contributes a larger portion of the deformation of the structure.

This brief description underlines the fact that no special steps need to be taken for the treatment of softening elements in the proposed analysis method. Within the algorithm the transition from a positive to a negative element stiffness matrix does not have to be detected and, both, positive and negative deformation increments, deformation corrections, force increments, unbalanced forces, and, finally, stiffness and flexibility matrices at the section as well as at the element level can be accommodated. Consequently, unloading of elements is also treated without requiring a reduction of load step size or special computational steps.

The advantage of the proposed method in the analysis of softening systems can be best illustrated with a simple example that is shown in Fig. 4.5. It consists of two extensional springs connected in series. Spring A is linear elastic, while spring B is bilinear elastic strain softening. In a series model the system deformation is the sum of the component deformations, while the element forces are equal to the force applied on the entire system. For the two spring system and with the notation of Fig. 4.5 these conditions can be written as:

$$Q = D_A = D_B$$

$$q = q_A + q_B$$

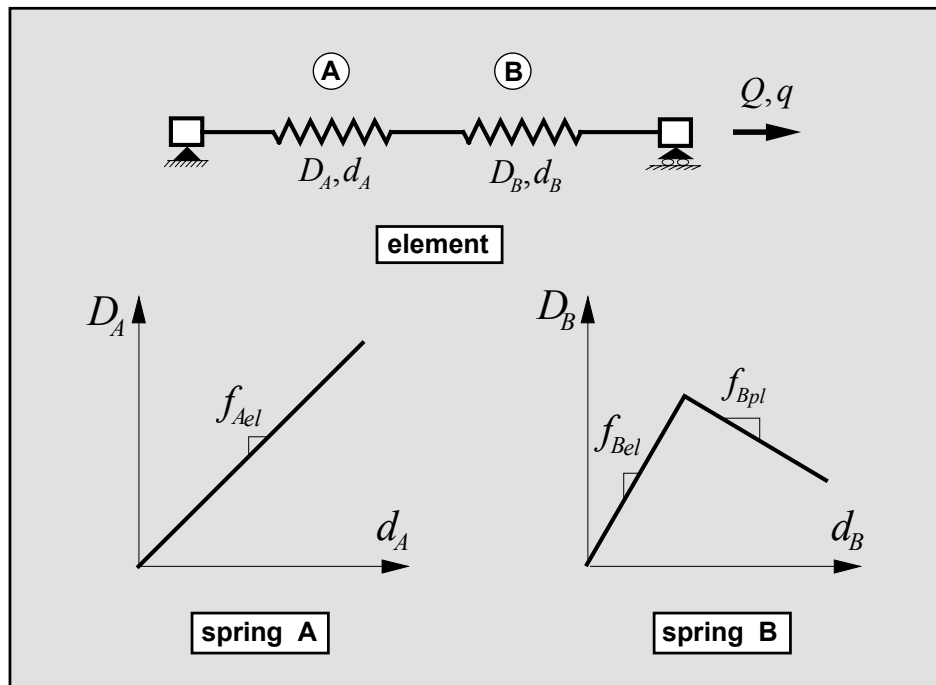


FIGURE 4.5 A SIMPLE SOFTENING ELEMENT: TWO SPRINGS IN SERIES

It can be readily seen that the system flexibility F is the sum of the spring flexibilities, i.e.:

$$F = f_A + f_B$$

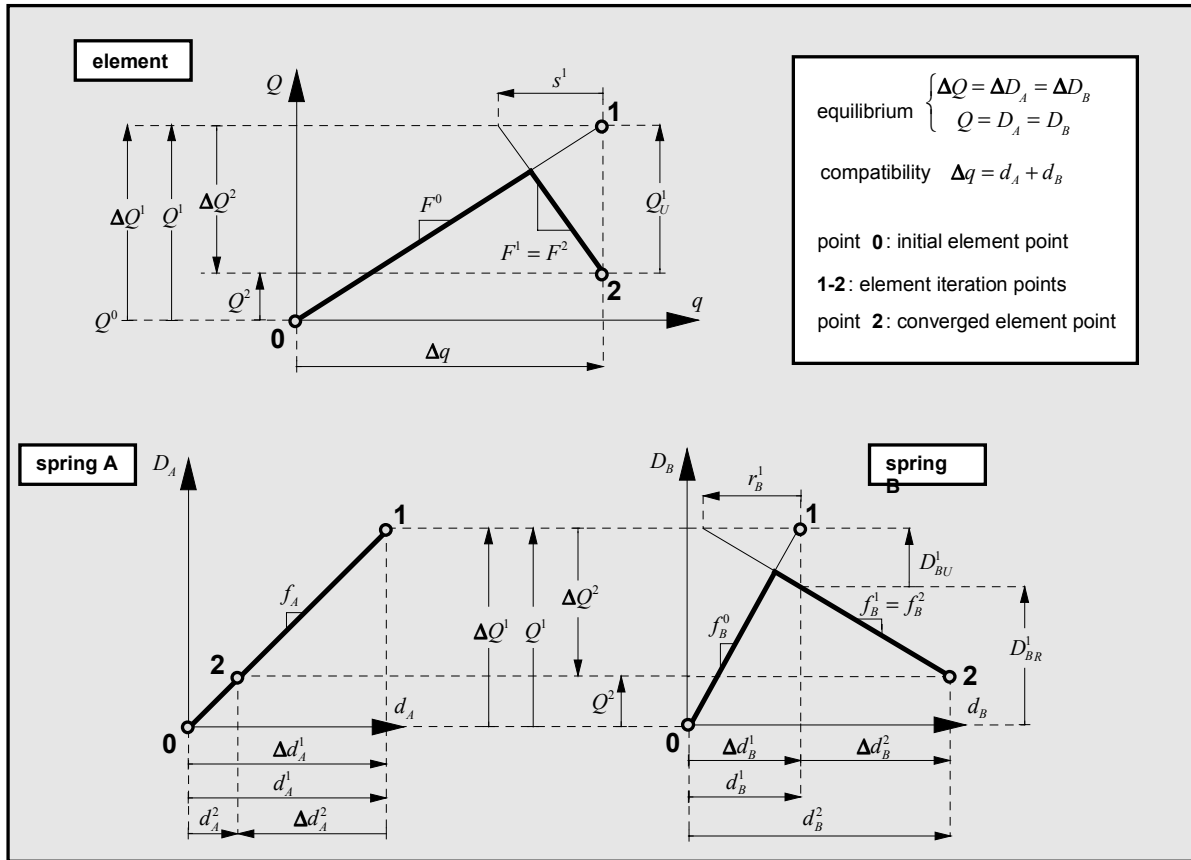


FIGURE 4.6 FORCE-DEFORMATION HISTORY IN THE SPRING SYSTEM

It is interesting to note the similarities between a series system and the beam-column element that is proposed in the present study: the equilibrium condition $Q = D_A = D_B$ amounts to a constant force distribution within the two spring element and is equivalent to Eq. (2.6) which defines a linear bending moment and a constant axial force distribution for the beam-column element. Similarly, the deformation of the two spring element is the sum of its components much like the deformations of the beam-column element are obtained by integration of the section deformations. To complete the analogy the analysis of the two spring system is performed for a given deformation increment Δq , for which the corresponding resisting force increment ΔQ is sought. Since the example is limited to the analysis of a single displacement increment and the behavior of the system is piecewise linear, there is no need for the use of superscripts k and i . An analysis summary is given in Fig. 4.6 with only two element iterations needed for convergence. Appendix C contains the complete solution process.

At the completion of the iterative analysis process the equilibrium and the compatibility of the system are strictly satisfied, as is the case for the proposed beam-column element. The force-displacement relation of the component springs is also strictly satisfied because of the piecewise linear nature of the constitutive relation. This is not the case, however, in a nonlinear system where the constitutive relation can only be satisfied within a specified tolerance.

It is interesting to note that the proposed analysis method does not need to detect the displacement level that corresponds to the stiffness change of the second spring. This is different from the procedure followed in the event-to-event solution strategy where each stiffness change needs to be traced in the search for the solution. While tracing each stiffness change may give a better estimate of the system response, the number of events required to reach convergence can be very large for a system with many components, such as a reinforced concrete column with several control sections and many fibers in each section. In this case the computation by an event-to event strategy becomes prohibitively expensive. Moreover, it is often advantageous, both, from a physical and a computational standpoint to specify continuous constitutive relations for which an infinite number of events would have to be accepted in an event-to event solution strategy.

CHAPTER 5

APPLICATIONS

5.1 General

A series of examples are presented in this chapter to demonstrate the ability of the proposed element to describe the hysteretic behavior of reinforced concrete beams and columns under imposed cyclic load and deformation histories. The analytical results in this chapter are obtained with the stand alone program **BEAMCOL** whose numerical implementation was discussed in the previous chapter.

When experiments are conducted, loads are applied to the specimen in a controlled fashion and the resulting displacements and deformations are measured. Typically, members that exhibit a relatively high stiffness are tested by controlling the force applied on the specimen. Once significant damage and stiffness deterioration of the specimen sets in, the test is continued under displacement control, whereby the applied forces are carefully adjusted in order to produce a given displacement history. In the numerical simulation of experiments a single method of load application has to be used for the entire analysis, since most finite element programs do not permit changes in the boundary conditions during the analysis. Numerical simulations under force control provide good results when the member stiffness is high, but fail to trace the nonlinear behavior near the ultimate strength of the member and the post-peak response. For this reason the numerical simulations in this chapter were conducted under displacement control.

Three tests have been selected for the verification of the proposed beam-column element. The tests comprise two reinforced concrete cantilever beams and a reinforced concrete beam-column. The first beam is selected for the study of the moment-curvature behavior of a single section and for the study of the effect of different tolerance measures and displacement increments on the accuracy of the analytical results. The second specimen is a cantilever beam under uniaxial bending and the third specimen is a cantilever column that was subjected to a constant axial force in combination with uniaxial and biaxial bending, both, monotonic and cyclic. For each test the geometry and the material characteristics of the specimen as well as the parameters of the material models for concrete and reinforcing steel are given. The material parameters are obtained from available experimental information

from coupon or concrete cylinder tests. Finally, the load and displacement history of the specimen and the boundary conditions used in the analysis are also specified.

The chapter concludes with a parameter study of the third specimen, the cantilever column. This study aims at investigating the sensitivity of the proposed model to the number of control sections within the column, both, in the presence and in the absence of an axial compressive force. It is important in this regard to establish whether the analytical results converge to the actual solution as the number of control sections in the column increases and, if so, to determine the smallest number of column control sections that yield sufficiently accurate results.

5.2 Moment-Curvature of a Section

Kaba and Mahin (1983) proposed a nonlinear method for describing the hysteretic behavior of reinforced concrete sections as was briefly discussed in the literature survey of Chapter 1. Their model is compared with the experimental response of a concrete cantilever beam tested by Kent (1969). The same experimental results are used here to test the validity of the beam-column element proposed in this study. The geometry of the specimen and the geometry of the cross section as well as the discretization used by Kaba and Mahin, are shown in Fig. 5.1 and summarized in Table 5.1. The material parameters for the concrete and reinforcing steel models are summarized in Tables 5.2 and 5.3, respectively.

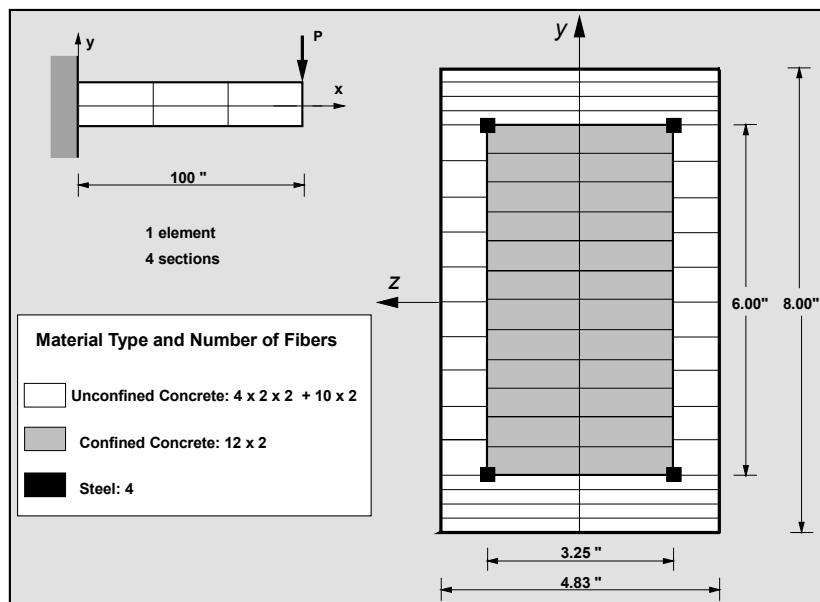


FIGURE 5.1 STRUCTURE DISCRETIZATION FOR KENT BEAM # 24

Kent Beam #24				
number of beam-column elements = 1				
Length of Element = 100 in.			Number of Sections = 4	
Number of fibers				
Section type	Unconfined Concrete	Confined Concrete	Steel	Total
I	18x2	12x2	4	64

TABLE 5.1 KENT BEAM #24 DISCRETIZATION

Concrete Properties				
Concrete type	E_c [ksi]	f'_c [ksi]	ϵ_0	ϵ_u
Unconfined (I)	3605	-6.95	-0.0027	-0.00292
Confined (I)	3605	-6.95	-0.0027	-0.03810

TABLE 5.2 MATERIAL PROPERTIES OF CONCRETE

Steel Properties			
Steel type	E_s [ksi]	f_y [ksi]	Strain hard. ratio
Steel type I (I)	29,000	48.4	0.0042

TABLE 5.3 MATERIAL PROPERTIES OF STEEL

The cantilever beam is loaded with a vertical load at the free end and the moment-curvature relation at the built-in section is studied. Fig. 5.2 shows, both, Kent's experimental results and the analysis with the model of Kaba-Mahin. This example is also selected for the study of the effect of tolerance measures and size of displacement increments on the accuracy of the analytical results.

In the examples presented in this chapter the structure and element tolerance are identical, which implies $TF = 1$, where TF is the parameter introduced in Section 4.4 to relate the structure with the element tolerance. Consequently, the general term tolerance will be used in the remainder of the chapter. Three sets of tolerance values have been selected in the analysis of Kent's cantilever beam in Fig. 5.1. Recalling from Section 4.4 that EAT and ERT stand for Element Absolute Tolerance and Element Relative Tolerance, respectively, the three sets of tolerance values are defined in the following table:

<i>Tolerance definition</i>		
small	$EAT = 1 \text{ kip}$	$ERT = 0.01\%$
medium	$EAT = 100 \text{ kips}$	$ERT = 1\%$
large	$EAT = 1000 \text{ kips}$	$ERT = 10\%$

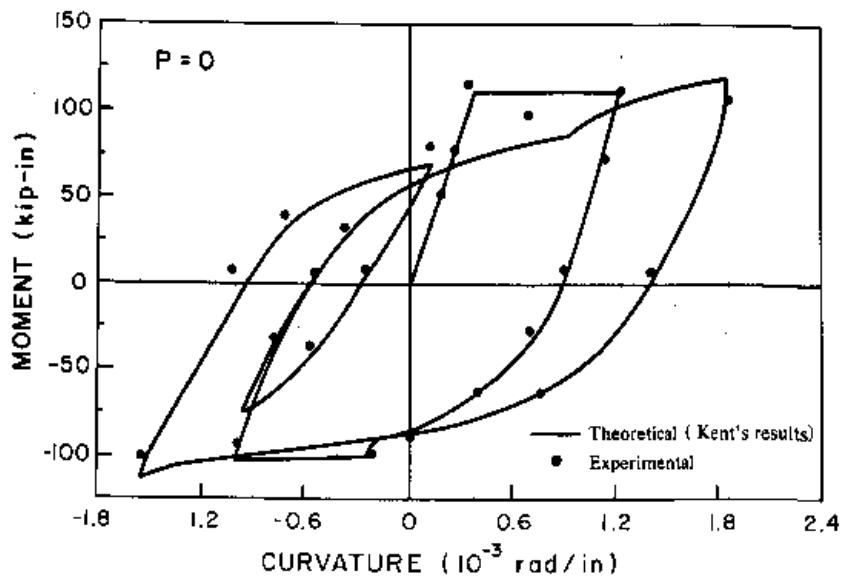


FIGURE 5.2 MOMENT-CURVATURE RELATION FROM KENT'S EXPERIMENT AND KABA-MAHIN ANALYSIS (KABA AND MAHIN 1983)

Fig. 5.3 shows the moment-curvature history obtained with program BEAMCOL. The results show very good agreement with those presented in Fig. 5.2. These results are obtained with a small load step size and with the three sets of tolerance values defined above. Small and medium tolerance values yield very similar results while a large tolerance value produces a slight overestimation of section strength. In a parallel parametric study on the effect of size of displacement increment it is observed that the accuracy of the results is not particularly affected by the tolerance value for small and medium step size corresponding to displacement increments of 0.05 in. and 0.5 in. at the cantilever tip, respectively. For a large step size, which corresponds to only four load steps per half cycle, a small tolerance has to be imposed to achieve convergence.

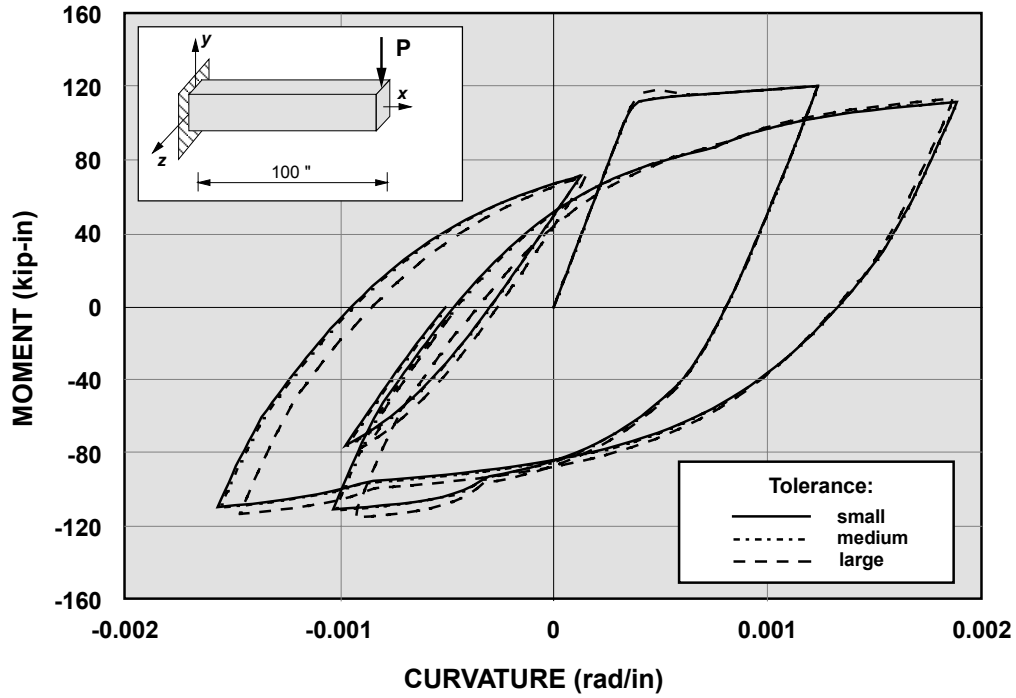


FIGURE 5.3 EFFECT OF TOLERANCE ON MOMENT-CURVATURE RELATION AT THE BUILT-IN SECTION

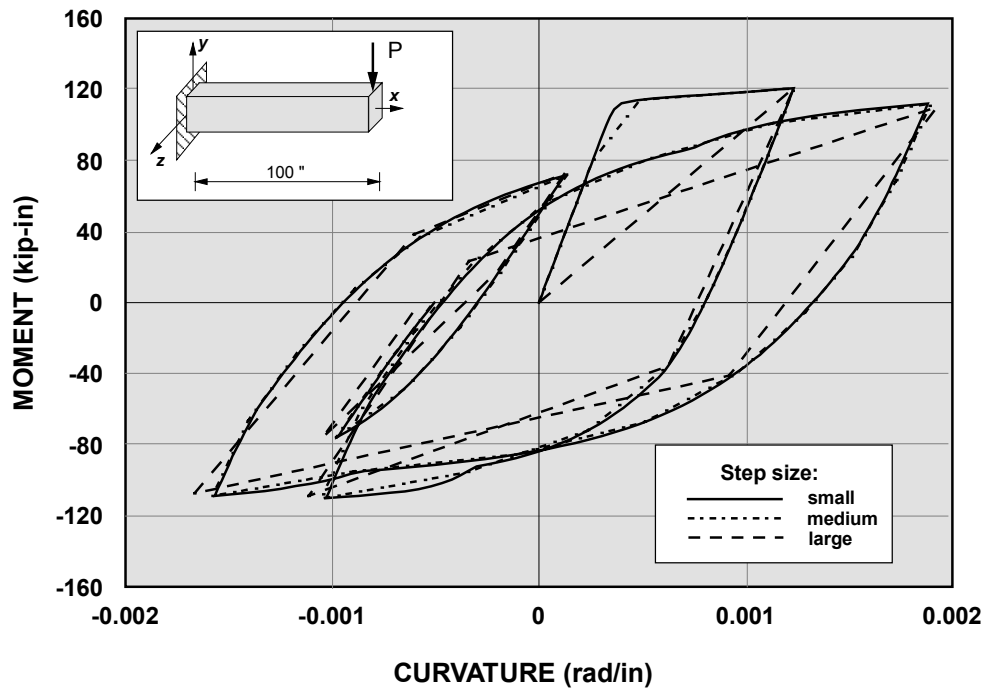


FIGURE 5.4 EFFECT OF LOAD STEP SIZE ON MOMENT-CURVATURE RELATION AT THE BUILT-IN SECTION FOR SMALL TOLERANCE

Fig. 5.4 shows the effect of displacement step size on the moment-curvature relation for a small tolerance. As the load step size increases, the number of element iterations per load step also increases. A measure of the algorithm efficiency is the total number of element iterations for a particular load history. For small load steps the total number of element iterations is large, even though only one or two iterations are needed for convergence in each step. In this case the total number of element iterations is essentially proportional to the number of load steps. As the load step size increases, more iterations are needed for convergence in each load step. This increase in the number of iterations in each load step is, however, not proportional to the corresponding increase of load step size, since not every load step involves significant nonlinear behavior and since the force unbalance decreases exponentially in the proposed algorithm. Consequently, the total number of iterations decreases with increasing load step size and, thus, leads to a more economic analysis. Unfortunately, this gain in economy is outweighed by numerical problems of solution flip-flop and lack of convergence in a few steps in the case of medium or large tolerance values under a large displacement increment. Thus, the selection of the appropriate tolerance value and load step size requires skill and experience or an intelligent, automatic load step subdivision algorithm. The need to accurately trace the load-deformation behavior of a structure imposes considerable restrictions on load step size, so that this issue loses much of its significance in practical cases.

5.3 Uniaxial Bending of Cantilever Beam

An extensive series of tests on rectangular and T-shaped reinforced concrete beams was conducted by Ma, Bertero and Popov (1976). The rectangular beam denoted as R-1 is used in the correlation studies. The geometry of the specimen and the discretization of the cross section are shown in Fig. 5.5. The relevant geometric data are summarized in Table 5.4, while Tables 5.5 and 5.6 contain the material parameters for the concrete and reinforcing steel models, respectively. These parameters are derived from available experimental information from coupon and concrete cylinder tests. In simulating the behavior of confined concrete the model by Scott et al. (1982) was used. In this model the degree of confinement depends on the volumetric ratio of transverse reinforcement relative to the confined concrete core ρ_s , which for beam R-1 was estimated at 0.60%. In the study of the hysteretic behavior of the cantilever beam the model consists of two elements: a beam-column element for the cantilever itself and a very stiff linear spring that is oriented in the load direction at the free end of the cantilever for the analysis under displacement control.

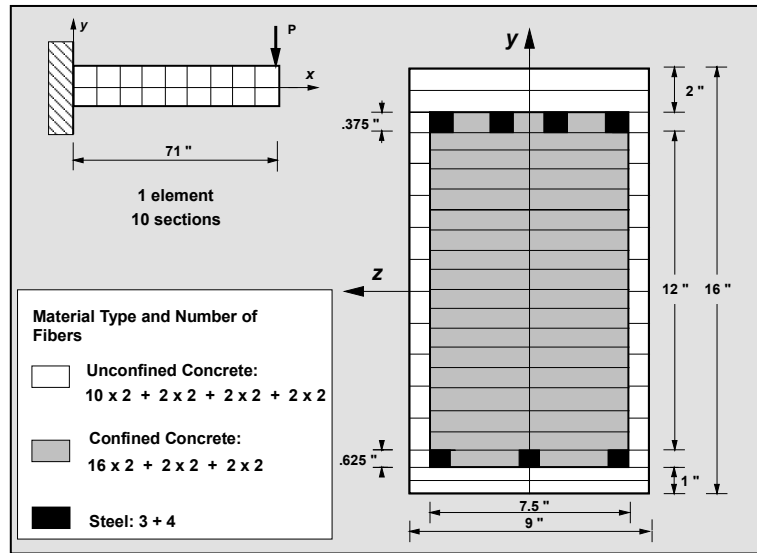


FIGURE 5.5 STRUCTURE DISCRETIZATION FOR BEAM R-1

Cantilever Beam R-1				
Number of beam-column elements: 1				
Length of Element = 71 in.		Number of Sections = 10		
Number of fibers				
Section type	Unconfined Concrete	Confined Concrete	Steel	Total
I	16x2	20x2	7	79

TABLE 5.4 BEAM R-1 DISCRETIZATION

Concrete Properties				
Concrete type	E_c [ksi]	f'_c [ksi]	ϵ_0	ϵ_u
Unconfined	3980	-5.07	-0.00200	-0.003
Confined	3980	-5.43	-0.00214	-0.069

TABLE 5.5 CONCRETE MATERIAL PROPERTIES

Steel Properties			
Steel type	E_s [ksi]	f_y [ksi]	Strain hard. ratio
Steel type 1	29,000	66.5	0.0085

TABLE 5.6 STEEL MATERIAL PROPERTIES

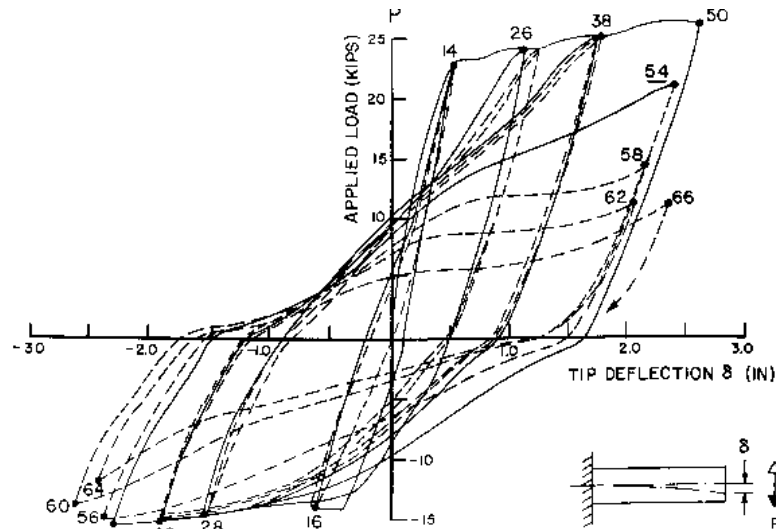


FIGURE 5.6 EXPERIMENTAL TIP LOAD-DISPLACEMENT RELATION FOR BEAM R-1 (MA ET AL. 1976)

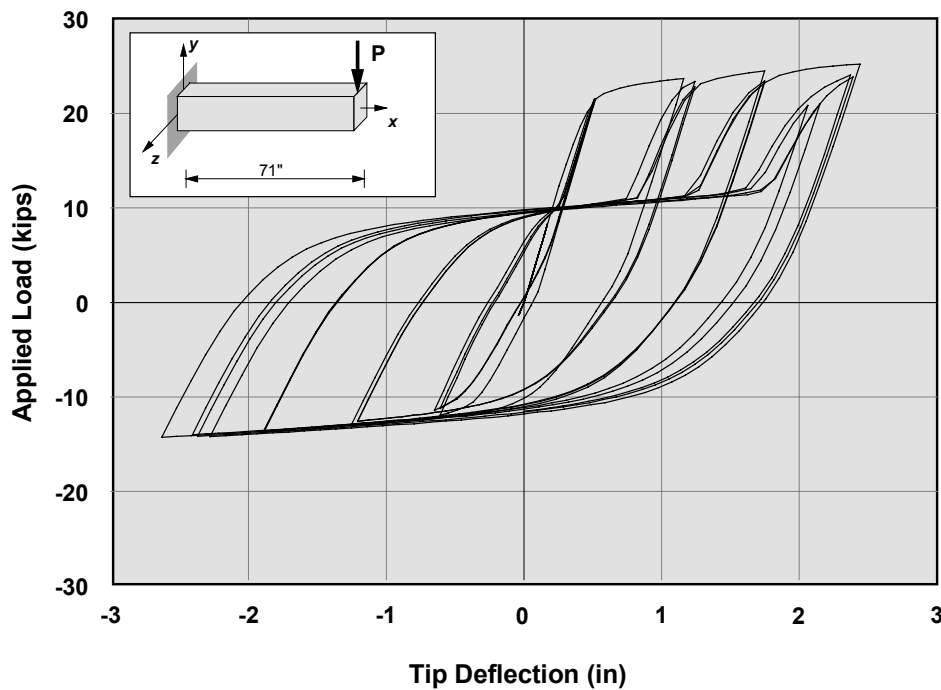


FIGURE 5.7 ANALYTICAL LOAD-TIP DISPLACEMENT RELATION FOR BEAM R-1

In the numerical simulation of the experiment the displacements measured at the tip of the cantilever are imposed on the model by applying a force that is the product of the end displacement with the large stiffness of the linear spring. The selected tolerance values for the

analysis are $EAT = 0.01$ kip and $ERT = 1\%$ and the tip displacements are imposed in increments of 0.1 in.

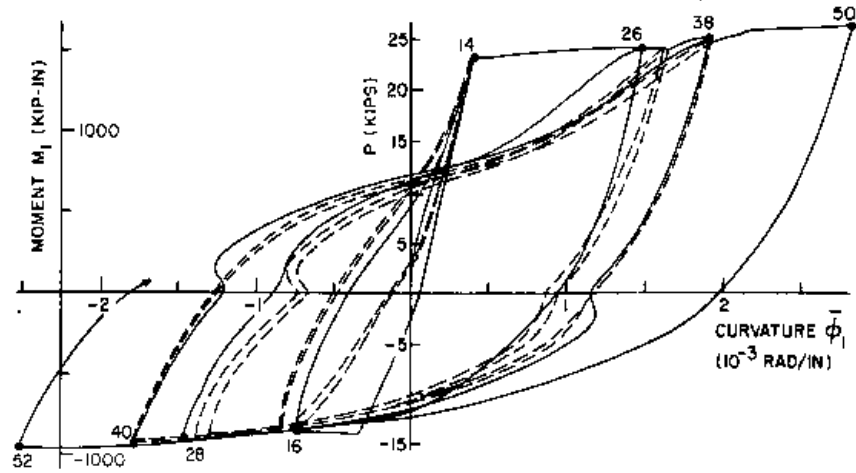


FIGURE 5.8 EXPERIMENTAL MOMENT-CURVATURE RELATION
NEAR THE BUILT-IN SECTION OF BEAM R-1 (MA ET AL. 1976)

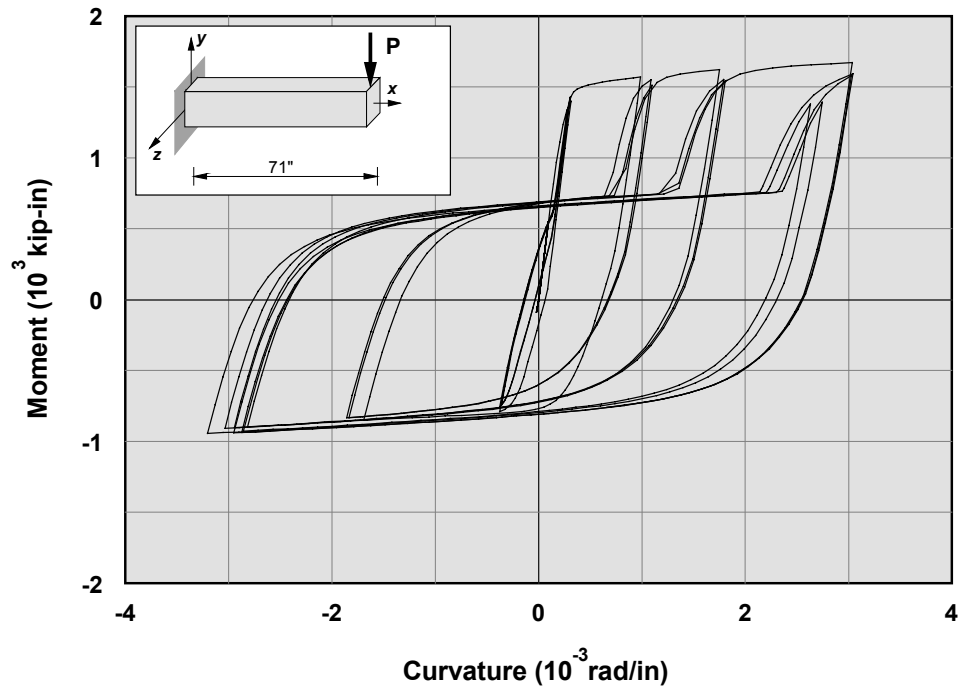


FIGURE 5.9 ANALYTICAL MOMENT CURVATURE RELATION
NEAR THE BUILT-IN SECTION OF BEAM R-1

The displacements at the tip of the cantilever are caused by flexural deformations, shear deformations, bond-slip between concrete and reinforcing steel and the rotation at the built-in section due to reinforcing bar pull-out from the column stub. The proposed model, however, only accounts for flexural deformations. As a result, the analytical results in Fig 5.7 deviate from the experimental data in Fig. 5.6. The discrepancy is small before yielding at the built-in section of the cantilever takes place, but increases in the post-yield cycles and is particularly notable during reloading in the "pinching" of the experimental hysteretic behavior due to shear and bond-slip. The analytical and experimental moment-curvature relation near the built-in section of the cantilever are compared in Figs 5.8 and 5.9. The agreement is much better in this case, since the other sources of inelastic deformation do not affect the hysteretic section response that much.

5.4 Uniaxial and Biaxial Bending of a Column under Axial Compression

A series of columns that were subjected to different load histories of uniaxial and biaxial bending under constant axial force were studied by Low and Moehle (1987). The geometry of the two column specimens that were selected for the correlation studies is shown in Fig. 5.10 which also shows the geometry of the cross section as well as the discretization used in the analytical studies. The relevant geometric data are summarized in Table 5.7.

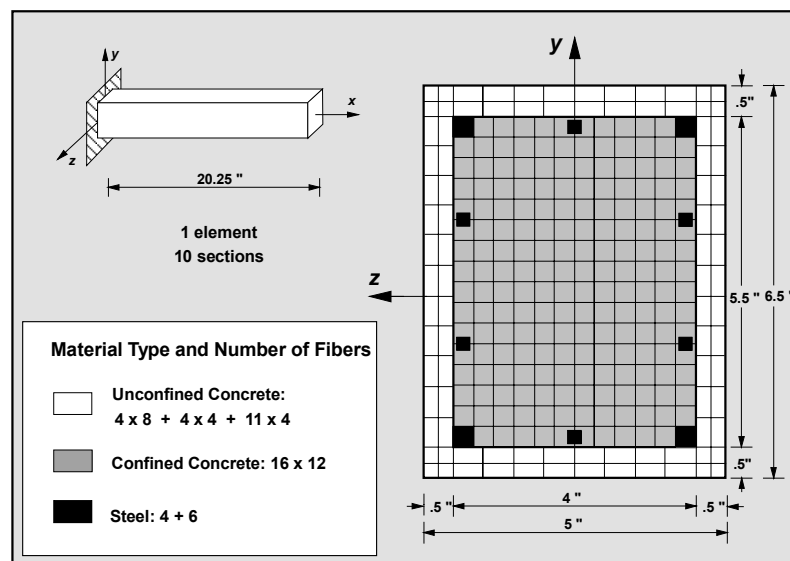


FIGURE 5.10 STRUCTURE MESH FOR LOW-MOEHLE SPECIMEN COLUMNS #1 AND #2

The model consists of a single beam-column element that contains two different types of section in accordance with the amount of transverse reinforcement in the specimen. The lower half of the column has a volumetric ratio of transverse reinforcement relative to the

confined concrete core ρ_s equal to 2%. This corresponds to section type I. The upper half of the column has a volumetric ratio of transverse reinforcement relative to the confined concrete core ρ_s equal to 1.3% and corresponds to section type II. The material parameters for the concrete and reinforcing steel models are summarized in Tables 5.8 and 5.9, respectively. These parameters are derived from available experimental information from coupon and concrete cylinder tests. In simulating the behavior of confined concrete the model by Scott et al. (1982) was used.

Low-Moehle specimens #1 and #2				
Number of beam-column elements: 1				
Length of Element = 20.25 in.			Number of Sections = 4	
Number of fibers				
Section type	Unconfined Concrete	Confined Concrete	Steel	Total
I and II	4x8+15x4	16x12	10	294

TABLE 5.7 LOW-MOEHLE SPECIMEN COLUMNS #1 AND #2 DISCRETIZATION

The tolerance values selected for the analysis are $EAT = 0.01$ kip and $ERT = 1\%$. The numerical simulations are conducted under displacement control and the lateral tip displacements along the y and z axis are imposed in increments ranging from 0.01 to 0.04 in.

The first comparison involves Low and Moehle specimen #1. The loading of this specimen consists of a cyclic lateral force along the weak axis z at the free end of the cantilever and an axial compression of 10 kips that is kept constant during the experiment. The analytical and experimental results for specimen #1 are compared in Fig. 5.11, which shows the lateral force versus tip displacement response of the specimen in the z -direction. The agreement between experimental and analytical results is good even though the model is clearly stiffer than the specimen, particularly, in the early stages of the hysteretic response. The stiffness discrepancy at the very early response stage can be attributed to the initial cracking of the specimen due to shrinkage and temperature. The discrepancy in hysteretic behavior under large displacement reversals, on the other hand, can be attributed to the significant effect of bond-slip and pull-out of the longitudinal reinforcing bars from the foundation. Since the numerical simulations are conducted under displacement control this effect is only evident in the "pinching" of the hysteretic response and the earlier loss of strength of the specimen relative to the model.

Concrete Properties				
Concrete type	E_c [ksi]	f'_c [ksi]	ϵ_0	ϵ_u
Unconfined (Sections I and II)	3700	-5.30	-0.00200	-0.0119
High Confinement (Section I)	3700	-6.53	-0.00246	-0.3710
Medium Confinement (Section II)	3700	-6.11	-0.00231	-0.2330

TABLE 5.8 CONCRETE MATERIAL PROPERTIES

Steel Properties			
Steel type	E_s [ksi]	f_y [ksi]	Strain hardening ratio
Steel type 1	29,000	64.9	0.0067
Steel type 2	29,000	64.4	0.0038
Steel type 3	29,000	73.1	0.0050

TABLE 5.9 STEEL MATERIAL PROPERTIES

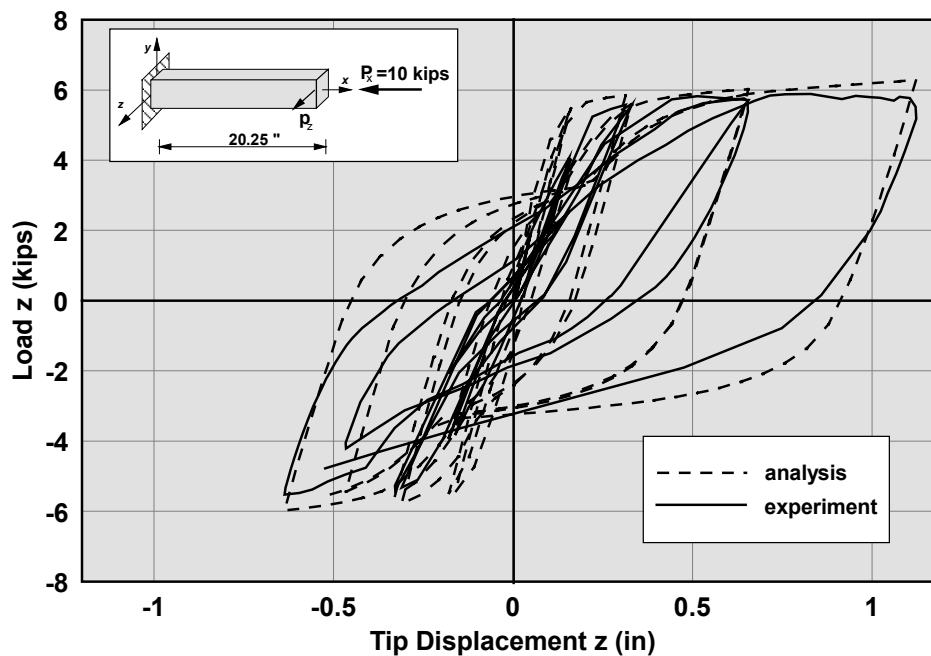


FIGURE 5.11 TIP LOAD-DISPLACEMENT RELATION IN THE z -DIRECTION FOR LOW-MOEHLE SPECIMEN #1: EXPERIMENTAL AND ANALYTICAL RESULTS

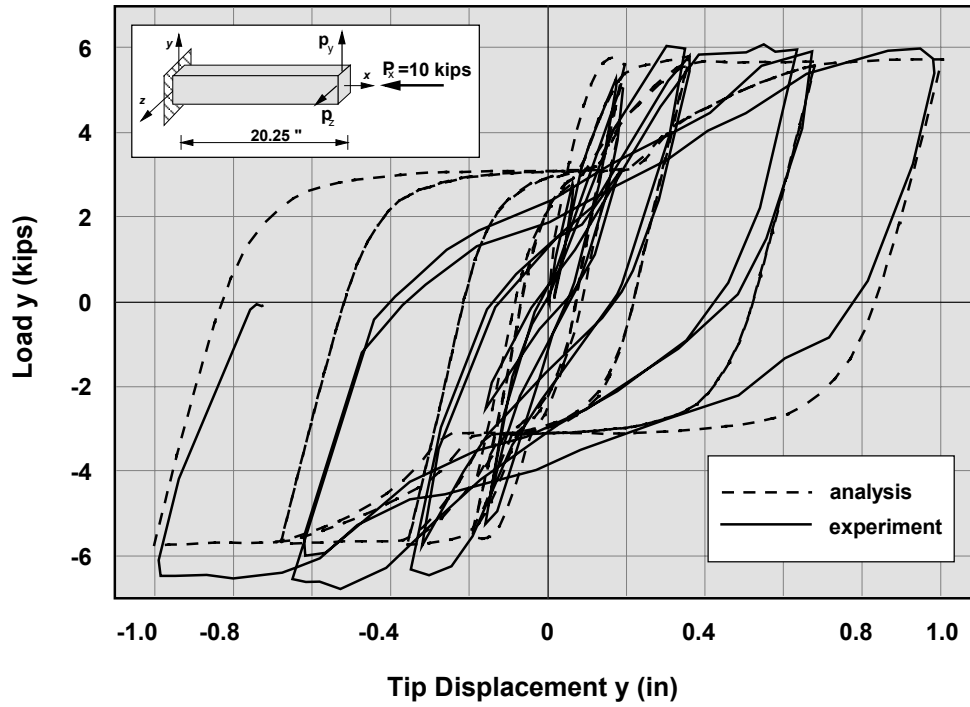


FIGURE 5.12 TIP LOAD-DISPLACEMENT RELATION IN Y-DIRECTION FOR LOW-MOEHLE SPECIMEN #2

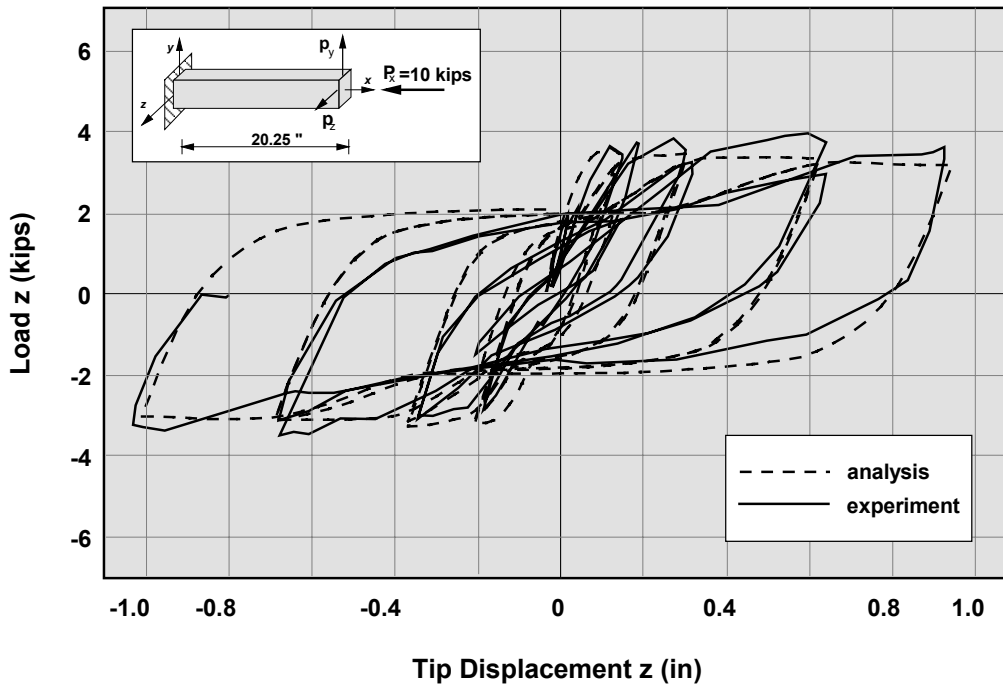


FIGURE 5.13 TIP LOAD-DISPLACEMENT RELATION IN Z-DIRECTION FOR LOW-MOEHLE SPECIMEN #2

The second comparison involves Low and Moehle specimen #2. The loading of this specimen consists of a cyclic lateral force acting at 45 degrees relative to the principal y and z axes of the specimen at the free end of the cantilever and an axial compression of 10 kips that is kept constant during the experiment. Figs. 5.12 and 5.13 compare the analytical with the experimental results in terms of the lateral force versus corresponding tip displacement response in the y -direction, strong axis bending, and z -direction, weak axis bending, respectively. For specimen #2 the $P-\Delta$ effect is taken into account by modifying the computer results to include the effect of lateral displacements on the bending moments at the base of the cantilever. In this case the fixed-end rotation at the base of the column is rather small and accounts for only 4% of the maximum tip displacement. The agreement between experimental and analytical results is good even though the model is clearly stiffer than the specimen, particularly, in the early stages of the hysteretic response. The stiffness discrepancy at the very early response stage can be attributed to the initial cracking of the specimen due to shrinkage and temperature. The discrepancy in hysteretic behavior under large displacement reversals, on the other hand, can be attributed to the significant effect of bond-slip of the longitudinal reinforcing bars along the height of the column. Since the numerical simulations are conducted under displacement control this effect is only evident in the "pinching" of the hysteretic response and the earlier loss of strength of the specimen relative to the model.

Low-Moehle specimen #2 is used in several parameter studies to investigate the sensitivity of the analytical results to the number of control sections in the element. The model is subjected to monotonic uniaxial strong axis bending under, both, force and displacement control loading conditions and the load-tip displacement response is shown in Figs. 5.14 through 5.16.

Fig. 5.14 shows the load-tip displacement response of the cantilever beam under monotonic bending moment. The results show that the element flexibility increases as the number of control sections decreases. The fewer the number of integration points, the more significant becomes the contribution of the section at the built-in end to the flexibility of the element. Since in a cantilever beam that is loaded at the tip, the section at the built-in end undergoes the largest inelastic deformation, the tip displacement increases with the reduction in the number of control sections. The results for eight and ten integration points are indistinguishable indicating convergence to the analytical solution of the problem. For four and six integration points the results show very good agreement with the response obtained with ten integration points. The maximum force discrepancy is 5% and 2% for four and six integration points, respectively. For only two integration points a maximum force discrepancy of 20% is observed.

Fig. 5.15 shows the load-tip displacement response of the cantilever beam under monotonic bending moment and a constant axial compression of 75 kips. The analytical results are obtained under displacement control in order to trace the loss of column strength when the unconfined cover concrete spalls. The column softening is described well with at least four integration points in the element. With two integration points the initial response is more flexible and the yield strength is underestimated.

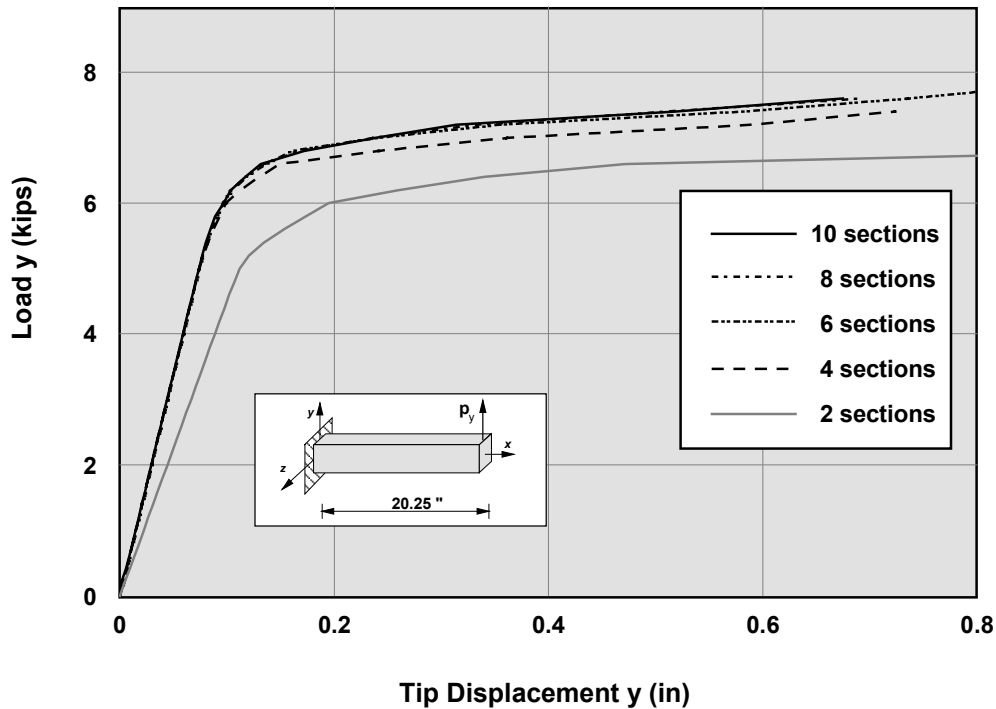


FIGURE 5.14 SENSITIVITY OF THE LOAD-DISPLACEMENT RESPONSE OF A CANTILEVER UNDER UNIAXIAL BENDING TO THE NUMBER OF CONTROL SECTIONS

Fig. 5.16 shows the response of the same cantilever column under the same loading history, but without the effect of confinement for the concrete that is enclosed by stirrup-ties. Even though the loss of strength is sudden and more abrupt in this case, the analytical results agree very well for cases with at least four integration points in the column. For two integration points the initial response is more flexible, while for two and three integration points the post-peak response deviates significantly from the other cases.

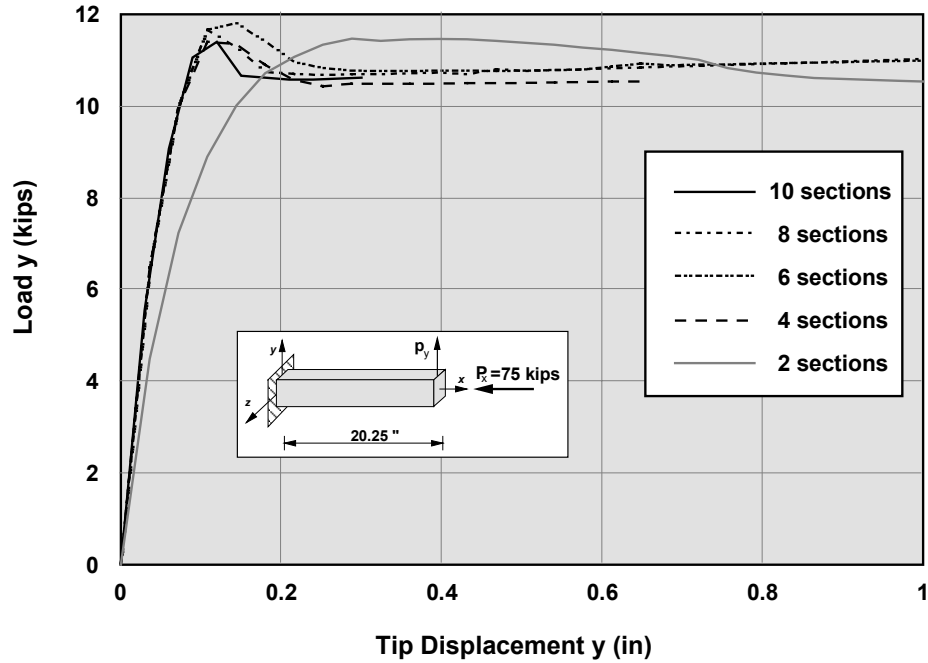


FIGURE 5.15 SENSITIVITY OF ANALYTICAL LOAD-DISPLACEMENT RESPONSE TO THE NUMBER OF CONTROL SECTIONS. CANTILEVER WITH CONFINED CONCRETE UNDER UNIAXIAL BENDING MOMENT AND AXIAL FORCE

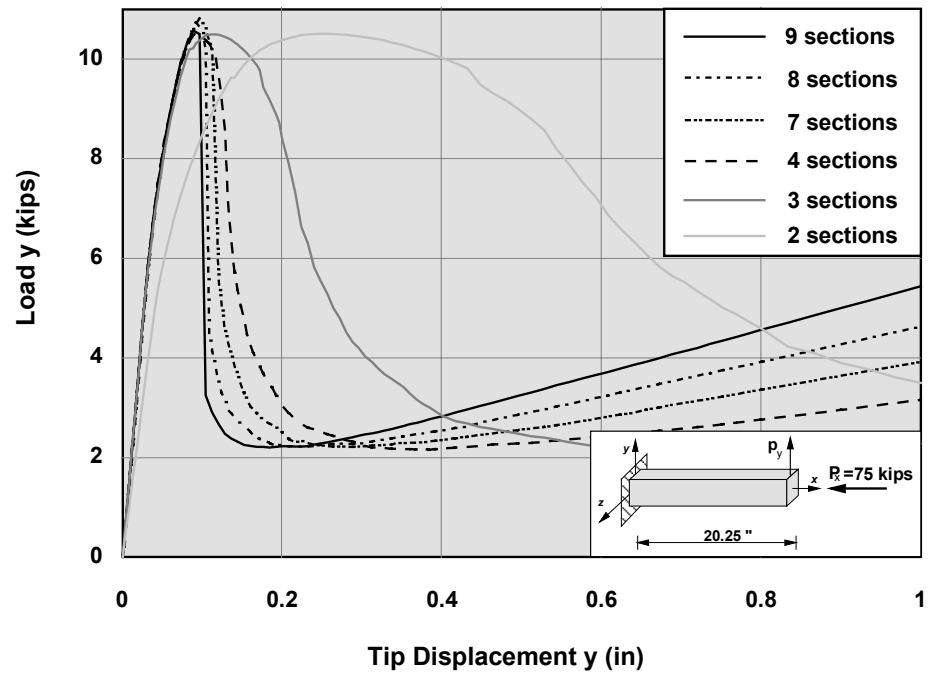


FIGURE 5.16 SENSITIVITY OF ANALYTICAL LOAD-DISPLACEMENT RESPONSE TO THE NUMBER OF CONTROL SECTIONS. CANTILEVER WITH UNCONFINED CONCRETE UNDER UNIAXIAL BENDING MOMENT AND AXIAL FORCE

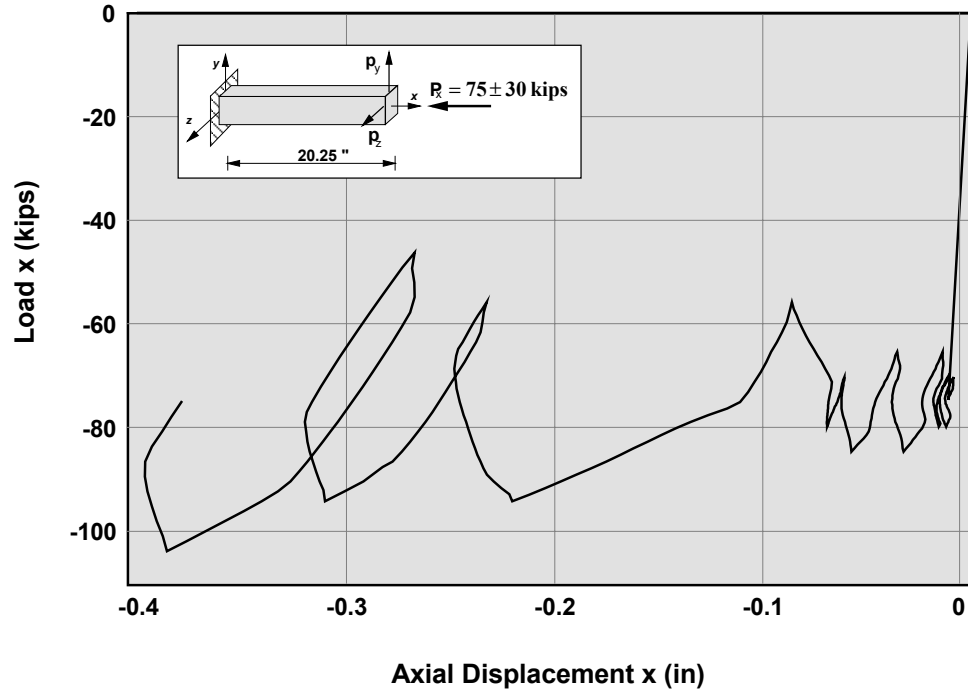


FIGURE 5.17 AXIAL LOAD-DISPLACEMENT RELATION IN THE x -DIRECTION UNDER CYCLIC AXIAL FORCE AND BIAXIAL BENDING

Another analytical study is conducted on specimen #2 in order to study the effect of a varying axial force on the hysteretic behavior. Unfortunately, no experimental data are available for this case. The confinement of the core concrete is reduced, so that the ultimate concrete strain ϵ_u is now equal to 0.12. The same displacement history is now imposed in both principal directions y and z with the tip displacements reaching a maximum value of +0.96 in. and -0.96 in. In the axial direction x the force fluctuates about an average compression value of 75 kips and reaches extreme values of 105 kips and 45 kips in compression. Thus, while the member is loaded under displacement control conditions in the y and z direction, the axial force is controlled in the x -direction.

The imposed loads and displacements change at the same rate: the displacement increment in the y and z direction is equal to 0.05 in., while the force increment in the x direction is equal to 1.5 kips. The selected convergence tolerance values are: in absolute terms $EAT = 0.1$ kip and in relative terms $ERT = 1\%$. The analytical results are shown in Figs. 5.17 through 5.19 and demonstrate the ability of the model to describe the complex response of the member without numerical problems, even under a complex load history of cyclically varying axial force and biaxial bending.

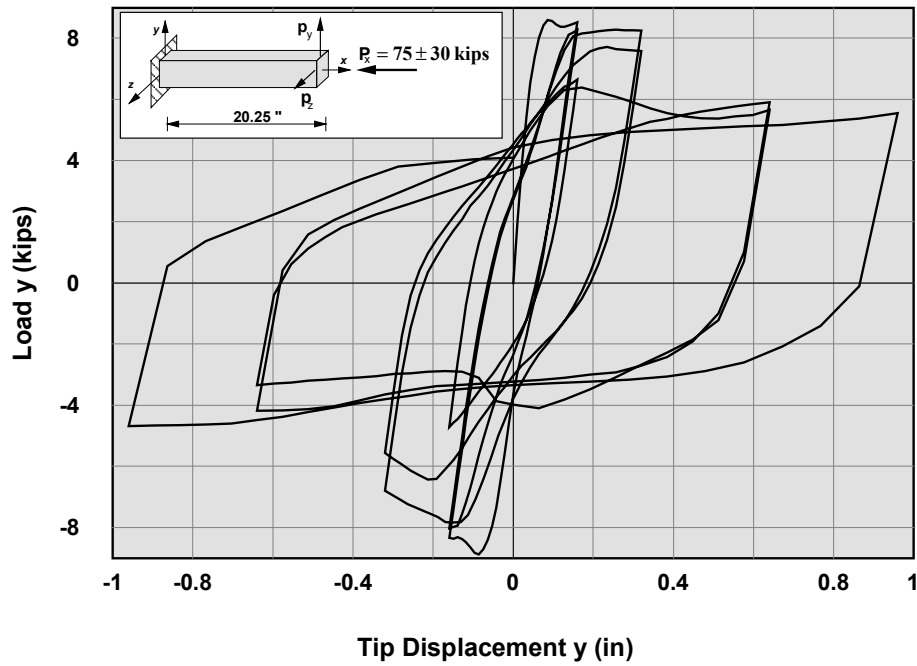


FIGURE 5.18 TIP LOAD-DISPLACEMENT RELATION IN THE y -DIRECTION UNDER CYCLIC AXIAL FORCE AND BIAxIAL BENDING

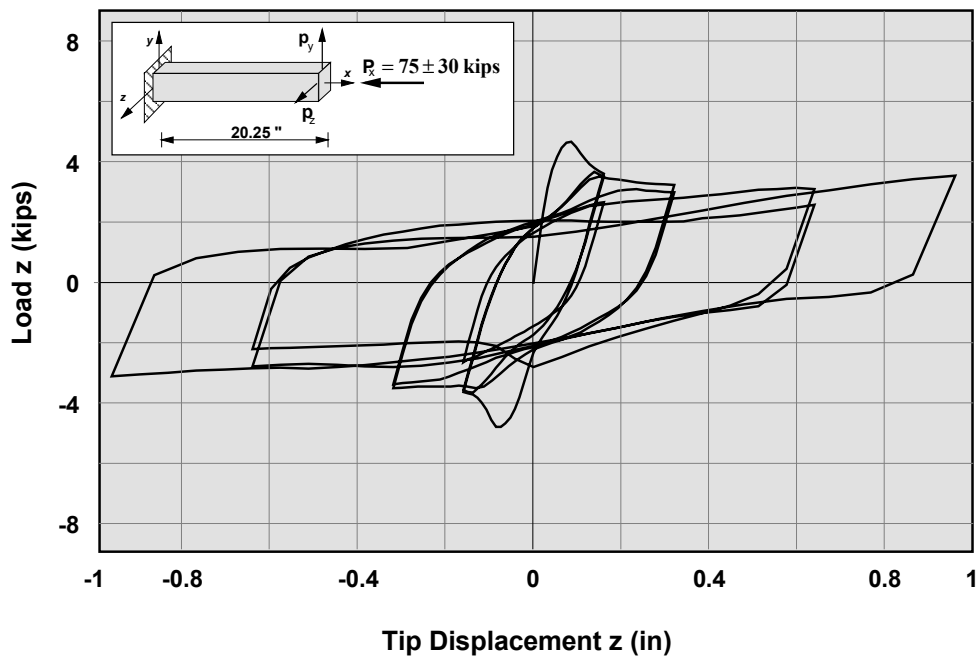


FIGURE 5.19 TIP LOAD-DISPLACEMENT RELATION IN THE z -DIRECTION UNDER CYCLIC AXIAL FORCE AND BIAxIAL BENDING

CHAPTER 6

CONCLUSIONS

The objective of this study is to develop a reliable and computationally efficient beam-column finite element model for the analysis of reinforced concrete members under cyclic loading conditions that induce biaxial bending and axial force. The element is discretized into longitudinal steel and concrete fibers such that the section force-deformation relation is derived by integration of the stress-strain relation of the fibers. At present the nonlinear behavior of the element derives entirely from the nonlinear stress-strain relation of the steel and concrete fibers. The element formulation is based on bending moment and axial force distribution functions that satisfy the equilibrium along the element, and, thus, requires a flexibility based state determination algorithm for the computation of the stiffness matrix and resisting forces of the element. The model does not consider relative slip between fibers, which are assumed to be perfectly bonded, so that plane sections before deformation remain plane.

The proposed nonlinear algorithm for the element state determination is general and can be used with any nonlinear section force-deformation relation. The procedure involves an element iteration scheme that converges to a state that satisfies the material constitutive relations within the specified tolerance. During the element iterations the equilibrium and the compatibility of the element, are always satisfied in a strict sense by the assumed force and deformation interpolation functions. The number of element iterations required to reach convergence depends on the element stiffness and on the tolerance that is selected for the problem. In general, a very small element tolerance involves a large number of element iterations. By contrast, a larger element tolerance requires a large number of iterations at the structure level in order to achieve convergence at the structural degrees of freedom. The proposed method proved to be computationally stable and robust, while being able to describe the complex hysteretic behavior of reinforced concrete members, such as strain hardening, "pinching" and softening under cyclic nodal and element loads.

A new scheme for the application of element loads in flexibility based beam finite elements is also presented in the report. The procedure is a natural extension of the element state determination algorithm and is based on the use of the exact internal force distribution under the applied element loads. The corresponding fixed end forces at the element ends are

determined during iterations of the element state determination. The presence of element loads is important in the study of the effect of gravity loads on structures undergoing lateral load reversals.

Compared with similar stiffness based beam-column elements, the proposed model offers three major advantages: (a) with the use of the exact force distribution function along the element fewer elements are needed to discretize a structure, (b) element softening can be dealt with without numerical difficulties, and, (c) the application of element loads is rather straightforward with the use of the exact internal force distribution function under the given element loads. The element belongs to the family of flexibility based elements, but distinguishes itself by the general and clearly formulated state determination process that relies on the same equilibrium and compatibility conditions used in the formulation of the element stiffness matrix and does not resort to ad hoc approximations and special solution strategies to avoid numerical difficulties. Compared with fiber beam-column elements that are based on the event-to-event solution scheme, the proposed model is more general, since it is not limited to piecewise linear force-deformation relations. It is also more efficient in the analysis of large structures that may experience a very large number of events during severe cyclic loading, since it does not require tracing of every stiffness change in the structure.

Comparisons between the results of the proposed model with experimental data show very good correlation, especially, for cycles that induce small to average damage in the members under investigation. Since the shear deformations are not included in the proposed beam-column element, the selection of specimens for testing the validity of the model is limited to cases with negligible contribution of shear deformations to the overall response. Under very large inelastic deformations the model exhibits higher resisting forces than those measured in the experiment. This is predictable, since the model does not include several important effects in the material models of the constituent fibers, such as the effect of cyclic damage on the unconfined and confined concrete response, the buckling of the longitudinal reinforcing bars and the effect of shear and bond-slip of reinforcing bars on the state of damage of the member. Moreover, the model does not account for the fixed end rotation due to reinforcing bar pull-out from the base of the specimen. Under imposed displacement conditions the bar pull-out has a slight effect on the load carrying capacity of the specimen, but it affects significantly the reloading stiffness and the energy dissipation capacity of the specimen.

The proposed element that is now clearly formulated and implemented in the stand alone computer program **BEAMCOL** offers several opportunities for future studies:

-
- The effect of more sophisticated material models for unconfined and confined concrete as well as for reinforcing steel on the local and global hysteretic response of reinforced concrete members needs to be studied. The present study is limited to rather simple constitutive models, which lack important features, such as the effect of cyclic damage on the concrete stress-strain relation, the buckling of reinforcing steel, etc.
 - Parametric studies are required to establish the sensitivity of the element response to the number of integration points (control sections) in the member. The case studies in this report are conducted under displacement control and show that, while the load-displacement response is well represented with as few as 3 integration points, the section moment-curvature response is very sensitive to the number of integration points. This has very important practical ramifications, since it is the local response, such as steel and concrete strains at the most critical section, that will determine the failure of the element. Thus, modeling guidelines are needed for the selection of the number of integration points in order to predict with confidence curvature and rotation ductility demands and plastic hinge lengths in reinforced concrete members.
 - Second order effects, such as those arising from P- Δ actions, should be included in the element in order to study the importance of overturning moments under the large lateral sways caused by strong ground motions.
 - The effect of fixed end rotations due to reinforcing bar pull-out from foundations and beam-column joints should be included in the model by modification of the behavior of the end sections or by the addition of special hinge elements at the beam ends.
 - The reinforcing bar slip relative to concrete is also important along the element, particularly, for members with insufficient development length, lap splices, etc. The rational inclusion of this effect in the section constitutive relation is a challenging task that requires further study.
 - The proposed element does not account for deformations due to shear and torsion. It is presently not clear whether these effects can be included in a rational way in a fiber beam-column element, but the subject merits further study.
 - The proposed element enhanced with the new method for the inclusion of element loads is suitable for the analysis of prestressed concrete members. These can be modeled as a group of prestressing tendons that are connected in parallel with the proposed reinforced concrete beam-column element. Such an element is the subject of a current study.
-

- The proposed nonlinear solution algorithm is generally applicable. Its implementation in elements with different nonlinear section force-deformation relations should be explored. Similarly, the extension of the algorithm to systems that are composed of a combination of several springs in series and/or in parallel should be studied.
 - The implementation of the proposed beam-column element in a general finite element computer program for the nonlinear static and dynamic analysis of large structures is a very important task. The implementation of the element in the finite element program FEAP is presently complete. It is only briefly discussed in this study and will be the subject of a future report. Topics to be addressed in this future study include parametric studies for the development of modeling guidelines for the nonlinear analysis of reinforced and prestressed concrete structures under earthquake excitations and the exploration of different nonlinear solution strategies within the framework of program FEAP.
 - Starting from the existing capabilities of the finite element program FEAP with respect to nonlinear solution strategies and pre- and post-processing utilities, an integrated computer environment for the nonlinear static and dynamic analysis of reinforced and prestressed concrete structures needs to be developed. This analysis package should encompass elements with different levels of complexity, from simple linear elastic elements to very sophisticated nonlinear 3-D finite elements, and should allow for their seamless integration within the same nonlinear structural model.
-

REFERENCES

- Anagnostopoulos, S. (1981). "Inelastic Beams for Seismic Analysis of Structures." *Journal of Structural Engineering*, ASCE, 107(ST7), pp. 1297-1311.
- Banon, H., Biggs, J. and Irvine, M. (1981). "Seismic Damage in Reinforced Concrete Frames." *Journal of Structural Engineering*, ASCE, 107(ST9), pp. 1713-1729.
- Bazant, S. and Bhat, P. (1977). "Prediction of Hysteresis in Reinforced Concrete Members." *Journal of Structural Engineering*, ASCE, 103(ST1), pp. 151-167.
- Bertero, V.V., Aktan, A., Charney, F. and Sause, R. (1984). "Earthquake Simulator Tests and Associated Experimental, Analytical and Correlation Studies of One-Fifth Scale Model." in, Earthquake Effects on Reinforced Concrete Structures, *American Concrete Institute*, SP-84-13, Detroit, pp. 375-424.
- Brancaleoni, F., Ciampi, V. and Di Antonio, R. (1983). "Rate-Type Models for Non Linear Hysteretic Structural Behavior." *EUROMECH Colloquium*, Palermo, Italy.
- Charney, F. and Bertero, V.V. (1982). "An Evaluation of the Design and Analytical Seismic Response of a Seven Story Reinforced Concrete Frame-Wall Structure." *Report EERC 82-08*, Earthquake Engineering Research Center, Berkeley.
- Chen, W. and Atsuta, T. (1977). **Theory of Beam-Columns**. McGraw Hill, New York.
- Ciampi, V. and Carlesimo, L. (1986). "A Nonlinear Beam element for Seismic Analysis of Structures." *8th European Conference on Earthquake Engineering*, Lisbon.
- Ciampi, V. and Nicoletti, M. (1986). "Parameter Identification for Cyclic Constitutive Models with Stiffness and Strength Degradation." *8th European Conference on Earthquake Engineering*, Lisbon.
- Clough, R. and Benuska, L. (1967). "Nonlinear Earthquake Behavior of Tall Buildings." *Journal of Mechanical Engineering*, ASCE, 93(EM 3), pp. 129-146.
- Clough, R. and Johnston, S. (1966). "Effect of Stiffness Degradation on Earthquake Ductility Requirements." *Transactions of Japan Earthquake Engineering Symposium*, Tokyo, pp. 195-198.
- Darvall, L.P. and Mendis, P. (1985). "Elastic-Plastic-Softening Analysis of Plane Frames." *Journal of Structural Engineering*, ASCE, 11(ST4), pp. 871-888.
- Filippou, F.C., Popov, E.P. and Bertero, V.V. (1983). "Effects of Bond Deterioration on Hysteretic Behavior of Reinforced Concrete Joints." *EERC Report 83-19*, Earthquake Engineering Research Center, Berkeley.
- Filippou, F.C., and Issa, A. (1988). "Nonlinear Analysis of Reinforced Concrete Frames under Cyclic Load Reversals." *EERC Report 88-12*, Earthquake Engineering Research Center, Berkeley.
- Giberson, M. (1967). "The Response of Nonlinear Multi-Story Structures Subjected to Earthquake Excitations." *Earthquake Engineering Research Laboratory*, Pasadena.
- Hellesland, J. and Scordelis, A. (1981). "Analysis of RC Bridge Columns Under Imposed Deformations." *IABSE Colloquium*, Delft, Netherlands, pp. 545-559.
- Iwan, W. (1978). "Application of Nonlinear Analysis Techniques." in, Iwan W. ed., *Applied Mechanics in Earthquake Engineering*, ASME, AMD, 8, New York, pp. 135-161.
- Kaba, S. and Mahin, S.A. (1984). "Refined Modeling of Reinforced Concrete Columns for Seismic Analysis." *EERC Report 84-03*, Earthquake Engineering Research Center, University of California, Berkeley.
- Karsan, I.D., and Jirsa, J.O. (1969). "Behavior of Concrete under Compressive Loadings", *Journal of the Structural Division*, ASCE, 95(ST12).
- Kent, D.C. (1969). "Inelastic Behavior of Reinforced Concrete Members with Cyclic Loading". Ph.D. Thesis, University of Canterbury, Christchurch, New Zealand.

- Kent, D.C., and Park, R. (1971). "Flexural Members with Confined Concrete", *Journal of the Structural Division*, ASCE, 97(ST7).
- Keshavarzian, M. and Schnobrich, W. (1985). "Inelastic Analysis of RC Coupled Shear Walls." *Earthquake Engineering and Structural Dynamics*, 13, pp. 427-448.
- Lai, S., Will, G. and Otani, S. (1984). "Model for Inelastic Biaxial Bending of Concrete Members." *Journal of Structural Engineering*, ASCE, 110(ST11), pp. 2563-2584.
- Low, S.S. and Moehle J.P. (1987). "Experimental Study of Reinforced Concrete Columns Subjected to Multi-Axial Cyclic Loading." *EERC Report 87-14*, Earthquake Engineering Research Center, University of California, Berkeley.
- Ma, S.Y., Bertero, V.V. and Popov, E.P. (1976). "Experimental and Analytical Studies on the Hysteretic Behavior of Reinforced Concrete Rectangular and T-Beams", *EERC Report 76-2*, Earthquake Engineering Research Center, University of California, Berkeley.
- Mahasuverachai, M. (1982). "Inelastic Analysis of Piping and Tubular Structures." *EERC Report 82-27*, Earthquake Engineering Research Center, University of California, Berkeley.
- Mander, J.B., Priestley, M.J.N. and Park, R. (1988). "Theoretical Stress-Strain Model for Confined Concrete." *Journal of Structural Engineering*, ASCE, 114(ST8), pp. 1804-1826.
- Mari, A. and Scordelis, A. (1984). "Nonlinear Geometric Material and Time Dependent Analysis of Three Dimensional Reinforced and Prestressed Concrete Frames." *SESM Report 82-12*, Department of Civil Engineering, University of California, Berkeley.
- Menegotto M., and Pinto, P.E. (1973). "Method of Analysis for Cyclically Loaded Reinforced Concrete Plane Frames Including Changes in Geometry and Non-Elastic Behavior of Elements under Combined Normal Force and Bending", *Proceedings, IABSE Symposium on Resistance and Ultimate Deformability of Structures Acted on by Well Defined Repeated Loads*, Lisbon, pp. 15-22.
- Menegotto, M. and Pinto, P.E. (1977). "Slender RC Compressed Members in Biaxial Bending." *Journal of Structural Engineering*, ASCE, 103(ST3), pp. 587-605.
- Meyer, C., Roufaiel, M.S. and Arzoumanidis, S.G. (1983). "Analysis of Damaged Concrete Frames for Cyclic Loads." *Earthquake Engineering and Structural Dynamics*, Vol. 11, pp. 207-228.
- Okada, T., Seki, M. and Asai, S. (1976). "Response of Reinforced Concrete Columns to Bi-directional Horizontal Forces and Constant Axial Force." *Bulletin of ERS*, 10, Tokyo, pp. 30-36.
- Otani, S. (1974). "Inelastic Analysis of R/C Frame Structures." *Journal of the Structural Division*, ASCE, 100(ST7).
- Ozdemir, H., (1981). "Nonlinear Transient Dynamic Analysis of Yielding Structures." *Ph. D. Thesis*, Department of Civil Engineering, University of California, Berkeley.
- Prager, W. and Hodge, P. (1951). **Theory of Perfectly Plastic Solids**, John Wiley and Sons, New York.
- Roufaiel, M.S.L. and Meyer, C. (1987). "Analytical Modeling of Hysteretic Behavior of R/C Frames." *Journal of Structural Engineering*, ASCE, 113 (ST3), pp. 429-444.
- Scott, B.D., Park, R. and Priestley, M.J.N. (1982). "Stress-Strain Behavior of Concrete Confined by Overlapping Hoops at Low and High Strain Rates", *ACI Journal*, Vol. 79, No. 1, pp. 13-27.
- Sheikh, S. and Yeh, C.C. (1990). "Tied Concrete Columns Under Axial Load and Flexure." *Journal of Structural Engineering*, ASCE, 116 (ST10), pp. 2780-2800.
- Soleimani, D., Popov, E.P. and Bertero, V.V. (1979). "Nonlinear Beam Model for R/C Frame Analysis." *7th ASCE Conference on Electronic Computation*, St. Louis.
- Spacone, E., Ciampi, V. and Filippou, F.C. (1992). "A Beam Element for Seismic Damage Analysis." *EERC Report*, to be published, Earthquake Engineering Research Center, University of California, Berkeley.
- Takayanagi, T. and Schnobrich, W. (1979). "Non Linear Analysis of Coupled Wall Systems." *Earthquake Engineering and Structural Dynamics*, Vol. 7, pp. 1-22
- Takeda, T., Sozen, M.A. and Nielsen, N. (1970). "Reinforced Concrete Response to Simulated Earthquakes." *Journal of Structural Engineering*, ASCE, 96(ST12), pp. 2557-2573.
-

- Takizawa, H. (1976). "Notes on Some Basic Problems in Inelastic Analysis of Planar RC Structures." , *Trans. of Arch. Inst. of Japan*, 240, Part I in Feb. 1976, pp. 51-62, Part II in March 1976, pp. 65-77.
- Takizawa, H. and Aoyama, H. (1976). "Biaxial Effects in Modeling Earthquake Response of RC Structures." *Earthquake Engineering and Structural Dynamics*, 4, pp. 523-552.
- Zeris, C.A. (1986). "Three Dimensional Nonlinear Response of Reinforced Concrete Buildings." *Ph. D. Thesis*, University of California, Department of Civil Engineering, Berkeley.
- Zeris, C.A. and Mahin, S.A. (1988). "Analysis of Reinforced Concrete Beam-Columns under Uniaxial Excitation." *Journal of Structural Engineering*, ASCE, 114(ST4), pp. 804-820.
- Zeris, C.A. and Mahin, S.A. (1991). "Behavior of Reinforced Concrete Structures Subjected to Biaxial Excitation." *Journal of Structural Engineering*, ASCE, 117(ST9), pp. 2657-2673.
- Zienkiewicz, O.C. and Taylor, R.L. (1989). **The Finite Element Method**. Volume 1. Basic Formulation and Linear Problems. Fourth Edition. McGraw Hill, London.
- Zienkiewicz, O.C. and Taylor, R.L. (1991). **The Finite Element Method**. Volume 2. Solid and Fluid Mechanics, Dynamics and Non-Linearity. Fourth Edition. McGraw Hill, London.
-

APPENDIX A
SUMMARY OF SOLUTION ALGORITHM

The numerical procedure for the stand alone computer program is summarized here in a series of steps that parallel those at the end of Chapters 2 and 3. While the summaries at the end of Chapters 2 and 3 were limited to a basic description of the sequence of steps for the sake of clarity, this appendix contains the detailed numerical implementation of the procedure with the state of each variable within the nested iteration process denoted by superscripts according to the notation introduced in Section 4.2. The steps of the algorithm are also illustrated in Figs. A.1-A.4:

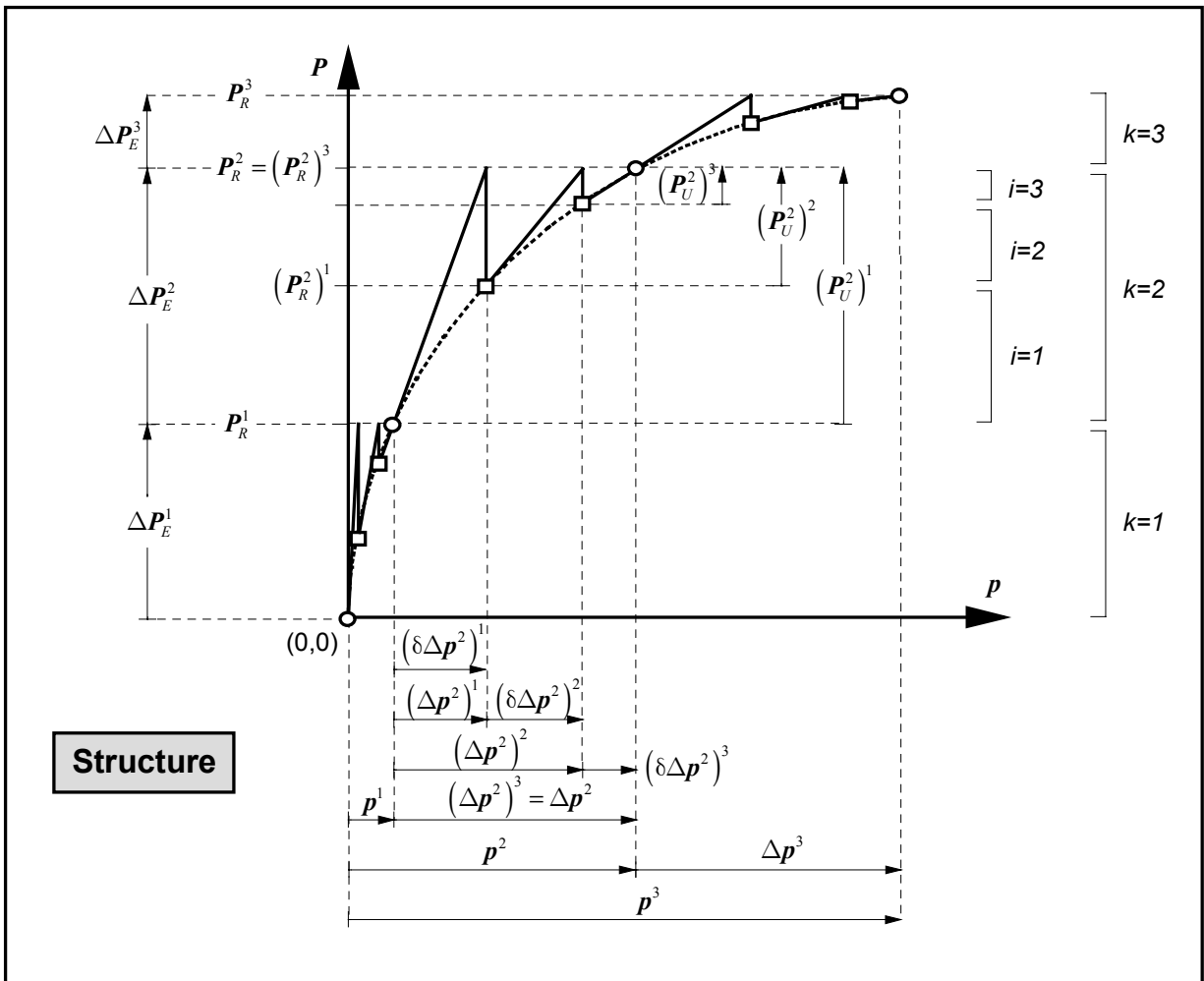


FIGURE A.1 EXAMPLE OF FORCE-DISPLACEMENT HISTORY AT THE STRUCTURE LEVEL

(1) *Start the analysis.*

Set $k=1$

(2) *Start the Newton-Raphson iterations.*

Set $i=1$.

(3) *Solve the global system of equations and update the structure displacement increments.*

Using the unbalanced force vector $(\mathbf{P}_U^k)^{i-1}$ and the structure tangent stiffness matrix $(\mathbf{K}_s^k)^{i-1}$ from the previous Newton-Raphson iteration $i-1$, the change in the structure displacement increments $(\delta\Delta\mathbf{p}^k)^i$ is computed from the solution of the linear system of equations

$$(\mathbf{P}_U^k)^{i-1} = (\mathbf{K}_s^k)^{i-1} \cdot (\delta\Delta\mathbf{p}^k)^i \quad (\text{A.1})$$

The unbalanced force vector $(\mathbf{P}_U^k)^{i-1}$ is obtained as the difference between total applied loads and total resisting forces at the conclusion of the previous Newton-Raphson iteration $i-1$ in step (19). When $k=1$ and $i=1$, $(\mathbf{P}_U^1)^0 = \Delta\mathbf{P}_E^1$. The tangent stiffness matrix $(\mathbf{K}_s^k)^{i-1}$ is based on the state of the structure at the end of the previous Newton-Raphson iteration and is determined in step (18). When $i=1$, two alternatives exist:

$k=1$: The initial tangent stiffness \mathbf{K}_s^0 is determined by imposing a very small deformation increment on the sections of all elements. The fiber material modules return the initial tangent modulus of elasticity E_{tan} from which the section, element and, finally, the structure stiffness is assembled. For the proposed concrete model, which has zero stiffness in tension, the initial tangent modulus always corresponds to the initial tangent stiffness in compression.

$k>1$: The structure stiffness is equal to the tangent stiffness at the end of the last load step $k-1$, that is $(\mathbf{K}_s^k)^0 = \mathbf{K}_s^{k-1}$;

The structure displacement increments $(\delta\Delta\mathbf{p}^k)^i$ are added to the displacement increments $(\Delta\mathbf{p}^k)^{i-1}$ at the end of the previous Newton-Raphson iteration $i-1$ to obtain the displacement increment $(\Delta\mathbf{p}^k)^i$ for iteration i .

$$(\Delta\mathbf{p}^k)^i = (\Delta\mathbf{p}^k)^{i-1} + (\delta\Delta\mathbf{p}^k)^i \quad (\text{A.2})$$

When $i=1$, $(\Delta \mathbf{p}^k)^0$ is initialized to zero.

(4) *Compute the element deformation increments.*

Using the compatibility matrix \mathbf{L}_{ele} the change in the element deformation increments $(\delta \Delta \mathbf{q}^k)^i$ is computed from the structure displacement increments $(\delta \Delta \mathbf{p}^k)^i$:

$$(\delta \Delta \mathbf{q}^k)^i = \mathbf{L}_{ele} \cdot (\delta \Delta \mathbf{p}^k)^i \quad (\text{A.3})$$

The element deformation increments are updated for iteration i :

$$(\Delta \mathbf{q}^k)^i = (\Delta \mathbf{q}^k)^{i-1} + (\delta \Delta \mathbf{q}^k)^i \quad (\text{A.4})$$

When $i=1$, $(\Delta \mathbf{q}^k)^0$ is initialized to zero. Note that the element displacement increments do not change during the element iteration loop j .

(5) *Start the element state determination.*

Set $j=1$.

(6) *Compute the change in the element force increments.*

Two cases are possible:

$j=1$: $\left((\delta \Delta \mathbf{Q}^k)^i \right)^1$ is obtained from the change in the element displacement increments $(\delta \Delta \mathbf{q}^k)^i$ for the current Newton-Raphson iteration i using the element tangent stiffness matrix $(\mathbf{K}^k)^{i-1}$ at the end of Newton-Raphson iteration $i-1$

$$\left((\delta \Delta \mathbf{Q}^k)^i \right)^1 = (\mathbf{K}^k)^{i-1} \cdot (\delta \Delta \mathbf{q}^k)^i \quad (\text{A.4})$$

$j>1$: $\left((\delta \Delta \mathbf{Q}^k)^i \right)^j$ is obtained from the residual element deformations $\left((\mathbf{s}^k)^i \right)^{j-1}$ at the end of iteration $j-1$ and the corresponding element stiffness matrix

$$\left((\delta \Delta \mathbf{Q}^k)^i \right)^j = - \left((\mathbf{K}^k)^i \right)^{j-1} \cdot \left((\mathbf{s}^k)^i \right)^{j-1} \quad (\text{A.5})$$

(7) *Update the element force increments and the element resisting forces.*

With the change in the element force increments $\left((\delta \Delta \mathbf{Q}^k)^i \right)^j$, the element force increments $\left((\Delta \mathbf{Q}^k)^i \right)^{j-1}$ are updated for iteration j :

$$\left((\Delta \mathbf{Q}^k)^i\right)^j = \left((\Delta \mathbf{Q}^k)^i\right)^{j-1} + \left((\delta \Delta \mathbf{Q}^k)^i\right)^j \quad (\text{A.6})$$

When $i=1$ and $j=1$, $\left((\Delta \mathbf{Q}^k)^1\right)^0$ is initialized to zero.

The current element resisting forces are obtained by adding the element force increments to the resisting force vector \mathbf{Q}^{k-1} at the end of the converged load step $k-1$:

$$\left((\mathbf{Q}^k)^i\right)^j = \mathbf{Q}^{k-1} + \left((\Delta \mathbf{Q}^k)^i\right)^j \quad (\text{A.7})$$

(8) *Compute the section force increments.*

The change in the section force increments is computed with the interpolation function $\mathbf{b}(x)$ and the corresponding force increments are updated

$$\left((\delta \Delta \mathbf{D}^k(x))^i\right)^j = \mathbf{b}(x) \cdot \left((\delta \Delta \mathbf{Q}^k)^i\right)^j \quad (\text{A.8})$$

$$\left((\Delta \mathbf{D}^k(x))^i\right)^j = \left((\Delta \mathbf{D}^k(x))^i\right)^{j-1} + \left((\delta \Delta \mathbf{D}^k(x))^i\right)^j \quad (\text{A.9})$$

When $i=1$ and $j=1$, $\left((\Delta \mathbf{D}^k(x))^1\right)^0$ is initialized to zero.

Update the current section forces

$$\left((\mathbf{D}^k(x))^i\right)^j = \mathbf{D}^{k-1}(x) + \left((\Delta \mathbf{D}^k(x))^i\right)^j \quad (\text{A.10})$$

When $k=1$, $\mathbf{D}^{k-1}(x) = \mathbf{0}$.

(9) *Compute the change in section deformation increments.*

The change in section deformation increments $\left((\delta \Delta \mathbf{d}^k(x))^i\right)^j$ is obtained by adding the effect of the change in section force increments $\left((\delta \Delta \mathbf{D}^k(x))^i\right)^j$ to the residual section deformations at the end of the $j-1$ iteration:

$$\left((\delta \Delta \mathbf{d}^k(x))^i\right)^j = \left((\mathbf{r}^k(x))^i\right)^{j-1} + \left((\mathbf{f}^k(x))^i\right)^{j-1} \cdot \left((\delta \Delta \mathbf{D}^k(x))^i\right)^j \quad (\text{A.11})$$

When $j=1$, $\left((\mathbf{r}^k(x))^i\right)^0 = \mathbf{0}$.

The section deformation increments are then updated:

$$\left((\Delta \mathbf{d}^k(x))^i \right)^j = \left((\Delta \mathbf{d}^k(x))^i \right)^{j-1} + \left((\delta \Delta \mathbf{d}^k(x))^i \right)^j \quad (\text{A.12})$$

When $i=1$ and $j=1$, $\left((\Delta \mathbf{d}^k(x))^1 \right)^0 = \mathbf{0}$.

(10) *Compute the fiber deformation increments.*

The change in fiber deformation increments is computed with the section compatibility matrix $\mathbf{l}(x)$ and the deformation increments are updated

$$\left((\delta \Delta \mathbf{e}^k(x))^i \right)^j = \mathbf{l}(x) \cdot \left((\delta \Delta \mathbf{d}^k(x))^i \right)^j \quad (\text{A.13})$$

$$\left((\Delta \mathbf{e}^k(x))^i \right)^j = \left((\Delta \mathbf{e}^k(x))^i \right)^{j-1} + \left((\delta \Delta \mathbf{e}^k(x))^i \right)^j \quad (\text{A.14})$$

The fiber deformations are updated:

$$\left((\mathbf{e}^k(x))^i \right)^j = \mathbf{e}^{k-1}(x) + \left((\Delta \mathbf{e}^k(x))^i \right)^j \quad (\text{A.15})$$

When $i=1$ and $j=1$, $\left((\Delta \mathbf{e}^k(x))^1 \right)^0 = \mathbf{0}$.

(11) *Compute fiber stresses and update the tangent modulus of the fibers.*

For the current fiber deformations $\left((\mathbf{e}^k(x))^i \right)^j$ the fiber material modules return the new fiber stresses $\left((\mathbf{E}^k(x, y_{fib}, z_{fib}))^i \right)^j$ and the updated tangent stiffness modulus of the fibers $\left((E_{tan}^k(x, y_{fib}, z_{fib}))^i \right)^j$.

(12) *Compute the section tangent stiffness and flexibility matrices.*

The updated tangent modulus of the fibers $\left((E_{tan}^k(x, y_{fib}, z_{fib}))^i \right)^j$ is used in the calculation of the current section tangent stiffness matrix

$$\left((\mathbf{k}^k(x))^i \right)^j = \begin{bmatrix} \sum_{ifib=1}^{n(x)} (EA)_{ifib} \cdot y_{ifib}^2 & -\sum_{ifib=1}^{n(x)} (EA)_{ifib} \cdot y_{ifib} \cdot z_{ifib} & -\sum_{ifib=1}^{n(x)} (EA)_{ifib} \cdot y_{ifib} \\ -\sum_{ifib=1}^{n(x)} (EA)_{ifib} \cdot y_{ifib} \cdot z_{ifib} & \sum_{ifib=1}^{n(x)} (EA)_{ifib} \cdot z_{ifib}^2 & \sum_{ifib=1}^{n(x)} (EA)_{ifib} \cdot z_{ifib} \\ -\sum_{ifib=1}^{n(x)} (EA)_{ifib} \cdot y_{ifib} & \sum_{ifib=1}^{n(x)} (EA)_{ifib} \cdot z_{ifib} & \sum_{ifib=1}^{n(x)} (EA)_{ifib} \end{bmatrix} \quad (\text{A.16})$$

with

$$(EA)_{ifib} = \left((E_{tan}^k(x, y_{ifib}, z_{ifib}))^i \right)^j \cdot A_{ifib}$$

$n(x)$ is the total number of fibers in the section. The section stiffness matrix is then inverted to yield the current section flexibility matrix:

$$\left((\mathbf{f}^k(x))^i \right)^j = \left[\left((\mathbf{k}^k(x))^i \right)^j \right]^{-1} \quad (\text{A.17})$$

(13) *Compute the section resisting forces.*

The section resisting forces are determined from equilibrium between the fiber stresses $\left((\sigma^k(x, y_{ifib}, z_{ifib}))^i \right)^j$ and the section resisting forces.

$$\left((\mathbf{D}_R^k(x))^i \right)^j = \left\{ \begin{array}{l} - \sum_{ifib=1}^{n(x)} \left((\sigma^k(x, y_{ifib}, z_{ifib}))^i \right)^j \cdot A_{ifib} \cdot y_{ifib} \\ \sum_{ifib=1}^{n(x)} \left((\sigma^k(x, y_{ifib}, z_{ifib}))^i \right)^j \cdot A_{ifib} \cdot z_{ifib} \\ \sum_{ifib=1}^{n(x)} \left((\sigma^k(x, y_{ifib}, z_{ifib}))^i \right)^j \cdot A_{ifib} \end{array} \right\} \quad (\text{A.19})$$

(14) *Compute the section unbalanced forces.*

The section unbalanced forces are the difference between applied loads and resisting forces:

$$\left((\mathbf{D}_U^k(x))^i \right)^j = \left((\mathbf{D}^k(x))^i \right)^j - \left((\mathbf{D}_R^k(x))^i \right)^j \quad (\text{A.20})$$

Check whether the unbalanced force vector satisfies the specified section tolerance.

(15) *Compute the residual section deformations.*

$$\left((\mathbf{r}^k(x))^i \right)^j = \left((\mathbf{f}^k(x))^i \right)^j \cdot \left((\mathbf{D}_U^k(x))^i \right)^j \quad (\text{A.18})$$

(16) *Compute the element flexibility and stiffness matrices.*

The element flexibility matrix is obtained by numerical integration of section flexibilities:

$$\left((\mathbf{F}^k)^i \right)^j = \sum_{nsec=1}^m \left[w_{nsec} \cdot \mathbf{b}^T(x_{nsec}) \cdot \left((\mathbf{f}^k(x_{nsec}))^i \right)^j \cdot \mathbf{b}(x_{nsec}) \right] \quad (\text{A.19})$$

where m is the number of monitored sections in the beam-column element x_{nsec} the x-coordinate of the section in the local reference system and w_{nsec} the corresponding weight factor. The element stiffness matrix is obtained by inverting the flexibility matrix.

$$\left((\mathbf{K}^k)^i \right)^j = \left[\left((\mathbf{F}^k)^i \right)^j \right]^{-1} \quad (\text{A.20})$$

(17) *Check for element convergence.*

Element convergence is achieved when all section unbalanced forces satisfy the specified section tolerance. Two cases are possible:

- a) *If convergence is achieved go to step (18)*
- b) *If convergence is not achieved then compute the residual element deformations*

$$\left((\mathbf{s}^k)^i \right)^j = \sum_{nsec}^m \left[w_{nsec} \cdot \mathbf{b}^T(x_{nsec}) \cdot \left((\mathbf{r}(x_{nsec})^k)^i \right)^j \right] \quad (\text{A.21})$$

increment j by 1 and *return to step (6)*.

(18) *Compute the structure resisting forces and update the structure stiffness matrix.*

When all elements have converged, the i -th Newton-Raphson iteration is complete. The structure resisting forces $(\mathbf{P}_R^k)^i$ are determined by assembly of all element resisting forces $(\mathbf{Q}^k)_{ele}^i$ according to the expression

$$(\mathbf{P}_R^k)^i = \sum_{ele=1}^n \mathbf{L}_{ele}^T \cdot (\mathbf{Q}^k)_{ele}^i \quad (\text{A.22})$$

The structure tangent stiffness matrix is updated by assembly of the element stiffness matrices:

$$(\mathbf{K}_s^k)^i = \sum_{ele=1}^n \mathbf{L}_{ele}^T \cdot (\mathbf{K}^k)_{ele}^i \cdot \mathbf{L}_{ele} \quad (\text{A.23})$$

(19) *Compute the structure unbalanced forces.*

The structure unbalanced forces $(\mathbf{P}_U^k)^i$ are the difference between total applied loads \mathbf{P}_E^k and total resisting forces $(\mathbf{P}_R^k)^i$:

$$(\mathbf{P}_U^k)^i = \mathbf{P}_E^k - (\mathbf{P}_R^k)^i \quad (\text{A.24})$$

where \mathbf{P}_E^k is determined from the total applied load at the end of load step $k-1$ and the current load increment

$$\mathbf{P}_E^k = \mathbf{P}_E^{k-1} + \Delta\mathbf{P}_E^k \quad (\text{A.25})$$

For $k=1$ $\mathbf{P}_E^0 = \mathbf{0}$.

(20) *Check for structure convergence.*

If the unbalanced forces at the structure level satisfy the specified tolerance, convergence is achieved. Correspondingly, two cases are possible:

- a) *If convergence is not achieved, increment i by 1, return to step (3) and start the next Newton-Raphson iteration;*
- b) *If convergence is achieved, load step k is complete. Go to step (21).*

(21) *Update force and deformation vectors and start new load step.*

All force and deformation vectors are updated by adding the vector increments for load step k to the corresponding total forces and deformations at the end of load step $k-1$:

$$\mathbf{p}^k = \mathbf{p}^{k-1} + \Delta\mathbf{p}^k \quad (\text{A.26})$$

$$\mathbf{q}^k(x) = \mathbf{q}^{k-1}(x) + \Delta\mathbf{q}^k(x) \quad (\text{A.27})$$

$$\mathbf{d}^k(x) = \mathbf{d}^{k-1}(x) + \Delta\mathbf{d}^k(x) \quad (\text{A.28})$$

update $\mathbf{E}^{k-1}(x)$ to $\mathbf{E}^k(x)$

$$\mathbf{e}^k(x) = \mathbf{e}^{k-1}(x) + \Delta\mathbf{e}^k(x) \quad (\text{A.29})$$

At this point, two cases are possible:

- a) $k=kn$. The entire external load \mathbf{P}_E was applied and the analysis is complete.
- b) $k < kn$. Increment k by 1. Compute the new structure unbalanced force vector

$$\left(\mathbf{P}_U^k\right)^0 = \mathbf{P}_E^k - \mathbf{P}_R^{k-1} \quad (\text{A.30})$$

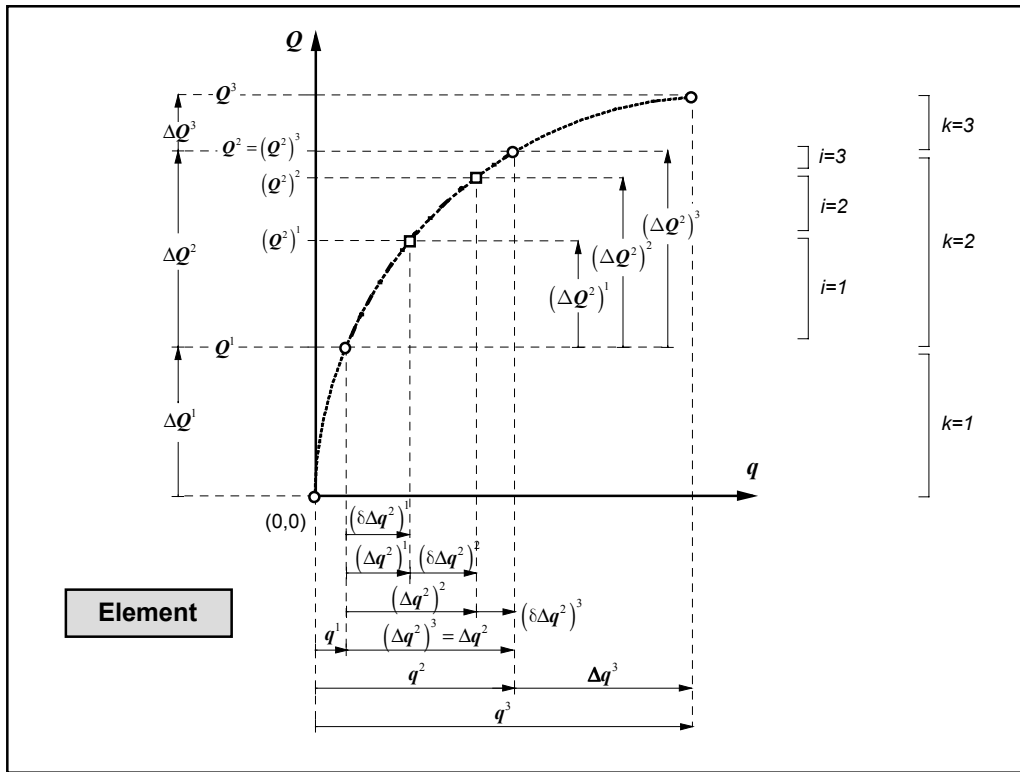
and return to step (2)

This summary refers to the stand alone implementation of the fiber beam-column element and differs in several points from the implementation in program FEAP. The updating of the variables in program FEAP follows more closely the summaries in Sections 2.5 and 3.6 and the corresponding figures. The convergence criteria, both, at the element and at the structural level are also different, as discussed in Chapter 4: the stand alone program checks element convergence by monitoring the unbalanced section forces. Similarly,

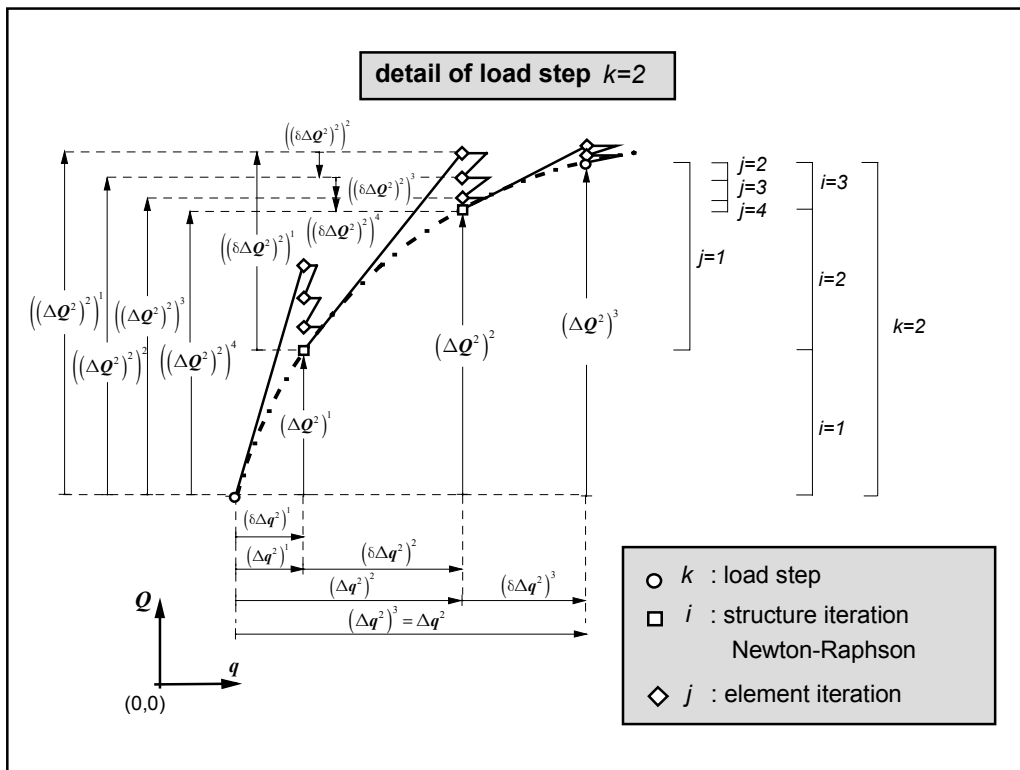
convergence at the structure level is checked by monitoring the unbalanced forces at the global degrees of freedom. In program FEAP, both, at the structure and at the element level convergence is checked by monitoring the work increments. The latter method is more general and is particularly suitable for structures near the ultimate load capacity, as discussed in Section 4.5.

The steps of the nonlinear solution algorithm are illustrated in Figs. A.1-A.4. Fig. A.1 depicts the load-displacement history at the structure level. The structure is subjected to three load step increments $\Delta \mathbf{P}_E^k$. Three Newton-Raphson iterations are performed within each load step to reach convergence to a structure state that satisfies equilibrium and compatibility. Figs. A.2, A.3 and A.4 depict the corresponding force-deformation histories at the element, section and fiber levels, respectively. Each figure contains two curves. The curve at the top shows the complete load history, while the curve at the bottom highlights the second load step $k=2$. Special marker symbols denote the state of the structure, the element, the section and the fiber. A circle denotes a converged state at the structure level. A square denotes a converged state at the element level. A diamond denotes a non converged intermediate element state that satisfies equilibrium and compatibility within the element, but violates the section force-deformation relation. Diamond markers are replaced by squares at the end of every Newton-Raphson loop i , and squares are replaced by circles at the end of every load step k . Squares and circles appear at all levels, i.e. at the structure, element, section and fiber level. Diamonds only appear at the element, section and fiber levels, since they refer to iteration loops within the element.

It is important to note that force and deformation vectors are not updated at the end of every Newton-Raphson iteration when all elements have converged, but at the end of every load step when convergence is reached at the structure level. The updating process is very important for the fiber constitutive relations. The fiber resisting force and tangent modulus is computed based on the total strain at the previous converged load step $\varepsilon^{k-1}(x_{nsec}, y_{ifib}, z_{ifib})$ and the current total strain increment $\left(\left(\Delta \varepsilon^k(x_{nsec}, y_{ifib}, z_{ifib}) \right)^i \right)^j$. This procedure guarantees the path-independence of the nonlinear solution algorithm and has the advantage that in the case of non-convergence the analysis can be restarted from the previous converged load step with a smaller increment. The same updating procedure is used, both, in program FEAP and in the stand alone program.



A) THREE LOAD STEPS



B) DETAIL OF LOAD STEP $k=2$

FIGURE A.2 FORCE-DEFORMATION HISTORY AT THE ELEMENT LEVEL

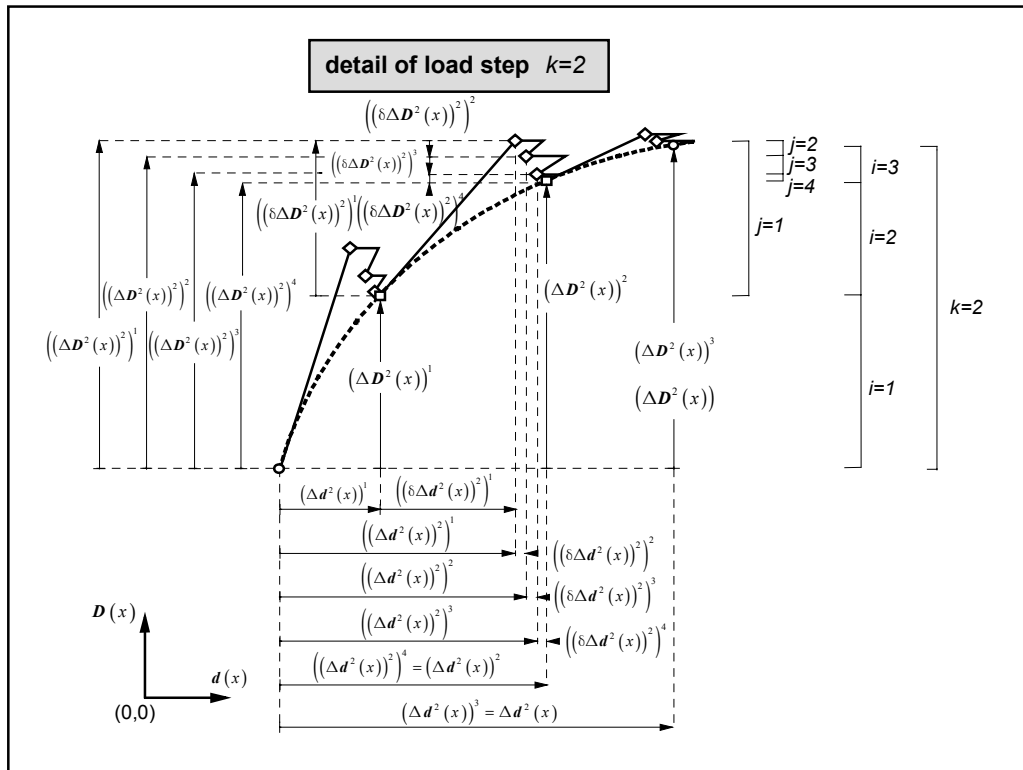
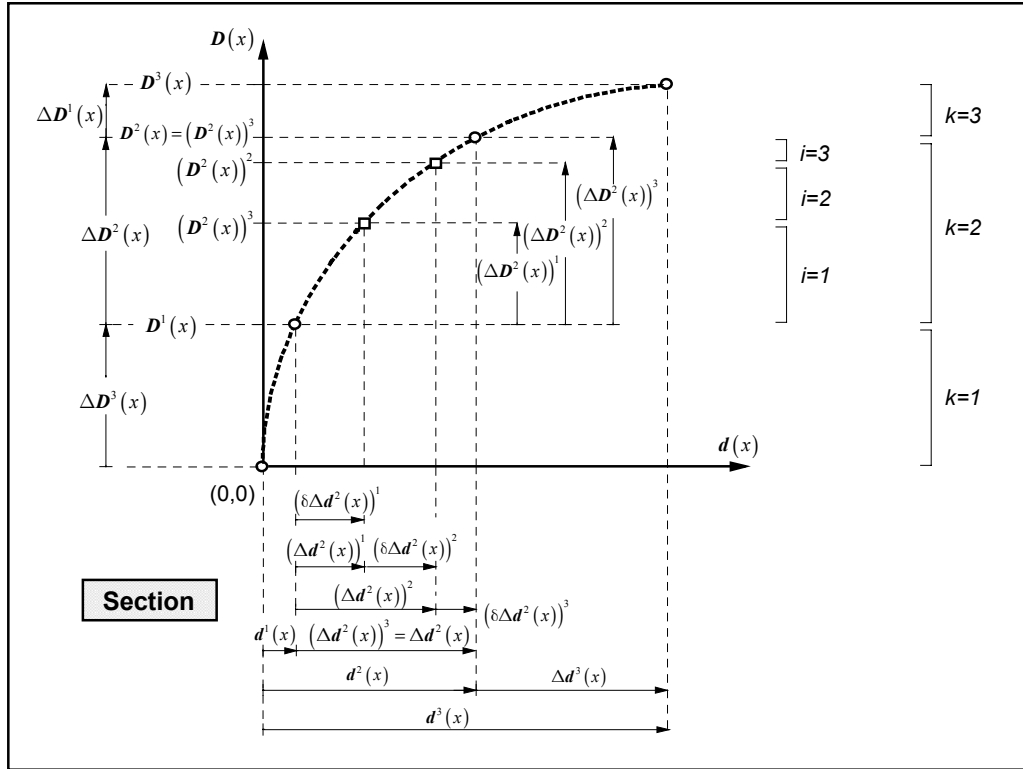
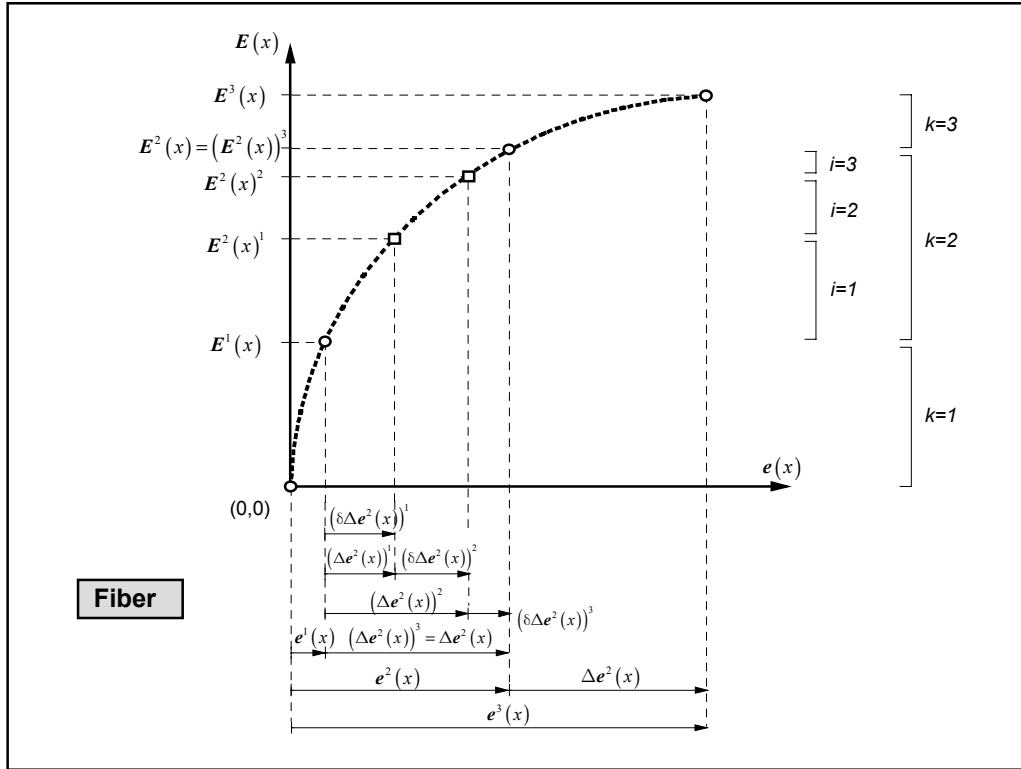
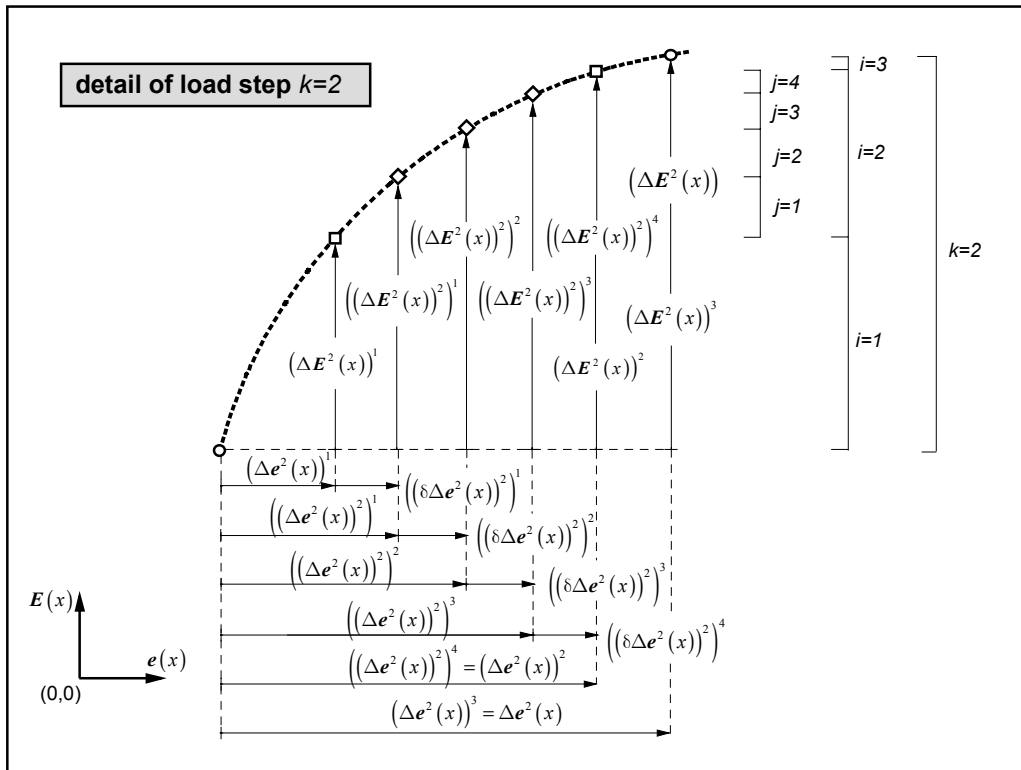


FIGURE A.3 FORCE-DEFORMATION HISTORY AT THE SECTION LEVEL



A) THREE LOAD STEPS



B) DETAIL OF LOAD STEP $k=2$

FIGURE A.4 FORCE-DEFORMATION HISTORY AT THE FIBER LEVEL

APPENDIX B

APPLICATION OF A UNIFORMLY DISTRIBUTED LOAD

ON A LINEAR ELASTIC CANTILEVER

The computational steps involved in the simple example in Section 4.5 are presented in this appendix. The linear elastic cantilever beam with a uniformly distributed vertical load is shown in Fig. 4.2. Figs. B.1 and B.2 are similar to Figs 4.3 and 4.4 but contain more information on the evolution of the variables during the solution process. With the notation of Chapter 4 superscripts denote the iterations at the structure and element level: k indicates the load step, i indicates the Newton-Raphson iteration at the structure level and j indicates the element iteration. Stiffness and flexibility matrices do not carry any superscripts in this example, since they do not change for a linear elastic element. The flexibility-based solution algorithm used in the example is described in Chapters 2 and 3.

The application of a uniformly distributed load on a linear cantilever beam involves the following sequence of computational steps:

$k=1$

$i=1$

$$\Delta \mathbf{P}_E^1 = \mathbf{0}$$

$$(\mathbf{P}_U^1)^1 = \mathbf{0}$$

$$(\delta \Delta \mathbf{p}^1)^1 = \mathbf{0}$$

$$(\delta \Delta \mathbf{q}^1)^1 = \mathbf{0}$$

$j=1$

$$\left((\delta \Delta \mathbf{Q}^1)^1 \right)^1 = \mathbf{K} \cdot \left((\delta \Delta \mathbf{q}^1)^1 \right)^1 = \mathbf{0}$$

$$\left((\Delta \mathbf{Q}^1)^1 \right)^1 = \mathbf{0}$$

$$\left((\mathbf{Q}^1)^1 \right)^1 = \mathbf{0}$$

$$\left((\delta \Delta \mathbf{D}^1(x))^1 \right)^1 = \mathbf{b}_g(x) \cdot \mathbf{W} = \left[\frac{w_y}{2} x(x-L) \quad 0 \quad 0 \right]^T$$

$$\begin{aligned}
\left(\left(\delta\Delta\mathbf{D}^1(L/2)\right)^1\right)^1 &= \left[-\frac{w_y}{8}L^2 \quad 0 \quad 0\right]^T \\
\left(\left(\Delta\mathbf{D}^1(x)\right)^1\right)^1 &= \mathbf{0} + \left(\left(\delta\Delta\mathbf{D}^1(x)\right)^1\right)^1 \\
\left(\left(\mathbf{D}^1(x)\right)^1\right)^1 &= \mathbf{0} + \left(\left(\Delta\mathbf{D}^1(x)\right)^1\right)^1 \\
\left(\left(\mathbf{D}^1(L/2)\right)^1\right)^1 &= \left[-\frac{w_y}{8}L^2 \quad 0 \quad 0\right]^T \\
\left(\left(\delta\Delta\mathbf{d}^1(x)\right)^1\right)^1 &= \mathbf{f}(x) \cdot \left(\left(\delta\Delta\mathbf{D}^1(x)\right)^1\right)^1 \\
\left(\left(\Delta\mathbf{d}^1(x)\right)^1\right)^1 &= \mathbf{0} \\
&\vdots \\
&\vdots \\
&\vdots
\end{aligned}$$

since the element is linear elastic

$$\begin{aligned}
\left(\left(\mathbf{D}_r^1(x)\right)^1\right)^1 &= \left(\left(\mathbf{D}^1(x)\right)^1\right)^1 \\
\left(\left(\mathbf{D}_v^1(x)\right)^1\right)^1 &= \left(\left(\mathbf{D}^1(x)\right)^1\right)^1 - \left(\left(\mathbf{D}_r^1(x)\right)^1\right)^1 = \mathbf{0} \\
\left(\left(\mathbf{r}^1(x)\right)^1\right)^1 &= \mathbf{f}(x) \cdot \left(\left(\mathbf{D}_v^1(x)\right)^1\right)^1 + \left(\left(\delta\Delta\mathbf{d}^1(x)\right)^1\right)^1 = \left(\left(\delta\Delta\mathbf{d}^1(x)\right)^1\right)^1 \\
&\text{the element has not converged, compute } \left(\left(\mathbf{s}^1\right)^1\right)^1
\end{aligned}$$

j=2

$$\begin{aligned}
\left(\left(\delta\Delta\mathbf{Q}^1\right)^1\right)^2 &= -\mathbf{K} \cdot \left(\left(\mathbf{s}^1\right)^1\right)^1 = \left[-\frac{w_y L^2}{12} \quad \frac{w_y L^2}{12} \quad 0 \quad 0 \quad 0\right]^T \\
\left(\left(\Delta\mathbf{Q}^1\right)^1\right)^2 &= \left(\left(\Delta\mathbf{Q}^1\right)^1\right)^1 + \left(\left(\delta\Delta\mathbf{Q}^1\right)^1\right)^2 = \left[-\frac{w_y L^2}{12} \quad \frac{w_y L^2}{12} \quad 0 \quad 0 \quad 0\right]^T \\
\left(\left(\mathbf{Q}^1\right)^1\right)^2 &= \mathbf{0} + \left(\left(\Delta\mathbf{Q}^1\right)^1\right)^2 = \left[-\frac{w_y L^2}{12} \quad \frac{w_y L^2}{12} \quad 0 \quad 0 \quad 0\right]^T \\
\left(\left(\delta\Delta\mathbf{D}^1(x)\right)^1\right)^2 &= \mathbf{b}(x) \cdot \left(\left(\delta\Delta\mathbf{Q}^1\right)^1\right)^2 \\
\left(\left(\delta\Delta\mathbf{D}^1(L/2)\right)^1\right)^2 &= \left[\frac{w_y}{12}L^2 \quad 0 \quad 0\right]^T
\end{aligned}$$

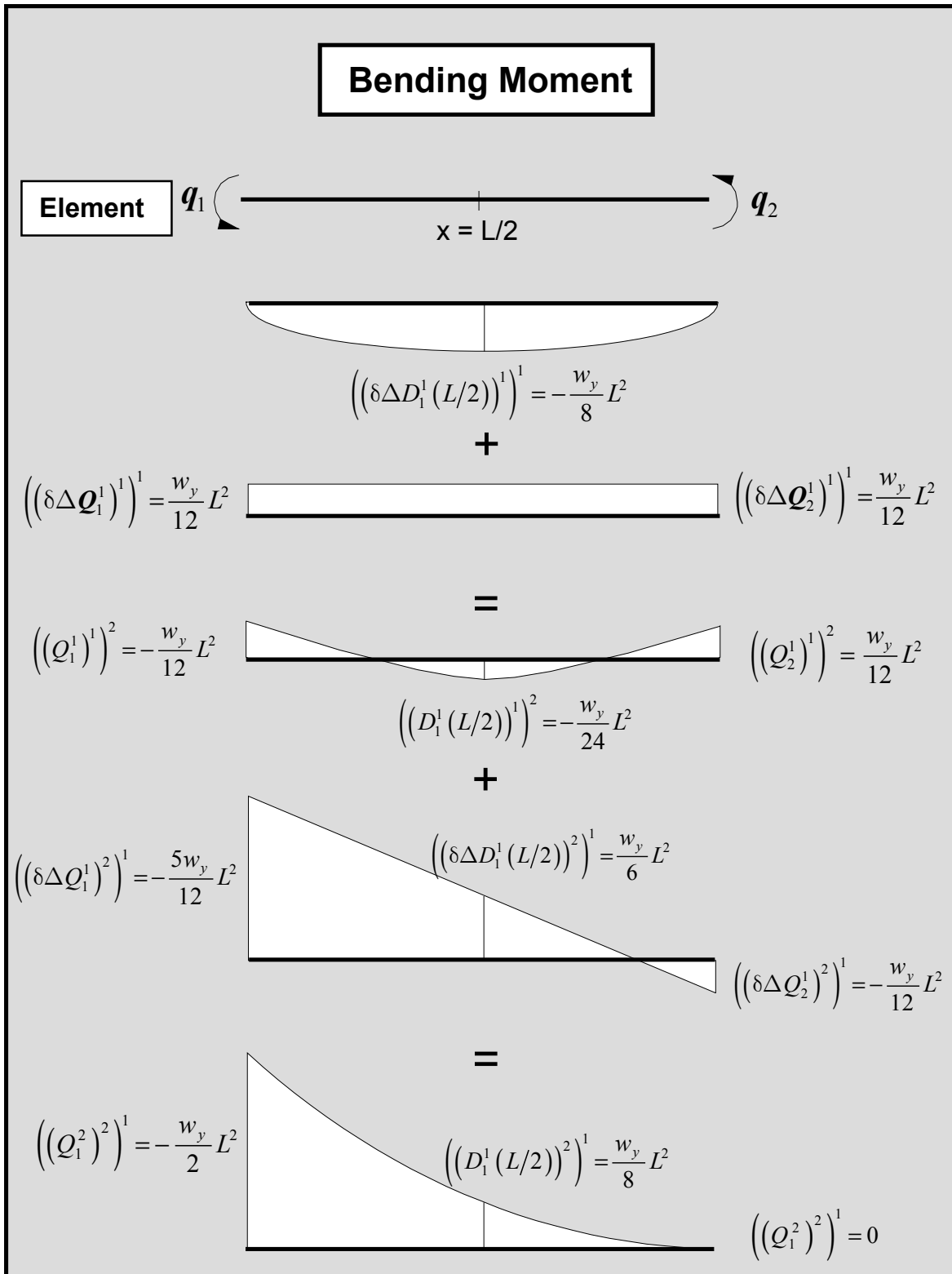


FIGURE B.1 CANTILEVER UNDER UNIFORMLY DISTRIBUTED LOAD: BENDING MOMENT HISTORY

$$\begin{aligned}
\left(\left(\Delta \mathbf{D}^1(x)\right)^1\right)^2 &= \left(\left(\Delta \mathbf{D}^1(x)\right)^1\right)^1 + \left(\left(\delta \Delta \mathbf{D}^1(x)\right)^1\right)^2 \\
\left(\left(\mathbf{D}^1(x)\right)^1\right)^2 &= \mathbf{0} + \left(\left(\Delta \mathbf{D}^1(x)\right)^1\right)^2 \\
\left(\left(\mathbf{D}^1(L/2)\right)^1\right)^2 &= \begin{bmatrix} -\frac{w_y L^2}{24} & 0 & 0 \end{bmatrix}^T \\
\left(\left(\delta \Delta \mathbf{d}^1(x)\right)^1\right)^2 &= \left(\left(\mathbf{r}^1(x)\right)^1\right)^1 + \mathbf{f}(x) \cdot \left(\left(\delta \Delta \mathbf{D}^1(x)\right)^1\right)^2 \\
\left(\left(\Delta \mathbf{d}^1(x)\right)^1\right)^2 &= \mathbf{0} + \left(\left(\delta \Delta \mathbf{d}^1(x)\right)^1\right)^2 \\
&\vdots \\
&\vdots \\
&\vdots
\end{aligned}$$

since the element is linear elastic

$$\begin{aligned}
\left(\left(\mathbf{D}_R^1(x)\right)^1\right)^2 &= \left(\left(\mathbf{D}^1(x)\right)^1\right)^2 \\
\left(\left(\mathbf{D}_U^1(x)\right)^1\right)^2 &= \mathbf{0} \\
\left(\left(\mathbf{r}^1(x)\right)^1\right)^2 &= \mathbf{f}(x) \cdot \left(\left(\mathbf{D}_U^1(x)\right)^1\right)^1 = \mathbf{0}
\end{aligned}$$

the element has converged

$$\begin{aligned}
\left(\bar{\mathbf{Q}}^1\right)^1 &= \begin{bmatrix} -\frac{w_y L^2}{12} & \frac{w_y L^2}{12} & 0 & 0 & 0 & 0 & 0 & 0 & 0 & 0 \end{bmatrix}^T \\
\left(\bar{\mathbf{Q}}^1\right)^1 &= \left(\bar{\mathbf{Q}}^1\right)^1 + \mathbf{t}_g \cdot \mathbf{W} = \begin{bmatrix} -\frac{w_y L^2}{12} & \frac{w_y L^2}{12} & 0 & 0 & 0 & -\frac{w_y L}{2} & -\frac{w_y L}{2} & 0 & 0 & 0 \end{bmatrix}^T \\
\left(\mathbf{P}_R^1\right)^1 &= \bar{\mathbf{L}} \cdot \left(\bar{\mathbf{Q}}^1\right)^1 = \begin{bmatrix} \frac{w_y L^2}{12} & -\frac{w_y L}{2} \end{bmatrix}^T \\
\left(\mathbf{P}_U^1\right)^1 &= \mathbf{P}_E^1 - \left(\mathbf{P}_R^1\right)^1 = \mathbf{0} - \left(\mathbf{P}_R^1\right)^1 = \begin{bmatrix} -\frac{w_y L^2}{12} & \frac{w_y L}{2} \end{bmatrix}^T
\end{aligned}$$

$i=2$

$$\begin{aligned}
\mathbf{K} \cdot \left(\delta \Delta \mathbf{p}^1\right)^2 &= \left(\mathbf{P}_U^1\right)^2 \\
\left(\Delta \mathbf{p}^1\right)^2 &= \left(\Delta \mathbf{p}^1\right)^1 + \left(\delta \Delta \mathbf{p}^1\right)^2 = \mathbf{0} + \left(\delta \Delta \mathbf{p}^1\right)^2 \\
\left(\delta \Delta \mathbf{q}^1\right)^2 &= \mathbf{L}_1 \cdot \left(\delta \Delta \mathbf{p}^1\right)^2 \\
\left(\Delta \mathbf{q}^1\right)^2 &= \left(\Delta \mathbf{q}^1\right)^1 + \left(\delta \Delta \mathbf{q}^1\right)^2
\end{aligned}$$

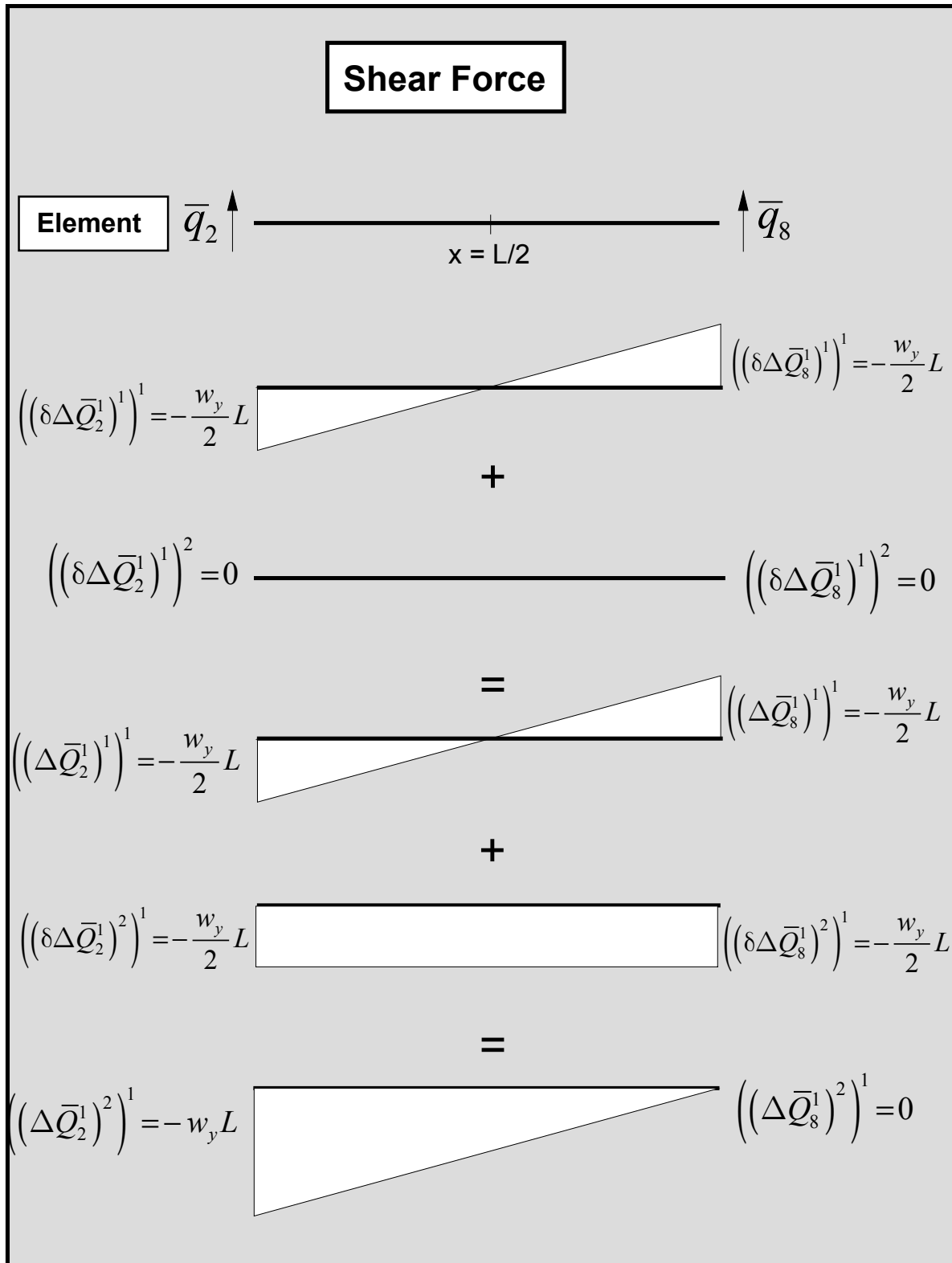


FIGURE B.2 CANTILEVER WITH UNIFORMLY DISTRIBUTED LOAD: SHEAR FORCE HISTORY

$j=1$

$$\left((\delta \Delta \mathbf{Q}^1)^2 \right)^1 = \mathbf{K} \cdot \left((\delta \Delta \mathbf{q}^1)^2 \right)^1 = \begin{bmatrix} -\frac{5w_y L^2}{12} & -\frac{w_y L^2}{12} & 0 & 0 & 0 \end{bmatrix}^T$$

$$\left((\Delta \mathbf{Q}^1)^2 \right)^1 = (\Delta \mathbf{Q}^1)^1 + \left((\delta \Delta \mathbf{Q}^1)^2 \right)^1 = \begin{bmatrix} -\frac{w_y L^2}{2} & 0 & 0 & 0 & 0 \end{bmatrix}^T$$

$$\left((\mathbf{Q}^1)^2 \right)^1 = \mathbf{0} + \left((\Delta \mathbf{Q}^1)^2 \right)^1 = \begin{bmatrix} -\frac{w_y L^2}{2} & 0 & 0 & 0 & 0 \end{bmatrix}^T$$

$$\left((\delta \Delta \mathbf{D}^1(x))^2 \right)^1 = \mathbf{b}(x) \cdot \left((\delta \Delta \mathbf{Q}^1)^2 \right)^1$$

$$\left((\delta \Delta \mathbf{D}^1(L/2))^2 \right)^1 = \begin{bmatrix} \frac{w_y L^2}{6} & 0 & 0 \end{bmatrix}^T$$

$$\left((\Delta \mathbf{D}^1(x))^2 \right)^1 = (\Delta \mathbf{D}^1(x))^1 + \left((\delta \Delta \mathbf{D}^1(x))^2 \right)^1$$

$$\left((\mathbf{D}^1(x))^2 \right)^1 = \mathbf{0} + \left((\Delta \mathbf{D}^1(x))^2 \right)^1$$

$$\left((\mathbf{D}^1(L/2))^2 \right)^1 = \begin{bmatrix} \frac{w_y L^2}{8} & 0 & 0 \end{bmatrix}^T$$

$$\left((\delta \Delta \mathbf{d}^1(x))^2 \right)^1 = \mathbf{0} + \mathbf{f}(x) \cdot \left((\delta \Delta \mathbf{D}^1(x))^2 \right)^1$$

$$\left((\Delta \mathbf{d}^1(x))^2 \right)^1 = (\Delta \mathbf{d}^1(x))^1 + \left((\delta \Delta \mathbf{d}^1(x))^2 \right)^1$$

\vdots
 \vdots
 \vdots

since the element is linear elastic

$$\left((\mathbf{D}_R^1(x))^2 \right)^1 = \left((\mathbf{D}^1(x))^2 \right)^1$$

$$\left((\mathbf{D}_U^1(x))^2 \right)^1 = \mathbf{0}$$

$$\left((\mathbf{r}^1(x))^2 \right)^1 = \mathbf{0}$$

the element has converged

$$\left(\bar{\mathbf{Q}}^1 \right)^2 = \begin{bmatrix} -\frac{w_y L^2}{2} & 0 & 0 & 0 & 0 & -\frac{w_y L}{2} & \frac{w_y L}{2} & 0 & 0 & 0 \end{bmatrix}^T$$

$$\left(\bar{\mathbf{Q}}^1 \right)^2 = \left(\bar{\mathbf{Q}}^1 \right)^2 + \mathbf{t}_g \cdot \mathbf{W} = \begin{bmatrix} -\frac{w_y L^2}{2} & 0 & 0 & 0 & 0 & -w_y L & 0 & 0 & 0 & 0 \end{bmatrix}^T$$

$$(\mathbf{P}_R^1)^2 = \bar{\mathbf{L}} \cdot (\bar{\mathbf{Q}}^1)^2 = \mathbf{0}$$

$$(\mathbf{P}_U^1)^2 = \mathbf{P}_E^2 - (\mathbf{P}_R^1)^2 = \mathbf{0}$$

the structure has converged

vector update

$$\mathbf{p}^1 = \mathbf{p}^0 + \Delta \mathbf{p}^1 = \Delta \mathbf{p}^1$$

$$\mathbf{q}^1(x) = \mathbf{q}^0(x) + \Delta \mathbf{q}^1(x) = \Delta \mathbf{q}^1(x)$$

$$\mathbf{d}^1(x) = \mathbf{d}^0(x) + \Delta \mathbf{d}^1(x) = \Delta \mathbf{d}^1(x)$$

update $\mathbf{E}^0(x) = \mathbf{0}$ to $\mathbf{E}^1(x)$

$$\mathbf{e}^1(x) = \mathbf{e}^0(x) + \Delta \mathbf{e}^1(x) = \Delta \mathbf{e}^1(x)$$

end of the analysis

APPENDIX C

APPLICATION OF SOLUTION ALGORITHM

TO A SIMPLE SOFTENING SYSTEM

The nonlinear solution algorithm for the element state determination is illustrated here with the aid of the simple system of two extensional springs in series shown in Fig. 4.5. One spring is linear elastic, while the other is linear elastic-strain softening. As discussed in Chapter 4, the equilibrium and compatibility of the two spring system leads to the following relations:

$$Q = D_A = D_B$$

$$q = q_A + q_B$$

$$F = f_A + f_B$$

In this illustrative analysis a single deformation increment Δq is applied and the corresponding resisting force increment ΔQ is sought. Consequently, there is no need for the use of superscripts k and i and only superscript j that describes the sequence of element iterations is sufficient to represent the evolution of the system variables. Superscript i is only used once to indicate that the element deformations are updated. Since the system is assumed to be initially unstressed, the initial state is characterized by:

$$Q^{j=0} = 0$$

$$q^0 = 0$$

$$d_A^0 = d_B^0 = 0$$

$$f_A^0 = f_{A,el}$$

$$f_B^0 = f_{B,el}$$

$$F^0 = f_A^0 + f_B^0$$

$$K^0 = [F^0]^{-1}$$

The steps for the nonlinear analysis of the two spring element are illustrated in Fig. 4.6. First, the deformation increment Δq is imposed. This increment remains unchanged during the iterations in order to satisfy the compatibility requirement. The total deformation of the element is updated

$$q^{i=1} = q^{i=0} + \Delta q^{i=1} = 0 + \Delta q = \Delta q$$

and the element iterations start:

$j=1$ Based on the initial element stiffness K^0 a first estimate of the element force increment ΔQ^1 due to Δq is computed and the deformation increments caused by this force in the extensional springs are determined:

$$\Delta Q^1 = K^0 \cdot \Delta q$$

$$Q^1 = Q^0 + \Delta Q^1 = \Delta Q^1$$

$$\Delta D_A^1 = \Delta D_B^1 = \Delta Q^1$$

$$\Delta d_A^1 = f_A^0 \cdot \Delta D_A^1$$

$$\Delta d_B^1 = f_B^0 \cdot \Delta D_B^1$$

Update the spring deformations and forces and determine the new spring flexibilities

$$d_A^1 = d_A^0 + \Delta d_A^1 + r_A^0 = \Delta d_A^1$$

$$d_B^1 = d_B^0 + \Delta d_B^1 + r_B^0 = \Delta d_B^1$$

$$D_A^1 = D_A^0 + \Delta D_A^1 = \Delta D_A^1$$

$$D_B^1 = D_B^0 + \Delta D_B^1 = \Delta D_B^1$$

$$f_A^1 = f_{A,el}$$

$$f_B^1 = f_{B,pl}$$

where r^0 are the initial residual deformations of the springs which are equal to zero. Compute the spring resisting forces $D_{A_R}^1$ and $D_{B_R}^1$ and the corresponding unbalanced forces:

$$D_{A_U}^1 = D_A^1 - D_{A_R}^1 = D_A^1 - D_A^1 = 0$$

$$D_{B_U}^1 = D_B^1 - D_{B_R}^1$$

Compute the residual spring deformations r_A^1 and r_B^1

$$r_A^1 = f_A^1 \cdot D_{Au}^1 = 0$$

$$r_B^1 = f_B^1 \cdot D_{Bu}^1$$

Update the element flexibility and stiffness matrices:

$$F^1 = f_A^1 + f_B^1$$

$$K^1 = [F^1]^{-1}$$

Check for element convergence: spring B has a significant force unbalance, and, consequently, the element has not converged. Compute the residual element deformation s^1 :

$$s^1 = r_A^1 + r_B^1 = r_B^1$$

$j=2$

Start a new element iteration. With the residual element deformation at the end of the previous iteration $j=1$ compute the new element force increment

$$\Delta Q^2 = -K^1 \cdot s^1$$

$$Q^2 = Q^1 + \Delta Q^2$$

$$\Delta D_A^2 = \Delta D_B^2 = \Delta Q^2$$

$$\Delta d_A^2 = f_A^1 \cdot \Delta D_A^2$$

$$\Delta d_B^2 = f_B^1 \cdot \Delta D_B^2$$

Update the spring deformations and forces and determine the new spring flexibilities:

$$d_A^2 = d_A^1 + \Delta d_A^2 + r_A^1 = d_A^1 + \Delta d_A^2$$

$$d_B^2 = d_B^1 + \Delta d_B^2 + r_B^1$$

$$D_A^2 = D_A^1 + \Delta D_A^2$$

$$D_B^2 = D_B^1 + \Delta D_B^2$$

$$f_A^2 = f_{A,el}$$

$$f_B^2 = f_{B,pl}$$

Compute the spring resisting forces $D_{A_R}^2$ and $D_{B_R}^2$ and the corresponding unbalanced forces:

$$D_{A_U}^2 = D_A^2 - D_{A_R}^2 = 0$$

$$D_{B_U}^2 = D_B^2 - D_{B_R}^2 = 0$$

Compute the residual spring deformations r_A^2 and r_B^2

$$r_A^2 = f_A^2 \cdot D_{A_U}^2 = 0$$

$$r_B^2 = f_B^2 \cdot D_{B_U}^2 = 0$$

Update the element flexibility and stiffness matrices:

$$F^2 = f_A^2 + f_B^2$$

$$K^2 = [F^2]^{-1}$$

Check for element convergence: both springs have zero force unbalance, and, consequently, the element has converged and this simple analysis is complete.
